D I S S E R T A T I O N

Microdevices for molecular diagnostics

Continuous flow PCR, nucleotide fluorescence labelling, DNA sensing and fluorescence enhancement

ausgeführt zum Zwecke der Erlangung des akademischen Grades eines Doktors der technischen Wissenschaften unter der Leitung von

Univ.-Prof. Dr. Michael J. Vellekoop

eingereicht an der Technischen Universität Wien
Fakultät für Elektrotechnik und Informationstechnik

von

Johannes R. Peham

Dingelstedtgasse 11/10, 1150, Wien
Matr.-Nr. 9931002

Wien, im Jänner 2012

Erstbegutachter	Univ.-Prof. Dr. Michael J. Vellekoop Vienna University of Technology Vienna, Austria
Zweitbegutachter	Univ.-Prof. Dr. Zlatko Trajanoski Innsbruck Medical University Innsbruck, Austria

In Memoriam
Dr. Peter Peham
(1931 - 2009)
Dr. Karl Schöpf
(1919 - 2012)

Contents

Abstract

This dissertation addresses microdevices, designed as advanced molecular diagnostic assays. The aim is to make tests and devices faster, less complex and more cost-effective than current methods. The molecular analysis of food-contamination, environmental threats, infectious pathogens or disease biomarkers can be improved significantly by such instruments. In particular four microsystems are presented: continuous-flow polymerase chain reaction (PCR), nucleotide fluorescence labelling, DNA sensing and fluorescence enhancement.

Continuous-flow PCR was realised with a microfluidic approach, processing consecutive sample droplets. The used micro-tubing was coiled around three heating plates with constant temperatures for denaturation, annealing and extension to implement a complete PCR protocol. Target lengths up to 1.3 kbp could be amplified and sample throughputs of up to 80 samples per hour could be realised, which is superior to other publications. Detection limits down to 1×10^2 bacterial cells per reaction were achieved.

Nucleotide fluorescence labelling was performed in a disposable microfluidic polycarbonate chip. Bacterial DNA is amplified and labelled in a single reaction, which results in a hybridisation-ready mix, ready for microarray analysis. The polycarbonate chip consists of a spiral channel, where the samples are pumped through. Injection moulding and thermal bonding was used for fabrication, which qualifies the device for large-scale production and for the application as single-use test. In comparison to the standard method an overall process acceleration from 6 h to 1.5 h could be achieved with sensitivities down to 1×10^2 bacterial cells per reaction.

For the detection of PCR products in continuous-flow, DNA sensing was realised with a fluorescence measuring microfluidic flow-cell. It comprises a LED-photodiode unit, sensing DNA samples in continuous flow. In particular it was designed for measuring unpurified PCR products including primers and polymerases, which was achieved by heating the flow cell to 60 °C. This approach suppresses signals from primer dimers and enables high sensitivities when detecting PCR products. Initial microbial DNA amounts before PCR of 10 cell equivalents per reaction were still detectable. The detection limit of purified DNA samples was $1\,\mathrm{ng\,\mu L^{-1}}$ at a throughput of

240 samples per hour. The detector can be directly connected to continuous-flow PCR devices like the tubing system or the polycarbonate fluorescence labelling chip.

Fluorescence enhancement was achieved with metal and metal oxide thin films fabricated by sputtering, dip- and spin-coating. Excitation and emission light from fluorescence sensing is amplified by the coatings and increases signal output. The different thin films were assessed by DNA microarrays with bacterial pathogens as biological samples. Gold coatings resulted in an 8-fold signal increase compared to bare glass slides. For diagnostic applications, this means a significant increase of sensitivity.

The presented microdevices and thin film coatings are superior to current assays. It could be shown, that they have the potential to improve molecular diagnostic methods in aspects of costs, process integration, sample throughput, miniaturisation, sensitivity and rapidness. In a further consequence, this leads to a superior analysis of pathogens, food- and environmental contaminations or disease biomarkers.

Kurzfassung

Diese Dissertation befasst sich mit Mikrogeräten als fortgeschrittene molekular-diagnostische Tests. Das Ziel sind Geräte, die Untersuchungen schneller, einfacher und günstiger durchführen können als derzeitige Verfahren. Die molekulare Analyse von Lebensmittel- oder Umweltkontaminationen, Infektionserregern oder Krankheitsindikatoren kann durch solche Instrumente erheblich verbessert werden. Im Speziellen werden vier Mikrosysteme präsentiert: Durchfluss Polymerase-Kettenreaktion (PCR), Nukleotid-Fluoreszenzmarkierung, DNS-Messung und Fluoreszenzverstärkung.

Durchfluss-PCR wurde mit einem mikrofluidischen Ansatz realisiert, bei dem aufeinanderfolgende Probentröpfchen bearbeitet werden. Der verwendete Mikroschlauch wurde um drei Heizplatten mit konstanten Temperaturen gewickelt. Die drei Temperaturzonen repräsentieren die DNS-Denaturierung, die Primerhybridisierung und die Elongation, um ein vollständiges PCR Protokoll umzusetzen. PCR-Produktlängen von bis zu $1.3\,\mathrm{kbp}$ konnten amplifiziert werden und ein Probendurchsatz von bis zu 80 Proben pro Stunde wurde erreicht, was eine Verbesserung im Vergleich zu bisher publizierten Verfahren darstellt. Detektionslimits von bis zu 1×10^2 bakterielle Zellen pro Reaktion wurden erzielt.

Nukleotid-Fluoreszenzmarkierung wurde mit einem Einweg-Mikrofluidik-Chip aus Polycarbonat realisiert. Bakterielle DNS wird in einer einzelnen Reaktion amplifiziert und markiert, was zu einem hybridisierungsfertigen Gemisch führt, welches direkt für DNS-Mikroarrays eingesetzt werden kann. Der Polycarbonat-Chip besteht aus einem spiralförmigen Kanal, durch den die Proben gepumpt werden. Für die Herstellung wurde Spritzguss und thermisches Bonden eingesetzt, was den Chip für die Massenfertigung und den Einsatz als Einweg-Test qualifiziert. Im Vergleich zur Standardmethode, konnte eine Prozessbeschleunigung von $6\,\mathrm{h}$ auf $1.5\,\mathrm{h}$ erreicht werden mit Detektionslimits von bis zu 1×10^2 bakterielle Zellen pro Reaktion.

Für die Durchfluss-Detektion von PCR-Produkten wurde DNS mit einer fluoreszenzmessenden Mikrofluidik-Kammer erfasst. Sie besteht aus einer LED-Photodioden Einheit, die DNS-Proben im Durchfluss misst. Im Spezi-

ellen wurde sie für die Messung von nicht gereinigten PCR-Produkten, welche auch Primer und Polymerasen enthalten, entwickelt. Dies wurde durch das Aufschmelzen von Primer-Dimeren mittels Temperierung der gesamten Kammer auf $60\,°C$ erreicht. Dieser Ansatz unterbindet Signale von Primer-Dimeren und ermöglicht hohe Sensitivitäten bei der Messung von PCR-Produkten. Mikrobielle DNS-Ausgangsmengen von 10 Zell-Äquivalenten pro Reaktion vor der PCR konnten noch detektiert werden. Das Detektionslimit von gereinigten DNS-Proben betrug $1\,ng\,\mu L^{-1}$, bei einem Durchsatz von 240 Proben pro Stunde. Der Detektor kann direkt nach Durchfluss-PCR Systemen, wie beispielsweise das schlauchbasierte System oder der Polycarbonat-Fluoreszensmarkierungs-Chip, angschlossen werden.

Fluoreszenzverstärkung wurde mit Hilfe von Metall- und Metalloxid-Dünnschichten erzielt, welche mittels Kathodenzerstäubung, Tauch- und Rotationsbeschichtung hergestellt wurden. Durch den aufgebrachten Dünnfilm werden Anregungs- und Emissionslicht der Fluoreszenzmessung verstärkt und die Signalintensität erhöht. Die verschiedenen Schichten wurden mit DNS-Mikroarrays und bakteriellen Erregern als biologische Proben getestet. Gold-Beschichtungen erreichten eine 8-fache Signalsteigerung im Vergleich zu gewöhnlichen Glas-Objektträgern. Für diagnostische Anwendungen bedeutet das eine wesentliche Erhöhung der Sensitivität.

Die präsentierten Mikrosysteme und Dünnschichten sind derzeitigen Testverfahren überlegen. Es konnte gezeigt werden, dass sie das Potential haben molekular-diagnostische Untersuchungen hinsichtlich Kosteneffizienz, Prozessintegration, Probendurchsatz, Miniaturisierung, Sensitivität und Schnelligkeit zu verbessern. Dies führt wiederum zu einer überlegenen Analyse von Infektionserregern, Lebensmittel- und Umweltkontaminationen oder Krankheitsindikatoren.

Nomenclature

0.1 List of Abbreviations

Symbol	Description
2D	two dimensional
3D	three dimensional
A	adenine
AFM	atomic force microscopy
AIDS	acquired immunodeficiency syndrome
APT	avalanche photodiode
bp	base pairs
BSA	bovine serum albumin
C	cytosine
CE	capillary electrophoresis
CF	continuous flow
CF-PCR	continuous flow PCR
CFU	colony forming units
ChIP	chromatin immunoprecipitation
CMOS	complementary metal oxide semiconductor
CNC	computerised numerical control
CVD	chemical vapour deposition
Cy3	green fluorescent dye of the cyanine family
Cy5	red fluorescent dye of the cyanine family
dCTP	deoxycytidine triphosphate
$\mathrm{ddH_2O}$	double distilled water

Symbol	Description
DMSO	dimethyl sulfoxide
DNA	deoxyribonucleic acid
dNTP	deoxynucleotide triphosphate
dsDNA	double stranded DNA
EDM	electrical discharge machining
EDTA	ethylenediaminetetraacetic acid
EHEC	enterohemorrhagic *Escherichia coli*
EtBr	ethidium bromide
FEM	finite element method
G	guanine
HT	high throughput
HIV	human deficiency virus
IFC	integrated fluidic circuit
IPA	isopropyl alcohol
IVD	in vitro diagnostics
kbp	kilo base pairs
LED	light emitting diode
LIF	laser induced fluorescence
LOC	lab on chip
LOD	limit of detection
μTAS	micro total analysis system
NH	amino-modified
NTC	negative temperature coefficient
PBS	phosphate buffered saline
PC	polycarbonate
PCR	polymerase chain reaction
PD	photodiode
PDMS	polydimethylsiloxane

Symbol	Description
PEEK	polyetheretherketone
PET	polyethylene terephtalate
PFA	perfluoroalkoxy
PID	proportional integral differential
PIN-PD	positive intrinsic negative photodiode
PMMA	polymethyl methacrylate
PMT	photomultiplier tube
POC	point of care
PS	polystyrene
PTFE	polytetrafluoroethylene
PVC	polyvinyl chloride
PVD	physical vapour deposition
PVP	polyvinylpyrrolidone
qPCR	quantitative PCR
RIE	reactive ion etching
RNA	ribonucleic acid
rRNA	ribosomal RNA
SDS	sodium dodecyl sulfate
SH	thiol-modified
SNP	single nucleotide polymorphism
SSC	saline sodium citrate
ssDNA	single stranded DNA
T	thymine
TEC	thermo electric cooling
USA	United States of America
USD	United States dollar

0.2 List of Variables

Symbol	Description	Unit
a	channel width at the top	m
A	cross section of channel	m^2
AF_{PCR}	amplification factor for PCR	1
AF_{PE}	amplification factor for primer extension	1
c	channel width at the bottom	m
C_P	specific heat capacity	$J\,kg^{-1}\,K^{-1}$
EF	enhancement factor	1
E_{em}	electrical field of emission light	$V\,m^{-1}$
$E_{em}{}^*$	enhanced electrical field of emission light	$V\,m^{-1}$
E_{ex}	electrical field of excitation light	$V\,m^{-1}$
η	reaction efficiency	1
k	thermal conductivity	$W\,m^{-1}\,K^{-1}$
N	number of cycles	1
$\mathbf{q}$	thermal flux	$W\,m^{-2}$
Q	heat source	$W\,m^{-3}$
R	radius of spiral	m
r_c	radius of curvature	m
R_{RMS}	root mean squared roughness	m
ρ	density	$kg\,m^{-3}$
S	arc length of spiral m	
SF	shrinkage factor	1
t	channel depth	m
T	temperature	K
T_g	glass transition temperature	°C

Symbol	Description	Unit
T_s	maximum service temperature	°C
V_{1turn}	volume of one spiral turn	m
φ	angle of the spiral	rad
w	distance between centres of channels	m

Chapter 1
Introduction

1.1 Molecular methods for diagnostics

The importance of molecular diagnostics in medicine is continuously rising. Molecular methods are used to substitute or complement classical diagnostics tests with the advantage of higher sensitivity and specificity, non-invasiveness, rapidness and high-throughput (HT) capability. In principle, molecular methods measure nucleic acids such as ribonucleic acid (RNA), deoxyribonucleic acid (DNA), proteins and products of metabolism. These molecules can be used as biomarkers, if their quantity can be correlated to disease status. However, the discovery of sensitive and specific human biomarkers is not trivial. The human genome, transcriptome and proteome are large, complex and often show high variations between individuals. This makes general assays difficult and requires technologies and data analysis methods capable of analysing biomolecules in a massively parallel way. High-throughput methods include microarrays, next generation sequencing and HT-mass-spectrometry. Therefore, molecular diagnostics not only require novel technologies for improved assays, measuring disease parameters, but also for the discovery of more specific and sensitive biomarkers.

Methods analysing nucleic acids include DNA microarrays, polymerase chain reaction (PCR) [1] and quantitative PCR. These technologies share the potential of highly sensitive and specific measurement of genomic or transcriptomic factors, which is the prerequisite for accurate diagnostic assays and biomarker screening. PCR can be described as one of the key methods, since it has the great potential of detecting minute amounts of DNA. This is performed by an exponential enzymatic reaction, which doubles the initial target DNA with every cycle. A PCR protocol usually includes three steps: denaturation, annealing and extension, which specifies one cycle. Firstly, denaturation is performed by heating the DNA to $95\,^{\circ}\mathrm{C}$, which melts the double strand into two single strands. Secondly, annealing is performed

between $50\,°C$ and $70\,°C$, where primers (short single stranded DNA) can attach to the previously melted target DNA. The DNA region of interest is defined by forward and reverse primer, which determine the start and end of the DNA replication by polymerases. Thirdly, extension of the primers is performed at $72\,°C$, where polymerases have the highest efficiency. These enzymes attach to the primed DNA and extend the target strand with its complementary sequence. These three steps are repeated, doubling the DNA amount at every step. PCR has therefore an amplification factor $\mathrm{AF_{PCR}}$, which is exponentially proportional to the number of cycles N and influenced by the reaction efficiency η ($0 < \eta < 1$), as defined in Equation 1.1.

$$AF_{PCR} = (1 + \eta)^N \tag{1.1}$$

Conventional PCR is the basis for several more advanced analysis methods including quantitative PCR (qPCR), fluorescent labelling reactions, digital PCR and as sensitivity gain for microarrays and sequencing. Quantitative PCR includes a fluorescent readout after each cycle, sensitive to double stranded DNA (dsDNA), which enables the acquisition of the growth curve for each reaction. Comparing the exponential phase of the curve to a known standard, makes a quantification of initial target DNA possible. This readout can be used to assess gene expression, used for tumour diagnostics or for measuring pathogen load to identify the severity of infectious diseases. Reactions similar to PCR are used for fluorescent labelling of DNA, like primer extension. There, modified polymerases, lacking exonuclease activity, incorporate fluorophore conjugated nucleotides into the newly synthesised strand (see Chapter 3, Fig. 3.2). This reaction is used for microarray analysis or solid-phase PCR. Digital PCR is another method derived from conventional PCR, which quantifies DNA by a discrete and countable signal [2]. Each sample is diluted and partitioned into multiple wells. Dilution has to be chosen in such a way, that one well holds one target (1) or no target at all (0). Cycling all wells simultaneously and performing an endpoint DNA measurement leads to a discrete number of positive wells, which are Poisson distributed. When only one or no target DNA strand resides in one well (achieved by dilution), this number of positive wells equals the number of target DNA molecules. Sample DNA quantity is therefore countable. One problem in conventional quantitative PCR is, that reaction efficiency of sample and reference can be different. Furthermore, only twofold differences can be resolved because of the exponential nature

of PCR. Digital PCR does not have these limitations, which makes it more precise and reliable. It has been used for cancer diagnostics [3] and recently the first commercial product was released from Fluidigm Inc., San Francisco, CA, USA. On the same platform high-throughput multiplex qPCR can be performed. In a matrix-like reaction pad, 96 samples are mixed with 96 primer pairs leading to 9216 reactions per plate and a reaction volume of 6.7 nL (Fig. 1.1). Fluidic control is achieved by pneumatic microvalves (NanoFlex™) on the elastic chip. With this approach pipetting effort is reduced by 100-fold and the costs per sample are reduces significantly. The system can be used for biomarker screening or multiplex diagnostic assays like gene expression analysis or pathogen identification.

1.2 Infectious diseases and their detection

Infectious diseases are a major health threat, especially in developing countries, including tuberculosis, pneumonia and human deficiency virus (HIV) / acquired immunodeficiency syndrome (AIDS) [4]. But also in the developed world the parasitic colonisation of humans is still a health issue ranging from nosocomial infections to food-borne illnesses. In May and June 2011 more than 3900 enterohemorrhagic *Escherichia coli* (EHEC) cases were reported in Germany and at least 46 died [5]. Beside these temporary outbreaks, permanent diseases include sepsis, pneumonia and urinary tract infections. Especially sepsis has a high mortality rate of up to 59 % [6] and an incidence of 51 to 300 cases per $100\,000$ inhabitants [7]. The average costs for severe sepsis are $22\,100$ USD per case, which is with a national estimate of $751\,000$ cases an overall annual cost of 16 billion USD in the USA [8]. Beside the motivation of health care itself, these costs are an economic driver for improved diagnostic and therapeutic methods reducing incidence and mortality.

For all infectious diseases, rapid diagnosis with subsequent species identification is important for early and species-targeted treatment. This early intervention is still the most promising approach for patient recovery. Furthermore, species specific antibiotic treatment has the potential to confine antibiotic resistances. In clinical routine, cultivation based methods remain the gold standard for bacterial caused diseases. Because pathogens have to multiply to be detectable in cultivation flasks, this method is time consuming, lasting at least 24 hours up to several days for slow growing organisms. Moreover, some strains are difficult to cultivate, which can cause

(a)

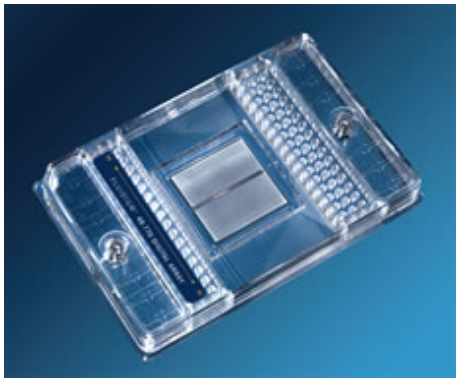

(b)

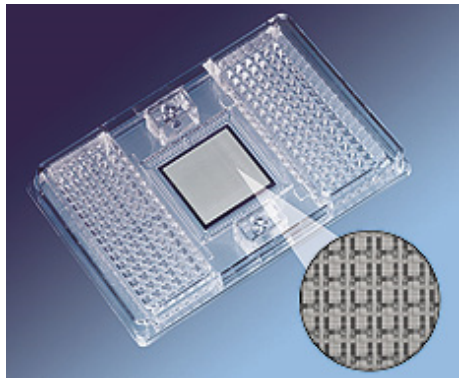

(c)

Figure 1.1: Fluidigm system: a) Biomark HD instrument for sample preparation, PCR cycling and readout; b) Digital Array™ integrated fluidic circuit (IFC) for digital PCR (48 samples, 770 reactions per sample (39 960 total reactions per run); c) Dynamic Array™ IFC for high throughput analysis of 96 samples × 96 assays (from www.fluidigm.com).

false negative signals. Molecular methods as described in Section 1.1 have the potential to significantly speed-up the analysis process of pathogen identification. Moreover, they are not dependant on optimised growth conditions, since they target the biomolecules of the organisms. PCR is a reliable method for pathogen genotyping, reducing analysis time significantly and its high sensitivity, low price and parallelisation capability are further advantages compared to cultivation techniques [9, 10]. This enables faster testing, which brings reduced mortalities, shorter hospital stay and reduced costs [11].

1.3 Microdevices for molecular methods

While molecular methods are well established in the laboratory, they have several limitations. They are labour intensive with long hands-on times, often depend on multiple devices and they require bulky equipment and trained personnel. Furthermore, standard methods require volumes in the range of microlitres for successful detection. Miniaturised systems like microdevices, Lab on Chip (LOC) systems and micro Total Analysis Systems (μTAS) have the potential to reduce sample and reagent volumes to nanolitres and picolitres. This brings increased sensitivity, reduced costs per sample and smaller device dimensions. μTAS have high system integration. They process the biological samples directly without pre-treatment and deliver the final results without further hands-on time (sample-in result-out). In diagnostics, this approach is interesting for mobile devices used for decentralised monitoring of disease parameters at or near the patient, called Point of Care (POC) testing. POC systems can be applied in clinics at the bedside, in the offices of general practitioners, in pharmacies, in emergency ambulances or at home for self-testing by the patient. In contrast, microdevices are used in research and diagnostic laboratories as well, because of their superior performance like sample-throughput, sensitivity or costs per sample. Examples for such systems are capillary electrophoresis systems on chip like the Agilent 2100 Bioanalyzer (Agilent Technologies Inc., Santa Clara, CA, USA) or the Shimadzu MCE-202 MultiNA (Shimadzu Corp., Kyoto, Japan) and sequencing on chip approaches like the ion torrent system (Ion Torrent Systems, Inc., Guilford, CA, USA). The ion torrent device uses a chip with up to 12 million wells for parallel non-optical sequencing [12]. Each well holds a unique DNA sequence, which is enzymatically elongated nucleotide by nucleotide. The different bases are added after each other to

identify, if a nucleotide is incorporated or not. This is performed by measuring H^+ ions, which are generated by the incorporation reaction. Technically, the ions are sensed by pH measurement with a complementary metal oxide semiconductor (CMOS) chip (Fig. 1.2).

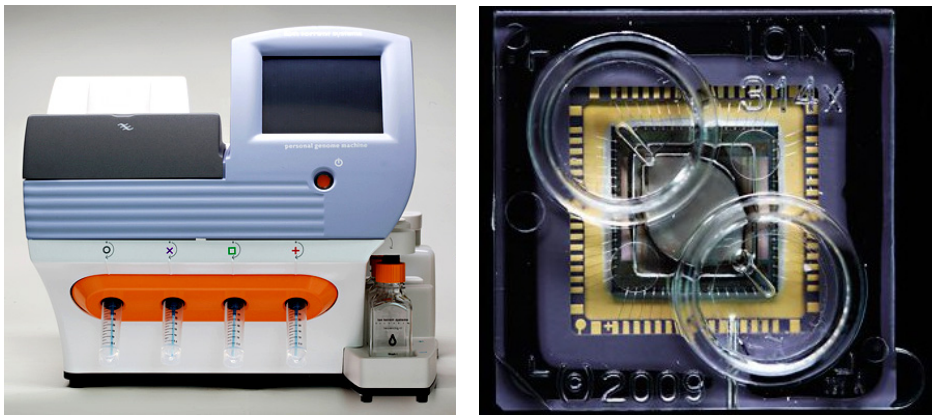

(a) (b)

Figure 1.2: Iontorrent sequencing system a) Personal Genome Machine™ instrument with the four containers (o, $\times$, $\square$ and $+$) for the different bases (A, C, T and G); b) semiconductor sequencing chip with 1.3 million wells (from www.iontorrent.com).

1.4 Outline

As discussed in the previous sections, there are several needs in molecular diagnostics including rapidness for early intervention, high-throughput analysis for biomarker discovery, process automation to reduce hands-on time, miniaturisation for handheld devices and increased sensitivity to detect diseases in an early stage. Microdevices have the potential to satisfy these requirements with improved diagnostics and biomarker discovery and novel and superior analysis approaches.

Chapter 2 addresses rapidness and high-throughput with a tubing-based continuous-flow (CF) PCR system for the amplification of long DNA targets. Samples are processed continuously and the system was assessed with DNA, extracted from different bacterial species. Sensitivity, throughput,

processing time and target length are compared to conventional systems and other publications.

Chapter 3 covers rapidness, process automation and miniaturisation with a disposable microfluidic plastic chip, used for PCR and fluorescent labelling in one reaction. The system was compared to the standard analysis method of PCR and labelling in a conventional thermocycler. The chip is fabricated by injection moulding and thermal bonding, which are capable for large-scale production.

Chapter 4 comprises a flow-through fluorescent DNA sensor for the high-throughput detection of PCR products. The system is lens-free and uses standard photodiodes for readout. It can be directly connected to the PCR- and direct labelling devices from Chapter 2 and 3.

Chapter 5 addresses increased sensitivity with metal and metal oxide coatings for the enhancement of fluorescence. The thin films were integrated into microarray fabrication and signal increase was assessed by DNA microarray assays.

Chapter 2

Tubing-based microfluidic polymerase chain reaction for high-throughput applications

As introduced in Section 1.1 PCR is one of the key methods in molecular diagnostics, providing highest sensitivity and specificity in detecting nucleic acids. Moreover, it is the fundamental principle for further techniques such as quantitative PCR, multiplex PCR, methylation specific PCR and solid-phase PCR. All those methods are well established in the laboratory, however they are time consuming and consist of labour intensive working steps. Miniaturised and automated systems for high-throughput analysis have the potential to outperform existing technologies in terms of rapidness, throughput and portability. This chapter presents a tubing-based continuous flow polymerase chain reaction system and is based on the paper:

J. R. Peham, W. Grienauer, H. Steiner, R. Heer, M. J. Vellekoop, C. Nöhammer and H. Wiesinger-Mayr, "Long target droplet polymerase chain reaction with a microfluidic device for high-throughput detection of pathogenic bacteria at clinical sensitivity", *Biomed Microdevices*, 2011, **13**:463-473. doi:10.1007/s10544-011-9514-x

2.1 Polymerase chain reaction in miniaturised environments

Generally, PCR relies on two operational principles: static cycling and cyclic flow. Static cycling is performed in a reaction chamber, where the sample volume is spatially fixed and the temperature of the container is changed periodically. In contrast, cyclic flow PCR is performed with a sample transported through heating zones of constant temperature. Because in cyclic flow systems the thermal mass exposed to different temperatures is reduced to sample and transport buffer, the transition times between different temperature levels are much lower. This enables a much faster amplification in comparison to a static thermocycler. In addition, a cyclic flow system is easier integrated in up- and downstream applications for continuous operation [13]. The throughput of such systems depends on the sample volume and fluidic geometries and ranges from 4000 [14] to 6000 [15] reactions per day per reactor without any hands-on time.

Although a successful amplification in a fluoropolymer capillary was presented before [14, 15], a complete comparison of the detection limit to a conventional thermocycler is missing. This means, that no results were presented observing yield reduction because of the contact to large surfaces of fluoropolymers [14]. These comparisons of perfluoroalkoxy (PFA) and standard PCR vials were shown in [15], however a comparison of the detection limits was not presented. Therefore, an efficiency comparison is not significant.

The miniaturisation and automation of the PCR in a microfluidic setting is a desirable objective, as it can bring high speed, less reagent consumption, cost reduction, increased sensitivity and parallelisation [16–19]. However, a holistic application-specific investigation of a continuous flow PCR system is rarely presented. Most literature demonstrate a proof of principle without concentrating on the limits and drawbacks important for a particular application. The major constraints are the restriction to phage DNA [15, 20], li-

mited amplicon lengths [21–23], lower sensitivity compared to conventional thermocyclers [24, 25] and the restriction to abundant DNA templates [26]. In aspect of species identification by DNA microarrays, long targets are especially important for the accurate discrimination between different bacteria [27, 28].

The next section describes how to overcome the trade-off between target length, sensitivity and sample throughput. A microfluidic PCR device with high sensitivity, high sample throughput and amplicons above 1 kbp for the amplification of the 16S rRNA gene is presented, with the application of bacterial detection.

2.2 Device design

Conventional thermocyclers alter the temperature after each processing step (denaturation, annealing, extension). A block of metal is heated and cooled by heating elements, Peltier elements and fans. This block usually holds 96 PCR tubes and has, therefore, a relatively high mass. This makes a rapid temperature change difficult and heating- and cooling rates in the range of $1\,\mathrm{K\,s^{-1}}$ to $4\,\mathrm{K\,s^{-1}}$ are typical. The largest temperature difference is the one between denaturation and annealing and is approximately $40\,\mathrm{K}$. In conventional thermocyclers this transition can last up to $40\,\mathrm{s}$. This transition time is longer than the reaction time itself for small targets ($5\,\mathrm{s}$ to $30\,\mathrm{s}$). Therefore, temperature adjustment accounts for a large part of overall processing time. Continuous flow PCR systems have the great advantage of reducing this transition time and providing high sample throughput. Because the tempered mass is the sample itself and not a metal block, temperature adjustment can be fast. However, the temperature gradient is dependent on the flow rate, which has to be considered (compare Section 2.5.4). Miniaturised chamber- or well-based systems [29–31] or single-loop systems [32] have reduced thermal mass as well, but they lack the capability of processing multiple samples consecutively. Therefore, their throughput is low and an integration into up- and downstream processes is difficult. Because throughput and integration into further analysis steps are important in molecular diagnostics, chamber-based systems were not considered.

Different concepts in continuous-flow PCR include planar designs (meander-, circular- and linear systems) [18] and 3D-circular devices [15, 25, 33]. Planar meander systems have the disadvantage, that the sequential protocol has one uncorrect annealing stage. Ins-

tead of denaturation-annealing-extension-denaturation the samples undergo denaturation-annealing-extension-annealing-denaturation. This drawback is not present in planar circular designs, however their channel length increases with increasing radius. This effect has to be compensated to guarantee correct PCR timings. Linear systems have a facile channel design, but they require multiple heating zones (three for each cycle), which makes the heating design more complex (see Chapter 3, Section 3.3.1 for a more detailed discussion of planar systems). Circular 3D devices are a convenient solution to be used with microtubings, which can be directly coiled around (Fig. 2.1). Because of its facile design the circular 3D approach was chosen for the presented device. A three-sided prismatic design was used, which is compatible with standard planar Peltier elements. This approach has low constructional complexity, which brings low costs.

The cyclic flow PCR reactor consists of a heating device in the shape of a triangular prism, where each side represents a temperature zone for denaturation ($95\,^{\circ}$C), annealing ($55\,^{\circ}$C) and extension ($72\,^{\circ}$C) respectively. A tubing is coiled around the heater in which the sample is pumped through the three temperature zones in every turn, realising a full thermal PCR protocol.

The sides of the triangular prism consists of an aluminium plate ($60\,$mm $\times$ $60\,$mm $\times$ $4\,$mm) with an attached peltier element (Tecoolers, Utrecht, The Netherlands) for heating. The hot side of the thermoelectric cooling (TEC) elements is in contact with the aluminium plate, while the cool side is attached to a steel frame. This frame is hollow to allow cooling with a fan. The corners between the heating plates are isolated with polycarbonate spacers, which additionally guarantee a round transition of the tubing (Fig. 2.2).

All connectors and fittings are made of polyetheretherketone (PEEK) or polytetrafluoroethylene (PTFE), which guarantee inertness and chemical stability [34]. The microfluidic tubing consists of transparent PTFE ($400\,\mu$m inner diameter, $800\,\mu$m outer diameter, ScanTube AB, Knivsta, Sweden) and is coiled around the triangular prism 40 times, representing 40 cycles. The tubing is attached with thermal grease to the aluminium plates and is isolated with $40\,$mm polystyrene on the other side to prevent heat loss, ensure temperature homogeneity and achieve high temperature stability over time (Fig. 2.3). Furthermore, the resistance of the polymers to cleaning reagents like NaOH and their temperature stability is important, which is fulfilled by both materials.

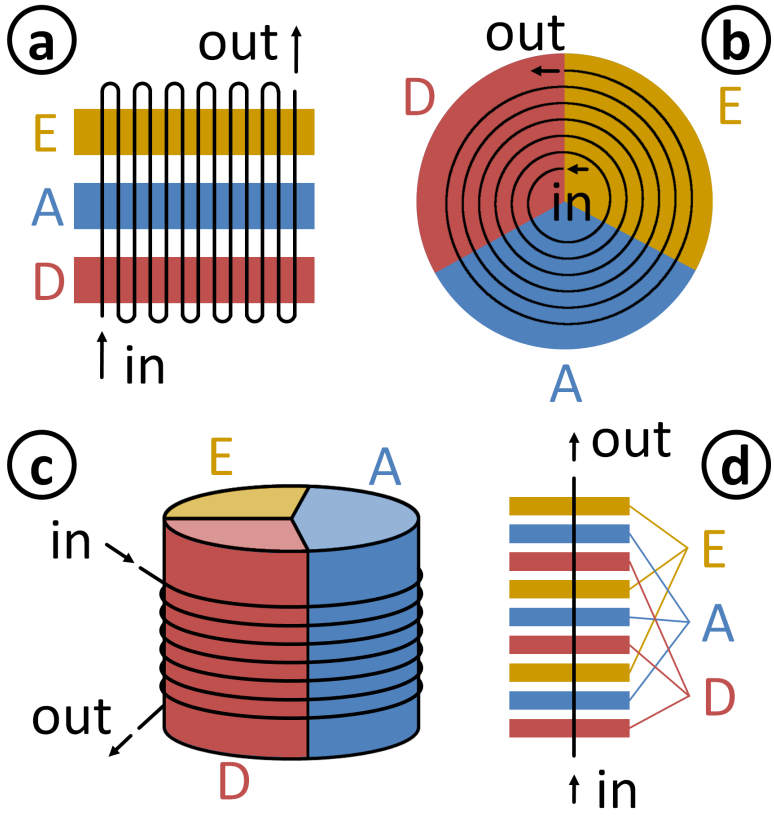

Figure 2.1: Concepts of continuous flow PCR: a) planar meander design, one uncorrect annealing step after extension (D-A-E-A-D); b) planar circular design; c) 3D circular design; d) linear design with multiple heating zones; D: denaturation; A: annealing; E: extension.

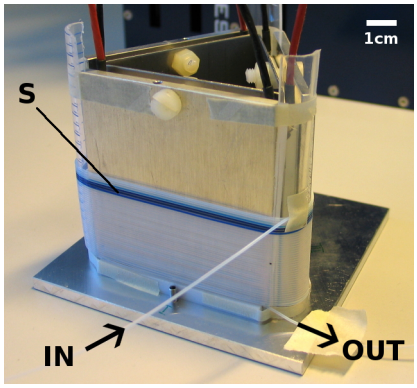

(a) Front view

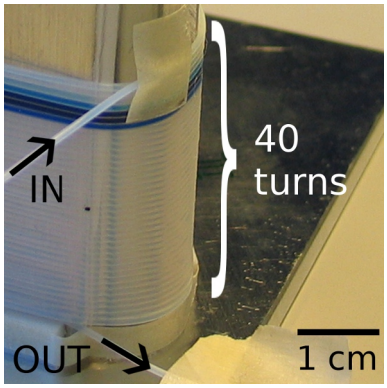

(b) Tubing detail

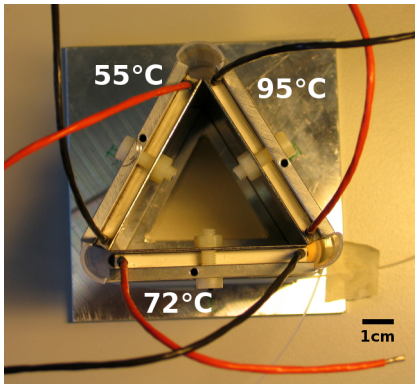

(c) Top view

Figure 2.2: Realisation of the PCR reactor: The three temperature zones (denaturation, annealing and extension) are represented by the three sides of the triangular prism. One turn of the polytetrafluoroethylene (PTFE) tubing represents one cycle of the PCR protocol. In total, 40 turns are coiled around the three heating plates. **S**: coloured sample sequence

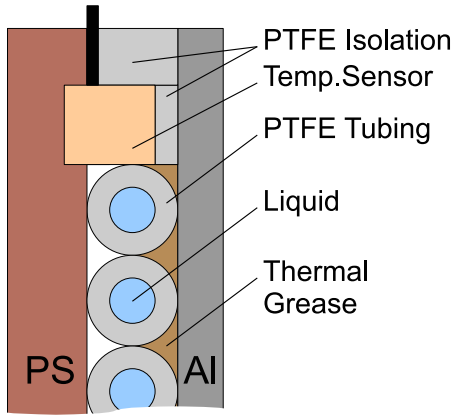

Figure 2.3: Cross section of heater: Thermal grease is applied between the tubing and the aluminium plate (Al) to optimise thermal conduction. On the other side the tubing is isolated with polystyrene (PS) to limit temperature loss and achieve a constant temperature. The temperature sensor is positioned at the location of the liquid and isolated with the same thickness of PTFE to guarantee accurate measurements.

The three TEC elements are driven by proportional integral differential (PID) controllers (TC M PCB, Electron Dynamics Ltd., Southampton, United Kingdom). High temporal stabilities down to 1 mK (controller specification) are possible with the continuously operating PID control unit, when the thermal load is isolated properly. The controller provides a pulse width modulated differential output for heating and cooling respectively. Minute temperature deviations in both directions can be compensated continuously, leading to the specified temperature stability. The temperature of each zone is measured by a negative temperature coefficient (NTC) sensor (B57540, EPCOS AG, München, Germany) mounted on the heating plate with 200 µm PTFE film, which equals the wall thickness of the tubing (Fig. 2.3). Therefore, the sensors experience the same thermal conditions as the liquid sample, which guarantees an accurate measurement. All temperatures were validated with a calibrated digital thermometer (Neuhold Elektronik, Graz, Austria).

2.3 Biological samples and reagents

2.3.1 Bacterial cells

The bacterial strains used in this study (*Escherichia coli*, *Pseudomonas aeruginosa* and *Staphylococcus aureus*) were originally isolated from clinical samples and stored as glycerol stocks (30 % glycerol) at −80 °C. Those stocks were used to cultivate the bacteria in caso bouillon at 37 °C overnight. The bacterial concentration in colony forming units (CFU) per mL was measured photometrically and compared to a reference (McFarland standard No. 0.5) for readjustment. Dilutions starting from 1×10^8 CFU mL^{-1} to 1×10^3 CFU mL^{-1} were prepared to test the limit of detection (LOD).

The cells were centrifuged (10 000 g for 10 min) and washed in phosphate buffered saline (PBS). After resuspending in double distilled water ($\mathrm{ddH_2O}$) the bacteria were thermally lysed at 95 °C for 15 min. Cell debris were spun down (10 000 g for 10 min) and the supernatant was transferred into a new tube and used straight away for the experiments. DNA was therefore isolated in a rather impure form, enabling to test for robustness of the amplification in a microfluidic environment.

2.3.2 PCR reagents and detection

The target for amplification was the 16S rRNA gene. Four primers (two forward, two reverse) were designed to generate three different amplicons with 418 bp (*E. coli* position 347 to 764), 720 bp (*E. coli* position 45 to 764) and 1324 bp (*E. coli* position 45 to 1368) respectively (Table 2.1). All primers were designed with the ARB software [35] and ordered from Microsynth (Balgach, Switzerland). The primers, targeting conserved regions of the 16S rRNA gene, are universal for all relevant pathogens causing infectious diseases. The region between the primers is species specific, which can be detected by DNA microarrays. The three species (*S. aureus*, *E. coli* and *P. aeruginosa*) were chosen as examples for assessing the system, because they are frequently associated with infectious diseases like blood stream infection, pneumonia or meningitis.

All PCR mixtures were prepared with the Mastermix 16S Basic (Molzym, Bremen, Germany) following the manufacturer's instructions. This mastermix is free of bacterial DNA and has a high amplification activity. Although the PTFE tubing has inert properties, it was crucial to add bovine serum albumin (BSA) into the mastermix for dynamic passivation. This

Table 2.1: Primers used for different amplicon lengths

Name	Sequence
45F	GCC TAW CAC ATG CAA GTC GA
347F	GAG GCA GCA GTR GGG AA
764R	TGT TTG CTC CCC AYG CTT T
1368R	CCG GGA ACG TAT TCA CCG

protein competitively binds to the surface, assuring that the DNA polymerase and nucleotides stay in solution. BSA is further described as a stabilising agent for DNA polymerases, which can lead to increased PCR efficiency [19, 36, 37].

For better sample visualisation in the tubing, a PCR compatible dye (Qiagen, Venlo, The Netherlands) was added. To avoid air bubbles, the PCR mastermix was degassed for 5 min at 95 °C with tube openings after 1.5 min and 3 min to release the formed gas.

Gel electrophoresis using a 1.7 % agarose gel stained with ethidium bromide ($0.2\,\mu g\,mL^{-1}$ final concentration) was applied to verify successfully amplified PCR products. The gels were photographed with a gel documentation system (UVP, Upland, CA, USA).

Image analysis was performed with the software ImageJ to obtain intensity plots for each lane and to quantify the gel bands. With the software the background was subtracted and the brightness of each lane was plotted against the vertical axis. Each peak, which represents a gel band, was quantified by calculating the area under the curve. All values were normalised to the band of the conventional thermocycler, resulting in a percentage value for each band [38]. A PCR product was defined as detectable when the band brightness was above 3-times the standard deviation of the background (blank), which is the definition of the detection limit.

2.4 Experimental setup

The PCR reactor was connected to a syringe pump (Cetoni GmbH, Korbußen, Germany), which was controlled by the supported software (Fig. 2.5). Since the realised prism is symmetric, a constant flow rate will result in equal times for denaturation (95 °C), annealing (55 °C) and extension

(72 °C). To achieve the desired retention times in each temperature zone, the flow rates were programmed accordingly (137 nL s^{-1} for 60 s per zone; 274 nL s^{-1} for 30 s per zone; 548 nL s^{-1} for 15 s per zone; 822 nL s^{-1} for 10 s per zone). To ensure a DNA free environment, all of the syringes and tubings were treated with 1M NaOH at 95 °C and rinsed with DNA-free ddH_2O before the first measurement.

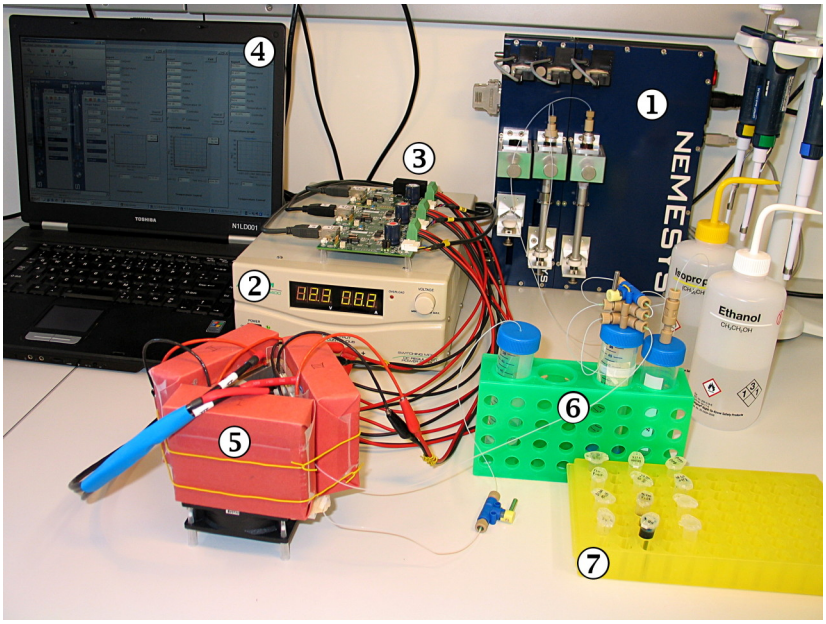

Figure 2.4: Experimental setup: syringe pumps (1); power supply (2); three temperature controllers (3); laptop (4); PCR-device (5); loading column, injection tip and waste (6), samples (7).

The used transport buffer was a low viscous silicone oil (Dow Corning, Midland, MI, USA) which is immiscible with the PCR mastermix and offers a low flow resistance. Surrounded by transport buffer the PCR samples were injected manually by direct aspiration into the PTFE tubing with the injection syringe. All samples, negative controls, washing plugs and buffer plugs were stored in separate tubes prior to processing, to avoid contamination. The maximum number of samples is restricted by the volume of the loading column between the two syringes (Fig. 2.5). For example one set requires 30 µL including the washing plug (W), negative control (N) and transport buffer separators (T), assuming a sample volume of 5 µL (Fig. 2.6). Therefore, a sample sequence consisting of 10 samples requires a loading column

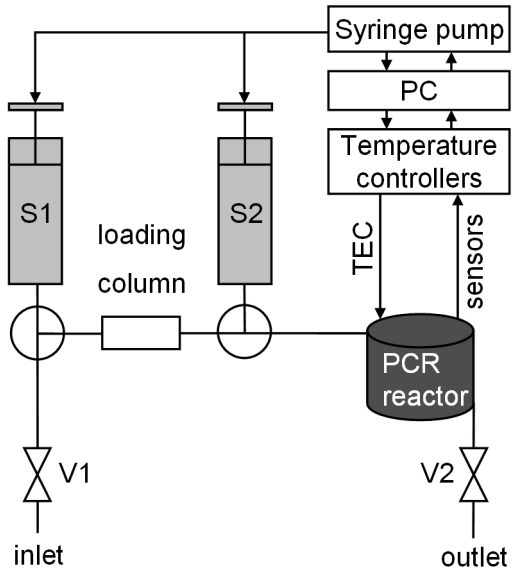

Figure 2.5: Fluidic and temperature control: The syringes, TEC elements and temperature sensors are controlled by software to establish process automation. The samples are aspirated with the injection syringe (S2) into the loading column (valve V1 open, valve V2 closed). After all samples are present in the loading column, the valves are inverted (V1 closed, V2 open) and the samples are driven into the reactor by the operation syringe (S1). The temperatures were held constant by the controllers for the whole process.

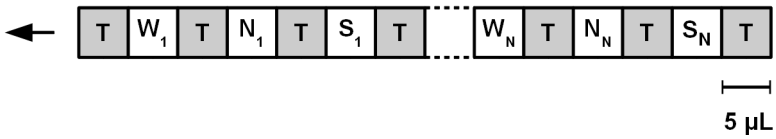

(a) Injection sequence

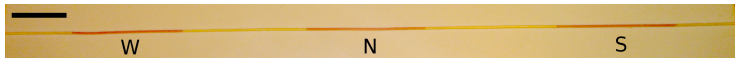

(b) Plug lengths

Figure 2.6: (a) Injection sequence: each sample (S) is preceded by a washing plug (W) and a negative control (N) for avoiding and detecting cross-contaminations respectively. The aqueous plugs (W, N and S) are inter-spaced by silicone oil as transport buffer (T). (b) Plug lengths: all plugs (W,N and S) are stained with a red dye, while the buffer plugs in between are colourless; black bar = 20mm.

of at least $300\,\mu L$. For the sample injection valve V1 was open and valve V2 was closed. In this setting the sample sequence was aspirated into the loading column with the injection syringe S2. When all samples were located in the loading column, the valves were reversed (V1 closed and V2 open) and the sequence was driven into the reactor with the operation syringe S1 (Fig. 2.5). The injection sequence starts with a washing plug (W) ($1\,\mu g\,\mu L^{-1}$ BSA) for washing, followed by the negative control (N) and the sample (S), as depicted in Fig. 2.6. Running a negative control before each sample ensures the detection of any contamination or carryover inside the tubing and connectors. The three plugs (W,N and S) are separated by $5\,\mu L$ transport buffer which equals approximately half the distance of one temperature zone. At the outlet of the reactor the samples are manually collected. For benchmarking the presented continuous flow PCR system, a positive control is run on a T3000 thermocycler (Biometra, Göttingen, Germany) using the same timing and the same volume ($5\,\mu L$). However, the transition times between the specific temperature levels of the thermocycler are longer ($1.4\,K\,s^{-1}$ for heating and $1.2\,K\,s^{-1}$ for cooling) than in the microfluidic reactor.

PCR sensitivity is dependent on polymerase activity, mastermix composition, fragment length, processing time and the amount of initial template DNA. The last three parameters were tested with a high yield DNA-polymerase using an optimised mastermix.

2.5 Results

2.5.1 Device quality

For an efficient PCR, accurate and precise temperature control is crucial. Temperature variations above $1\,K$ can lead to significant decrease of PCR efficiency. The presented device geometry with the used heaters, isolation, controllers and sensors achieved a temperature stability of $\pm 10\,mK$ over time and $\pm 0.5\,K$ spatially over one heating plate. The high temporal stability was possible with the continuously operating PID controller and the 40mm polystyrene isolation of the temperature zones (see Section 2.2 for details). The temperature accuracy of the overall system (controller and sensors) was $\pm 0.5\,K$. With these thermal specifications the heater is appropriate for running effective and reproducible PCRs.

Another important requirement for a successful microfluidic PCR is the

selection of a biocompatible material to avoid surface effects like adsorption or enzyme inhibition [34]. These effects were assessed by direct comparison of the PCR efficiency between the microfluidic PCR reactor and a conventional thermocycler. In particular, the surface effects of $9.6\,\mathrm{m}$ PTFE tubing with a total inner surface area of $1.2\,\mathrm{dm}^2$ in continuous flow was compared to a statically cycled standard PCR vial.

Although the tubing has low biomolecule adsorption, the included BSA in the mastermix was essential for dynamic blocking of polymerase adhesion. Other mastermixes without BSA showed much lower yields or did not function at all. The addition of BSA to those mastermixes led to improvements, but the efficiencies were still lower than the ready-mixed Molzym 16S Basic (Molzym, Bremen, Germany). Alternative enhancers for microfluidic PCRs like Tween 20, polyvinylpyrrolidone (PVP), gelatine, betaine and glycerol [39–43] showed no significant increase in efficiency. However, an additional washing plug before each sample increased the efficiency and avoided cross-contamination (see Fig. 2.6 for droplet sequence details). Without these washing plugs, carry-over between samples was unacceptable.

Polymerase, DNA or dNTPs were not adsorbed to the polymer surface, which would have resulted in a reduction of PCR yield in all measurements. The detection limit for the microfluidic device was not increased, which can be seen in Fig. 2.8. This proved the used polymers (PTFE and PEEK) as being biologically inert with respect to PCR reagents and resistant to the used washing solutions.

The used components of the microfluidic device such as thermal and fluidic control, tubing properties and reagents were appropriate for successful microfluidic PCRs. In addition, the geometry and dimensions can easily be adapted for improvements and miniaturisation, which makes it a very attractive setup for future experiments.

2.5.2 Fragment length

With standard PCR reagents it was not possible to amplify targets above $720\,\mathrm{bp}$ in the microfluidic reactor. The usage of a BSA-containing mastermix in addition with a droplet-based cyclic flow PCR made it possible to overcome this limit. To account for the constant polymerase activity, longer amplicons were cycled with longer extension times achieved with lower flow rates (compare Section 2.5.4).

Comparing the PCR products of the conventional thermocycler and the

microfluidic device, it was shown, that for the 1324 bp and the 720 bp fragment the microfluidic system performed better with an efficiency of up to 179 %. The 418 bp fragment was less effective in the cyclic flow device and showed a yield of 72 % (Fig. 2.7). Because this reduced efficiency was only observed with the short fragment, the primer itself accounts for the low yield. Further optimisation of the short primer pair could bring efficiencies like for the longer targets. In addition, no contaminations were observed in the microfluidic device, as evidenced by the negative negative controls (see Fig. 2.6 for droplet sequence details). These results proved the device capable of amplifying DNA targets up to 1324 bp in a sequential droplet setting without contaminations, which qualifies the system for high-throughput sequential sampling.

2.5.3 Limit of detection

The influence of primer pairs, bacterial species and initial cell amount on the sensitivity of the system was tested. The primer pair for the 720 bp amplicon lead to the lowest limit of detection (Table 2.2). All results of this primer pair for different cell amounts of *P. aeruginosa* are summarised in Fig. 2.8. The yield of the microfluidic device in comparison to the the conventional thermocycler was 91 % for a DNA concentration equivalent to 1×10^4 cells per reaction and 37 % for a DNA concentration equivalent to 1×10^3 cells per reaction. The highest achieved sensitivity is a DNA amount equivalent to 1×10^2 cells per reaction, where the microfluidic device showed an efficiency of 203 %. All negative controls showed no contaminations (FN and TN in Fig. 2.8). Furthermore, it was demonstrated, that *S. aureus* and *P. aeruginosa* could be detected with DNA concentrations equivalent to 1×10^2 cells per reaction, while *E. coli* was detected with DNA concentrations equivalent to 1×10^3 cells per reaction (Table 2.2).

Table 2.2: Limit of detection for different bacterial species and different fragment lengths. The values represent the cell equivalent of extracted DNA, detectable in one reaction.

Species	1.3 kbp	720 bp	418 bp
S. aureus	10^3	10^2	10^3
E. coli	10^3	10^3	10^3
P. aeruginosa	10^3	10^2	10^3

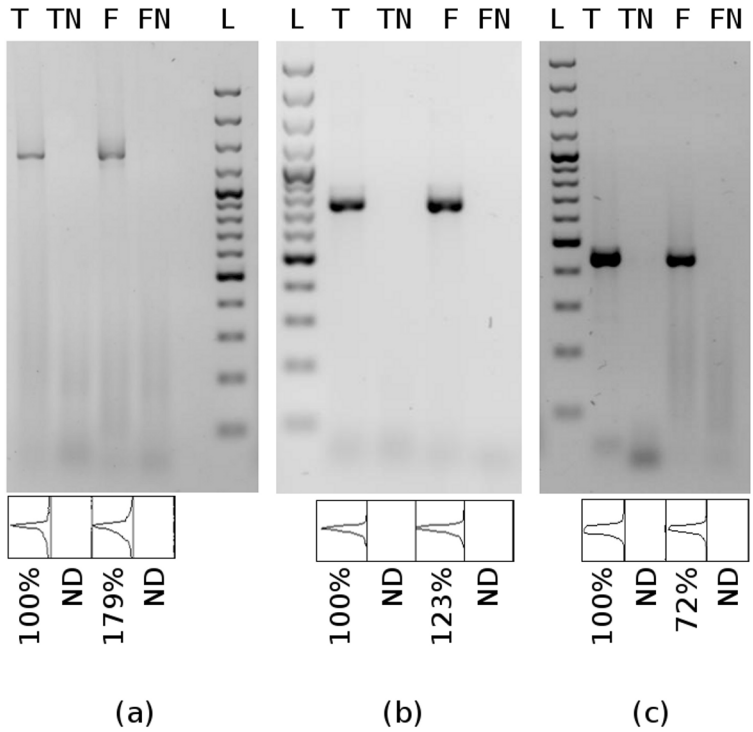

Figure 2.7: Fragment length comparison: (a) 1324 bp fragment, 45 s per temperature zone; (b) 720 bp fragment, 30 s per temperature zone; (c) 418 bp fragment, 15 s per temperature zone; *S. aureus*; DNA concentrations equivalent to 1×10^5 cells per reaction; **T**: positive control run in thermocycler; **TN**: negative control run in thermocycler; **F**: sample run in microfluidic reactor; **FN**: negative control run in microfluidic reactor; **L**: DNA ladder 100 bp; The plots beneath the gel image show the intensity of each lane across the vertical axis of the image; The values underneath the plots represent the band intensity in comparison to **T**; **ND**: not detectable.

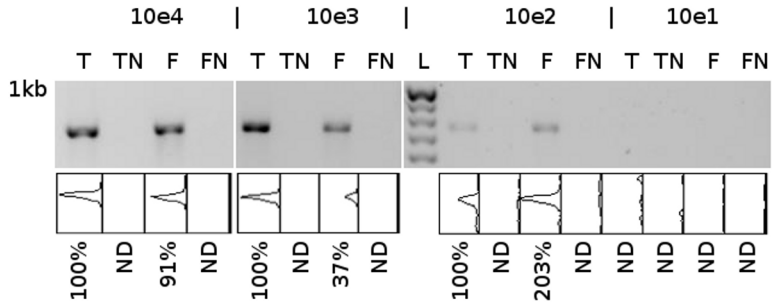

Figure 2.8: Limit of detection: Initial DNA concentrations are equivalent to 1×10^4 to 1×10^1 cells per reaction; 720 bp fragment; *P. aeruginosa*; **T**: positive control run in thermocycler; **TN**: negative control run in thermocycler; **F**: sample run in microfluidic reactor; **FN**: negative control run in microfluidic reactor; **L**: DNA ladder 100 bp; The plots beneath the gel image show the intensity of each lane across the vertical axis of the image; The values underneath the plots represent the band intensity in comparison to **T**; **ND**: not detectable.

2.5.4 Processing time

The transition time between the different temperature levels is much faster than in a conventional cycler. This leads to a significant shortening of the overall processing time. However, there is a trade-off between rapidness and PCR yield, because of limited polymerase speed and thermal lag effects [44, 45]. Three different flow rates were applied and the PCR yield was analysed by gel electrophoresis and image analysis (see Section 2.3.2 for details).

At a flow rate of $548\,\mathrm{nL\,s^{-1}}$ (15 s per temperature zone) the PCR efficiency for the 418 bp fragment was 54 % in comparison to the conventional thermocycler (15 s per temperature step without ramping) as depicted in Fig. 2.9. This reduction was only observed with the 418 bp fragment, which correlates with the results in Fig. 2.7. When the flow rate was increased to $822\,\mathrm{nL\,s^{-1}}$ (10 s per temperature zone) a further decrease in PCR yield to 15 % was observed and at a flow rate of $1644\,\mathrm{nL\,s^{-1}}$ (5 s per temperature zone) no amplification was detectable at all (Fig. 2.9). Although the negative control of the 15 s measurement (FN) was above the detecion limit and showed an intensity value of 0.8 %, it can be neglected because of the relatively high intensities of the samples (T, F).

The most rapid reaction was possible within 30 min, amplifying the

Table 2.3: Flow rates with according timings for different fragment lengths

Length	**FR** [a]	$\mathbf{t_z}$ [b]	$\mathbf{t_{tot}}$ [c]	**TP** [d]
bp	$nL\,s^{-1}$	s	min	$rxn\,h^{-1}$
1324	183	45	90(150)	26.7
720	274	30	60(120)	40
418	548	15	30(90)	80

[a] Flow Rate
[b] Time for one temperature zone
[c] Total processing time, values in parentheses are from conventional thermocycler
[d] Throughput in reactions per hour

shortest fragment of 418 bp. A process speedup of up to 3-fold compared to a conventional thermocycler was therefore possible (Table 2.3).

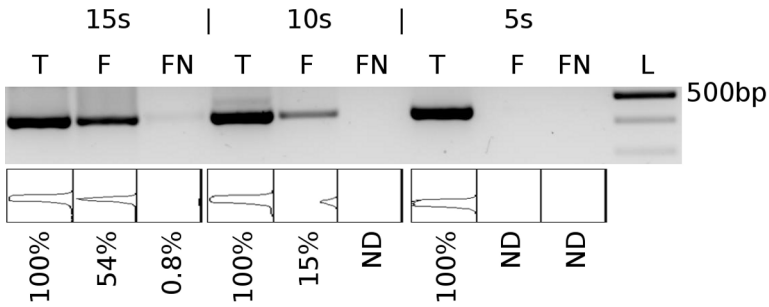

Figure 2.9: Comparison of different flow rates: **T**: Positive control run in thermocycler (times are exclusive ramping); **F**: Sample run in microfluidic reactor; **FN**: Negative control run in microfluidic reactor; **L**: DNA ladder 100 bp; **15s**: 15 s per temperature zone ($548\,nL\,s^{-1}$); **10s**: 10 s per temperature zone ($822\,nL\,s^{-1}$); **5s**: 5 s per temperature zone ($1644\,nL\,s^{-1}$); DNA template concentration: equivalent to 1×10^5 cells per reaction; PCR fragment length: 418 bp; Species: *S. aureus*; The plots beneath the gel image show the intensity of each lane across the vertical axis of the image; The values underneath the plots represent the band intensity in comparison to **T**; **ND**: not detectable.

2.5.5 Sample throughput

Each individual analysis set has a volume of 30 µL, consisting of washing plug, negative control, sample and their buffer separators (5 µL each, see Fig. 2.6 for details). The largest fragment can be processed within 90 min. With a total reactor volume of 1.2 mL this gives a throughput of 26.7 samples per hour. The fastest reaction with a processing time of 30 min gave a throughput of 80 samples per hour (compare Table 2.3).

2.6 Discussion

As evidenced by the presented results, the microfluidic device is capable of amplifying long targets at high-throughput and high sensitivities. Those properties qualify the system for accurate clinical species identification when combined with DNA microarrays. How this performance discriminates this work from other publications as well as its constraints and possible advances and extensions are discussed in this section.

2.6.1 Fragment length

Long genomic targets above 1 kbp amplified by PCR are essential, when they are employed as genomic markers for bacterial species identification. In particular, the number of misclassifications can be significantly reduced, when probing a longer genomic fragment [27]. Most of the recent microfluidic PCR articles are limited in amplicon lengths [21, 22, 46] and rarely present amplification above 400 bp. Addressing this constraint, our microsystem was proven to amplify fragments up to 1324 bp at high sensitivities (compare Section 2.5.3). These results qualify the system for the genotyping of bacteria with DNA microarrays and other applications requiring fragments above 1 kbp.

2.6.2 Limit of detection

Comparing the sensitivities in aspects of source species, *E. coli* showed a 10-fold higher LOD than *P. aeruginosa* and *S. aureus*. The reduced sensitivity may result from isolation specific variations, species specific variation or insufficiently optimised primers. However, the species specific sensiti-

vity variation cannot be correlated to the microfluidic system as evidenced by identical detection limits for the device and the thermocycler (Table 2.2).

Although DNA concentrations equivalent to 1×10^3 cells per reaction showed a reduced product yield of $37\,\%$ in Fig. 2.8, the limit of detection of the microfluidic system was not increased. It was equal to the conventional thermocycler with a DNA concentration equivalent to 1×10^2 cells per reaction. In contrast to this reduction, several PCR products amplified in the microfluidic device showed increased efficiencies of up to $203\,\%$ (Fig. 2.8). This may suggest a beneficial biochemical environment in the tubing, which boosts PCR efficiency. However, because of the large variation ($-64\,\%$ to $103\,\%$) this effect still has to be proven.

Thermally extracted DNA from bacterial samples was shown to be appropriate for successful microfluidic PCR and DNA concentrations equivalent to 100 cells per sample could be detected. In contrast to the amplification of phage DNA [15, 20] or abundant DNA templates [26], this approach is applicable to the detection of minute amounts of pathogenic bacteria. Furthermore, a reduced sensitivity compared to conventional thermocyclers [24, 25] was not observed using our microfluidic device.

Moreover, the presented system was specifically tested for the detection of bacterial pathogens. In particular, *Escherichia coli*, *Staphylococcuc aureus* and *Pseudomonas aeruginosa* were directly tested in the presented device. Those three species are under the top 5 of the most prevalent causative pathogens for infectious diseases. Together they account for more than 50% of species, responsible for blood stream infections, nosocomial pneumonia, skin and soft tissue infections and urinary tract infections [47]. The pathogen load of infections varies from 10 to 100 cells per mL in sepsis [48] to 10^4 to 10^6 cells per mL in wound fluid [49]. After bacterial isolation and DNA extraction, the concentration can be further increased by factors ranging from 10 to 1000. Elution volumes smaller than the initial volume, centrifugation and filtration steps yield to this up-concentration. With the presented device, this DNA amount after isolation can be detected. Therefore, the CF-PCR system is appropriate for high-sensitivity clinical applications like the diagnosis of blood stream infections, pneumonia, wound infections or urinary tract infections. In comparison to standard lab-equipment, it has the advantage of continuous sample processing, which brings high throughput and short analysis times.

2.6.3 Processing time and sample throughput

As shown in Section 2.5.4 there is a trade-off between detection limit and processing speed. Since the focus of this microfluidic device lies on pathogen detection, a reduction in sensitivity should be kept at a minimum. The efficiency of the shortest fragment (418 bp) is reduced to 54 % (Fig. 2.9) and 72 % (Fig. 2.7). On the other hand longer fragments showed increased efficiencies up to 203 % (compare Section 2.6.2). Therefore, the reduced signal cannot be linked to the device itself, but rather to a variance in primer efficiency in the microfluidic tubings, which correlates with the results in Table 2.2.

The tested flow rates represent a rapid setting, with a process acceleration of up to 3-fold (Table 2.3). This rapidity is crucial, when applying this system to diagnostics. In clinical testing, pathogens have to be detected fast to guarantee early antibiotic intervention. A therefore faster treatment correlates with a high probability of convalescence.

The dependency of the processing time on the fragment length could be shown (Table 2.3). Fragments below the tested 418 bp can be processed even faster. However, it is important to consider thermal lag effects because of high flow velocities, which have an exponential onset [44, 45]. This system was designed for species identification by downstream DNA microarray analysis, which requires fragments above 400 bp. Therefore, smaller sequences were not tested.

2.6.4 Trade-off between target length and throughput

While [50] (M in Fig. 2.10) reported successful amplification of a 1460 bp fragment. No evidence was shown, that the negative control is really negative in the microfluidic device. Moreover, the throughput of [50] with 0.7 samples per hour is far from our performance at 26.7 samples per hour and their sensitivity of 3.9×10^8 cells mL^{-1} is relatively low. High throughput was reported by [15] (L in Fig. 2.10) and [14] (N in Fig. 2.10) presenting 250 and 180 reactions per hour respectively. Although these values are in the range of our device, their fragment length is restricted to 600 bp [15] and 148 bp [14]. The presented microfluidic device overcomes this trade-off between throughput and fragment length with additional high sensitivities (A, B and C in Fig. 2.10). This was achieved by adding BSA into the mastermix, which is described as PCR-efficiency enhancer and stabilising agent (compare Section 2.3.2). Tubing material was another important factor for

PCR efficiency. PTFE showed high inertness and biocompatibility, preventing enzyme- or DNA-adhesion to the surfaces. High throughput was achieved by aqueous sample plugs in silicone oil transport buffer. The used plug sequence (wash, negative control, sample; compare Section 3.4) was crucial to avoid contamination and validate each sample by a negative control. With this design and mode of operation the CF-PCR device is capable of amplifying long targets at high sensitivity and high throughput.

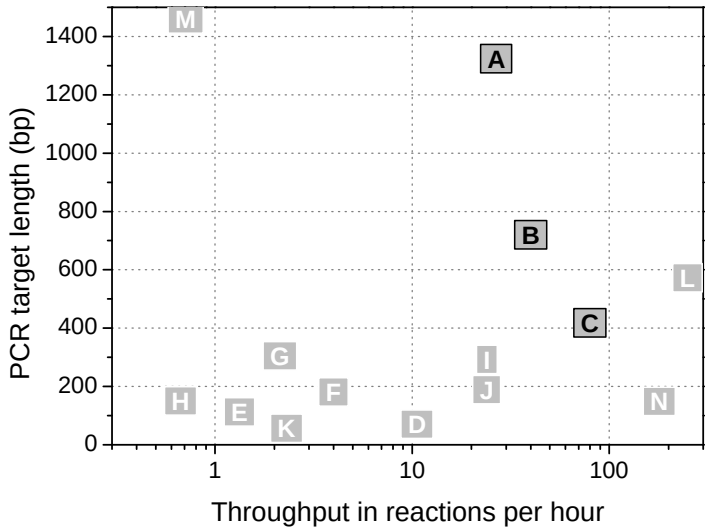

Figure 2.10: PCR target length and sample throughput of recent publications: Most of the recent publications report the amplification of targets below 400 bp and throughputs below 30 reactions per hour. This work overcomes these constraints. **A**: This work 1324 bp, **B**: This work 720 bp, **C**: This work 418 bp, **D**: [21], **E**: [22], **F**: [20], **G**: [51], **H**: [52], **I**: [33], **J**: [53], **K**: [54], **L**: [15], **M**: [50], **N**: [14]

2.6.5 Future advances and extensions

The limit of detection of the device was low with only 100 cells per reaction. However, some cases of infections have even lower bacterial loads, which would require lower detection limits. Further enhancement of sensitivity towards single cell detectability can be achieved by more sensitive dyes (e.g.

SYBR Green or SYBR Gold). They achieve a 10-fold signal increase compared to ethidium bromide (EtBr), which will bring a detection limit of 10 cells per reaction. Furthermore, the utilised thermal extraction of DNA, out of bacterial cells without purification (see Section 2.3.1), can be another constraint of higher sensitivities. Using more complex extraction methods, like solid phase extraction, including the digestion of proteins, may further decrease the limit of detection.

Although the presented PCR device is rapid, further acceleration can be performed by optimising the ratio of denaturation, annealing and extension. One possible experimental design would be a heater with 12 individual heating segments. This enables the testing of denaturation:annealing:extension ratios of 3:3:6, 2:2:8 and 1:1:10. The transition to a 2-step PCR reaction estimates a further decrease of the processing time by one third. In addition to process optimisation, the parallelisation of multiple tubing placed consecutively on one heater has the potential of further gain of throughput. Device dimensions can be reduced with smaller heaters and smaller Peltier elements. Temperature zones will be shortened as well, which requires lower flow rates. This can be beneficial for PCR efficiency, since reduced flow rates led to increased PCR yield (Fig. 2.9). The length of the coil can be reduced by thinner tubing or by placing multiple tubings above each other. However, two or more tubing layers require special heating (e.g from both sides), to guarantee correct and homogeneous temperatures in all locations. Another possibility for downscaling is the already mentioned 2-step PCR approach. Reducing the temperature zones from three to two, decreases the circumference of the device and therefore its dimensions. Miniaturisation will bring a relative increase of transition time between temperature zones. This has to be taken into account by improved heating and thermal design. Smaller devices have the potential of integration into mobile devices and point-of-care applications, both interesting for decentralised patient testing and bed-side diagnostics.

2.7 Conclusion

The presented cyclic flow PCR device is constructed in a robust manner using standard peltier elements and tubing, which can be adapted easily. Furthermore, the detailed description allows the assembly and application in any laboratory and the thermal and fluidic properties are perfectly suitable to guarantee an accurate and reproducible PCR. We have shown that

our system is able to rapidly amplify the species specific bacterial DNA region (16S rRNA) in a microfluidic sequential droplet setting. Three different species (*Escherichia coli*, *Staphylococcus aureus* and *Pseudomonas aeruginosa*) were tested in the device. They are under the top five causative pathogens for infecious diseases and are responsible for more than 50% of infections (sepsis, pneumonia and urinary tract infections). High sensitivities down to DNA concentrations equivalent to 1×10^2 cells per reaction were achieved without the need of DNA purification, which is appropriate for clinical applications. The reaction efficiency showed gains up to $203\,\%$ compared to conventional thermocyclers and cross-contaminations could be avoided, which qualifies the system for high-throughput sequential sampling. The 418 bp fragment in our study was proven to be processed in 30 min, resulting in a 3-fold acceleration in comparison to a conventional thermocycler. Most importantly we have overcome the trade-off between target length and sample throughput with our used design. In particular, we were able to amplify regions with 1.3 kbp in consecutive droplets at a throughput of 26.7 samples per hour (80 samples per hour for 418 bp). This length and sample rate is crucial for an accurate bacterial genotyping by DNA microarrays at high-throughput. Genomic screening can benefit from the achieved sample throughput, process acceleration and reduction of sample volume. Large sample sets can be processed in less time with less reagents and sample material. In addition to the reduces running costs, the presented continuous-flow system has a cost-effective design, which makes parallelisation of multiple reactors feasible. It is therefore an attractive alternative to plate-based PCR systems. Integration and coupling to other continuous-flow systems is straight forward and can bring additional functionalities, like up-stream DNA extraction or down-stream microarray analysis. Long targets, high sensitivity and rapid processing qualify the device for application in DNA microarray testing. It brings acceleration of the workflow, which enables early diagnostics and species specific antibiotic intervention. In the end, patient convalescence will be improved by such biomedical microdevices.

Chapter 3

Polycarbonate chip for rapid amplification and fluorescence labelling of nucleotides

The tubing-based continuous flow PCR system presented in Chapter 2 showed high sensitivities, high throughputs and the capability to amplify large DNA targets. Despite these achievements, the tubing-based design is limited, when it comes to system integration and mass manufacturing. When switching from tubing to a planar chip with integrated microfluidic channels, a higher system integration is possible. For example the combination of DNA extraction, PCR and microarray readout can be realised in a single chip. In addition, the planar design is suitable for mass production techniques, which makes it possible to fabricate a disposable device. This chapter describes an injection moulded microfluidic chip for nucleic acid amplification and fluorescence labelling in a single reaction. It is capable of synthesising a hybridisation ready mix out of microbial DNA to be used for DNA microarray analysis. The chapter is based on the following papers:

J. R. Peham, L.-M. Recnik, W. Grienauer, M. J. Vellekoop, C. Nöhammer and H. Wiesinger-Mayr, "Hybridisation mix synthesis in a spiral lab-on-chip device for fast-track microarray genotyping of human pathogens", *Proceedings of the SPIE - The International Society for Optical Engineering*, 2011, p. 806803 (8 pp.), Bioelectronics, Biomedical, and Bioinspired Systems V; and Nanotechnology V, 18-20 April 2011, Prague, Czech Republic. doi:10.1117/12.886620

J. R. Peham, L.-M. Recnik, W. Grienauer, M. J. Vellekoop, C. Nöhammer and H. Wiesinger-Mayr, "Disposable microfluidic chip for rapid pathogen identification with DNA microarrays", *Microsystem Technologies*, in press. doi:10.1007/s00542-011-1401-0

3.1 Diagnostic workflow with DNA microarrays

DNA microarrays have the great potential to screen for millions of DNA probes in a single sample. They are used for gene expression profiling, detection of single nucleotide polymorphisms (SNPs) or genotyping of organisms. The last method is used in the current approach to identify different human pathogens in case of sepsis. Although they can provide species specific information, the overall process consists of PCR, fluorescent labelling, microarray hybridisation, scanning and post processing. Besides time demanding single reactions, hands-on time between the steps further delays the overall process and limits automation. Therefore, the acceleration of each single reaction is important, but the integration of two or more processes into one device is equally important in aspects of time saving and automation. The workflow of microarray analysis consists of DNA amplification, fluorescent labelling, hybridisation, image scanning and statistical classification as depicted in Fig. 3.1 [27]. Since PCR and labelling are the most time demanding processes, our approach was to combine them into one single reaction and translate the process onto a microfluidic chip.

The direct labelling chip has to fulfil the task of synthesising a hybridisation ready mix out of minute amounts of microbial DNA in such a way, that it can be substituted in the existing workflow instead of the standard PCR and labelling reactions. In addition, the chip has to be suitable for mass production, an important requirement for in vitro diagnostics (IVD) [55].

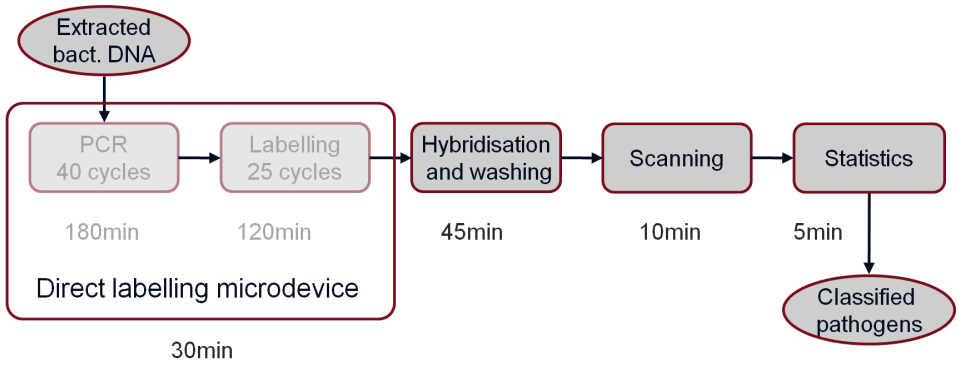

Figure 3.1: Workflow of DNA microarray analysis: Extracted microbial DNA is first amplified by PCR and labelled with fluorophores in a second step; Afterwards the abundant DNA copies are hybridised to the microarray, sensing up to 65 different pathogens; Image analysis and statistical classification determines the correct source species; The presented direct labelling chip is able to significantly shorten the analysis time by integrating DNA amplification and fluorescent labelling into an accelerated cyclic-flow reaction.

3.2 Enzymatic reaction and biological samples

The integration of DNA amplification and fluorophore incorporation in an one-step reaction is achieved with Cy3 labelled forward primers, which are directly used for PCR. The cyanine fluorophore is attached to the 5' end of the primer via an additional poly-T spacer, to minimise polymerase interference. With these primers it is possible to synthesise a hybridisation ready product, where the forward strand is fluorescently labelled (Fig. 3.2). The used primers target a 418 bp and a 720 bp region of the 16S rRNA gene, which is highly specific for bacterial genomes. Using this amplified target, it is possible to identify bacteria by applying subsequent microarray analysis (see Section 3.5.5). The details of the bacterial samples, PCR mastermix, including polymerase and dNTPs, were presented in Chapter 2. The reference method (primer extension) labels the PCR product in a separate step by incorporating Cy3 labelled dCTPs with a polymerase lacking exonuclease activity (Vent (exo-), New England Biolabs, Ipswich, MA, USA). This property makes it possible to incorporate the nucleotide-fluorophore conjugate, which represents an irregularity in the DNA strand. For this reaction only forward primers (not Cy3 labelled) are used, which leads to a linear amplification of the forward strand only. The primer extension method has

an amplification factor AF_{PE} depending linearly on the number of cycles N and the reaction efficiency η ($0 < \eta < 1$), as defined in Equation 3.1. In total, 25 cycles are run, leading to an amplification factor of maximal 25, depending on the reaction efficiency. A comparison of primer extension and direct labelling is depicted in Fig. 3.2. Because Cy3 conjugated dCTPs are incorporated every 30-40 nucleotides, the product itself contains more fluorophores than with the direct labelling approach. For the 720 bp long target, the product of the reference method holds 20-times more fluorophores than the direct labelling approach, while the shorter fragment of 418 bp has 14-times more incorporated fluorophores. This fact is important, when comparing signal intensities of the chip product and the reference (see Section 3.5.5).

$$AF_{PE} = \eta N \tag{3.1}$$

3.3 Device design and fabrication

3.3.1 Chip design

Continuous-flow PCR can be realised in various designs. In Chapter 2 a 3D-circular approach was presented, using fluoropolymer tubing and a prism-shaped heating device. This system is facile and cost-effective in design and has its strength in the high-throughput processing of consecutive samples for long PCR targets. Applications lie in the field of genomic screening in the form of a reusable device. Several other methods exist, including meander-, planar circular- and linear systems, depicted in Chapter 2, Fig. 2.1. All these approaches have constant temperature zones in common, over which the sample is pumped in microfluidic channels or tubings. Planar devices have all channels placed in one plane without changing their directions into three dimensional space. This enables reduced complexity in production, when compared to 3D systems. Furthermore, the integration of several processing steps into one device is easier.

Multiple fabrication methods exist, including etching of silicon, micro-milling, casting or injection moulding (see Section 3.3.2). Their potentials and limitations have to be considered, when designing microdevices, since they determine dimensions, accuracy and aspect ratios, but also production time and costs. A planar design was chosen, because of the potential to in-

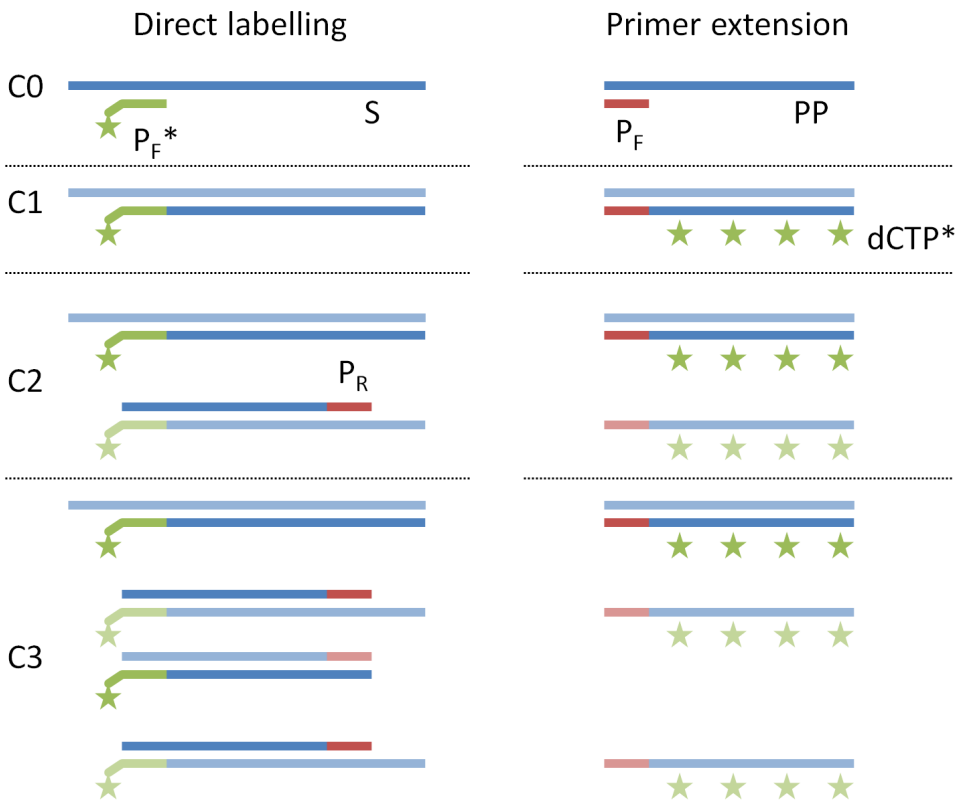

Figure 3.2: Direct labelling and primer extension: Direct labelling is performed with Cy3-conjugated forward primers ($P_F{}^*$) and a non-labelled reverse primer (P_R) directly from the sample DNA (S); Exponential amplification synthesises maximal 2^N DNA strands, where N is the number of cycles; Primer extension utilises non-conjugated forward primers (P_F) without any reverse primers, labelling already amplified PCR products (PP); Cy3-conjugated dCTPs are incorporated into every synthesised forward strand at a rate of one fluorophore every 30 to 40 nucleotides; Linear amplification synthesises maximal N DNA strands, where N is the number of cycles; C0: initial state; C1-C3: state after cycle 1-3.

tegrate further processing steps, like DNA extraction or microarray analysis within a single fabrication step. Furthermore, pre-denaturation meander and final-extension channel (Fig. 3.3(b)) can be easily integrated. In contrast, tubing systems, for example, do not allow the integration of microarrays, since a flat area is needed. Therefore, planar devices simplify system integration, which brings reduced fabrication time and costs.

As discussed in Chapter 2, Section 2.2, chamber-based systems are another alternative for microfluidic PCR [56, 57]. Although they are simple in design, requiring only one cavity for one sample, those devices require thermal cycling. Temperatures have to alternate between the different steps, which is time consuming for high thermal masses. Furthermore, connecting chamber-based devices to other operational steps is difficult. Continuous-flow systems can ease this integration, because of direct compatibility with up- and downstream processes. Planar PCR devices for continuous-flow processing have several design possibilities, including parallel meanders, circular spirals and linear systems. Parallel meanders are directed over three rectangular heating plates, traversing denaturation, annealing, extension and annealing again for one single cycle. Therefore, this method includes one additional annealing step, increasing total processing time. Moreover, this temperature sequence does not represent an optimised PCR protocol. Linear systems have the most facile microfluidic design, requiring only one single channel. Because of this complexity-reduction in microfluidics, three heating zones (denaturation, annealing and extension) are needed for each cycle. With typical cycle numbers in the range between 20 to 40, the total number of heating zones can increase up to 120. Microfluidic designs with circular spirals have the advantage of correct processing steps for each PCR-cycle and a simpler heater design than linear systems. Because of the mentioned advantages, a planar circular design was used for the continuous-flow PCR chip.

The chip reactor was designed to provide a spiral channel (Chapter 2, Fig. 2.1b), where the samples can run through the different temperature zones, provided by an underlying metal heater (see Section 3.4 for details). The spiral consists of 40 turns, representing 40 cycles of a PCR protocol. In addition, a pre-denaturation zone for initial denaturation of target DNA and a post-extension zone, to finish incomplete products, are present at the inlet and outlet respectively (Fig. 3.3). The channels themselves are $290\,\mu$m wide and the rims in between have a width of $150\,\mu$m. The Archimedean spiral is designed in such a way, that the volume per turn is constantly $5\,\mu$L. This

is important to guarantee the same timing for each temperature zone with increasing radius. In general, this can be realised by reducing the channel width or depth with increasing radius. Changing the width at constant depth will result in a significant narrowing of the outer channels. For example a starting width of $290\,\mu m$ has to decrease to $83\,\mu m$ for a constant turn volume of $5\,\mu L$. This results in an aspect ratio of 1:7 (width:depth), which adversely affects heating in the outer channels. Starting with a broader channel would result in larger chip diameters. As mentioned earlier, fabrication methods determine certain parameters. The used injection moulding machine restricts the maximal chip dimensions to $65\,mm$. Therefore, broader inner channels were not an option. Furthermore, the smallest possible width of the rims was $100\,\mu m$. Dimensions below this value cannot be fabricated by laser ablation. Moreover, the deforming with dimensions in this range is critical, risking the breakage of rims.

To meet the given constraints, the channel depth was decreased with increasing angle of the spiral, according to equation 3.3 to 3.5. The radius of the spiral (R), the arc length (S) and the cross section of the channel (A) are dependent on the angle (φ). The distance between the channels ($w = 0.44\,mm$) and the volume of each turn ($V_{1turn} = 5\,mm^3$) are constant. Since the cross section of the channels has trapezoidal shape, the depth of the channel (t) can be calculated in dependence of the angle (φ) to guarantee a constant volume for each turn. The depth is calculated with the channel width at the top ($c = 0.29\ mm$) and the channel width at the bottom ($a = 0.2\,mm$). Since the bottom of the channel is not angular, the constant radius of the curvature ($r_c = 0.1\ mm$) has to be included (see equation 3.5).

$$R(\varphi) = \frac{w}{2\pi}\varphi \tag{3.2}$$

$$S(\varphi) = \frac{w}{4\pi}\left(ln\left(\sqrt{(\varphi^2+1)}+\varphi\right)+\varphi\sqrt{\varphi^2+1}\right) \tag{3.3}$$

$$A(\varphi) = \frac{V_{1turn}}{\frac{w}{2}\left(\frac{2\varphi}{2\sqrt{\varphi^2+1}\left(\sqrt{(\varphi^2+1)}+\varphi\right)}+\sqrt{(\varphi^2+1)}+\frac{\varphi^2}{\sqrt{\varphi^2+1}}\right)} \tag{3.4}$$

$$t(\varphi) = \frac{2A(\varphi)-(r_c)^2\pi}{a+c}+r_c \tag{3.5}$$

The channel depth decreases from $597\,\mu m$ at the pre-denaturation zone and the beginning of the first turn to $175\,\mu m$ at the end of the last turn and

the post-extension zone, guaranteeing a constant volume of 5 µL per turn (Fig. 3.3 and 3.4).

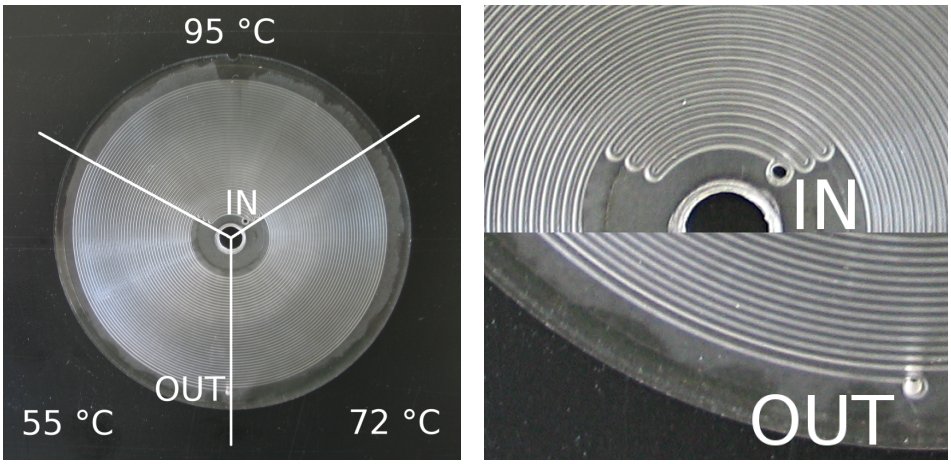

(a) (b)

Figure 3.3: Chip design: a) top view of chip with different heating zones for denaturation (95 °C), annealing (55 °C) and extension (72 °C) and inlet (IN) and outlet (OUT) ports; b) details of inlet with pre-denaturation zone and outlet with post-extension meander.

3.3.2 Chip material and fabrication

The selection of the chip material is crucial, since it determines temperature stability, fabrication and sealing methods, biomolecule interactions and optical properties. Plastics are cheap, easy to fabricate and they can be transparent, which is essential for optical readout systems or examination of test-chips. Because of these advantages, plastics were chosen as the material for this approach. However, the established injection moulding process is capable to process alternative materials like metals and ceramics, which is discussed in Section 3.6.1. Plastics can be categorised into thermoplasts, elastomers and thermosets. Elastomers are rubbery materials, which can deform several times of their dimensions. After releasing the deforming force, they return into their initial state. In microfluidics, one common example of an inorganic elastomer is polydimethylsiloxane (PDMS), where structures can be formed by casting. Although it is useful for prototyping, large-scale

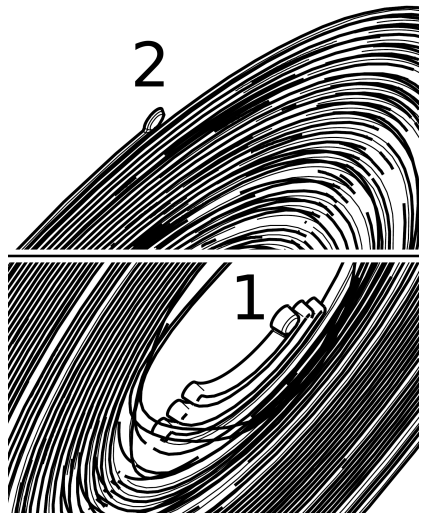

(a)

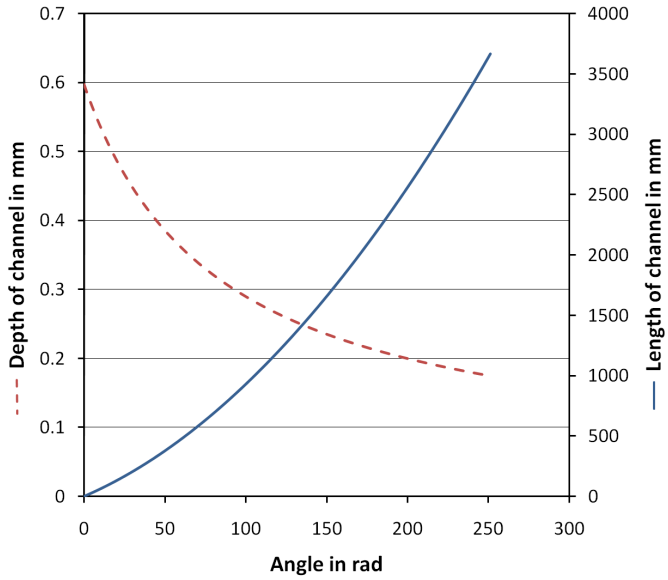

(b)

Figure 3.4: Spiral channel: a) 3D view of the spiral channel; inlet port and pre-denaturation meander (1) have 597 µm channel depth while the post-extension meander and outlet port (2) are 175 µm deep; b) Depth of channel and length of channel in dependency of the spiral angle (without pre-denaturation and post-extension sections), the depth decreases from 597 µm to 175 µm and the total channel length is 3761 mm including pre-denaturation and post-extension sections.

Table 3.1: Plastics and their thermal and adhesion properties

Name	T_g[a] °C	T_s[b] °C	DNA adhesion
PET	70 [58]	100 [59]	not tested
PVC	80 [58]	60 [59]	not tested
PS	95 [58]	75 [59]	not tested
PMMA	105 [58]	100 [59]	none measured[c]
PC	145 [58]	120 [59]	none measured[c]
PTFE	235 [58]	260 [59]	none measured[d]

[a] Glass transition temperature
[b] Maximum service temperature
[c] Fig. 3.5
[d] Chapter 2

production is more costly, because of long casting and curing times. Thermosets have the highest degree of cross-linking, which makes them rigid and they cannot be thermally deformed after they are set. Therefore, the thermal bonding of channel structures is not possible. Thermoplasts have this opportunity and are additionally easy to fabricate.

There are numerous types of thermoplasts including polyethylene terephthalate (PET), polyvinyl chloride (PVC), polystyrene (PS), polymethyl methacrylate (PMMA), polycarbonate (PC) and polytetrafluoroethylene (PTFE). They differ in mechanical, electrical, thermal and optical properties and have different resistances to chemicals. Temperature stability is a material property important for PCR. Common reactions are performed in the range between $50\,°C$ and $100\,°C$. For PET, PVC, PS and PMMA, the glass transition temperature (T_g) is below or in the range of $100\,°C$, which means they are in a rubbery state at the maximum PCR temperature. Therefore, they are prone to deformation, which adversely affects channel conformity and sealing. Maximum service temperatures of these plastics are below $100\,°C$ (Table 3.1). Moreover, they are not suitable to be operated at PCR temperatures. PTFE is a high temperature plastics, which is stable up to $260\,°C$. However, it is difficult to fabricate and bonding is complex. Polycarbonate has a maximum service temperature of $120\,°C$ and can be bonded thermally. Therefore, it was chosen as the primary feed stock for chip fabrication by injection moulding.

For all biochemical reactions, including PCR, the used containers and consumables have to be inert to biomolecules. Adhesion of DNA to channel walls, inlets and connectors has to be avoided, since it would drastically reduce reaction efficiency. Low initial DNA concentrations are prone to this effect, because the binding of template molecules to the surface hinders the polymerase to extend the strands. This can lead to no amplification at all. In the mastermix, primers and dNTPs are abundant, however surface adhesion of these nucleic acids reduces PCR efficiency, because of early reagent depletion, which reduces sensitivity. Furthermore, the transient adherence to channel walls is a cause for contaminations. DNA from the first sample sticks to the wall and releases, for example, in the second sample, which means a cross-contamination of sample two. Three different materials were tested in terms of DNA adhesion. PMMA was assessed in three types: untreated irradiated with $20\,\mathrm{kGy}$ and irradiated with $50\,\mathrm{kGy}$. The irradiation cross-links free surface groups, making the polymer more inert. Polycarbonate and an aldehyde surface were additionally tested. All different materials were incubated with an aqueous DNA solution ($20\,\mu\mathrm{L}$) for $5\,\mathrm{min}$ in a humid chamber. Concentrations of DNA were measured before and after surface contact to assess DNA adherence. All materials showed increased concentration after incubation, which indicates no attachment of nucleic acids to the tested surfaces (Fig. 3.5. The increase is caused by evaporation, which results in a reduction of volume and therefore enrichment. In addition to nucleic acids, the adherence of polymerases reduces efficiency. Surface attachment can lead to enzyme inhibition or reduced concentrations, both responsible for reduced catalytic activity.

Microdevices can be fabricated in numerous ways, including direct methods like silicon or glass etching, micromilling, electrical discharge machining (EDM), laser ablation and 3D printing and replica techniques like hot embossing, casting and injection moulding. Direct structuring methods remove material by mechanical, chemical or thermal means, fabricating the desired pattern. Alternatively, structures can be selectively deposited on a supporting surface, like 3D inkjet printing or photoresist methods. Moulding always requires a negative mould, from which the actual device can be replicated. The master has to be fabricated by direct methods, making moulding techniques an at least two-step approach. The fabrication method determines processing time, costs and the capability for mass manufacturing, which is crucial for disposable devices. In vitro diagnostic tests require these single-use approaches, requiring cost-effective and rapid me-

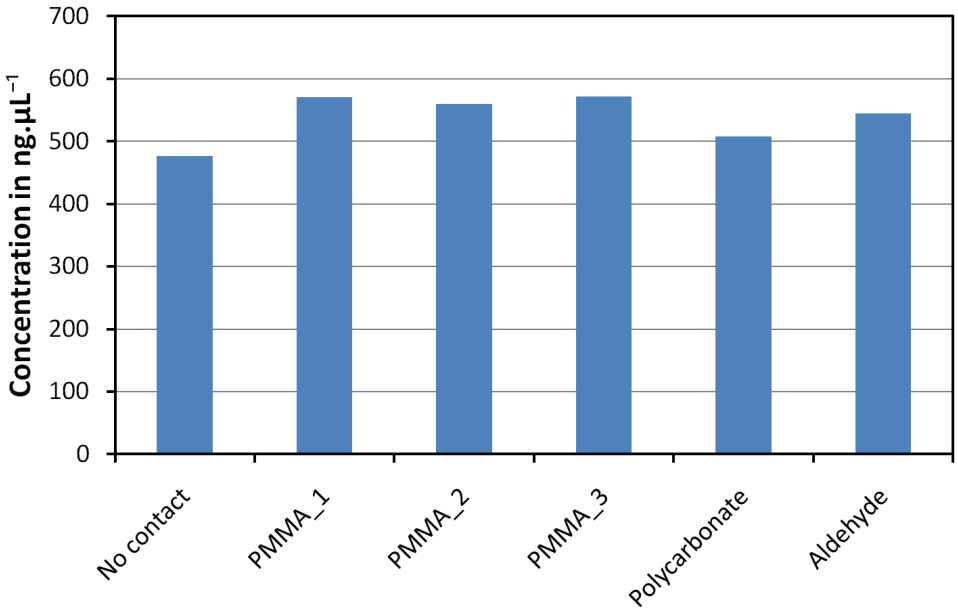

Figure 3.5: DNA adhesion of polymers: All assessed materials (PMMA, PC and aldehyde) showed no adherence of DNA, evidenced by an increase in DNA concentration after surface contact; The increase is caused by evaporation of sample volume; PMMA_1: bare PMMA; PMMA_2: PMMA irradiated with 20 kGy; PMMA_3: PMMA irradiated with 50 kGy.

thods. Replica methods are advantageous for large quantities, because a single master can be used for numerous devices. Cure times of casting methods make this process time demanding and therefore disadvantageous compared to hot embossing or injection moulding. Complex structures are difficult to realise with hot embossing techniques. Injection moulding overcomes these constraints by filling a chamber, containing the master, with liquid polymer and subsequent cooling. The device is instantly completed and can be ejected, which leads to throughputs in the range of one piece per second.

Injection moulding was used for chip fabrication, applying an optimised protocol for polycarbonate. Stainless steel was utilised as material for the master, guaranteeing durability. The negative mould was structured with a computerised numerical control (CNC) laser machine. Inlet and channel structures of the mould are depicted in Fig. 3.6. Polymer resin had to be dried prior to injection, to remove moisture, which can cause turbidity and incorrect forming. After moulding, the device was ejected manually.

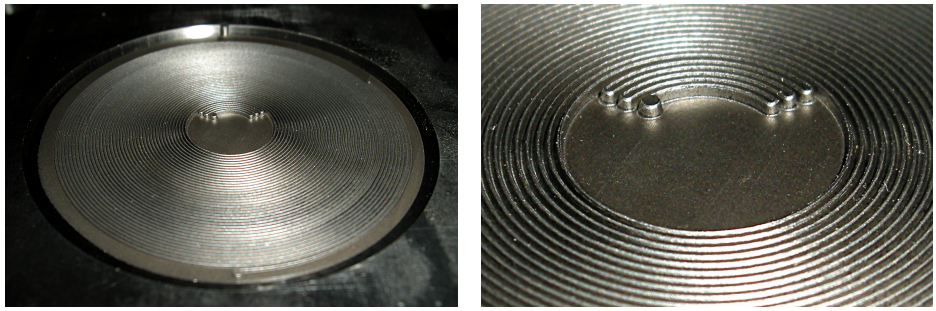

(a) (b)

Figure 3.6: Steel mould: a) overview of stainless steel mould fabricated by laser ablation; b) detail of steel mould, the negative of the inlet port and channel is depicted.

To achieve tight channels, the patterned structures have to be capped by a cover (same or a different materials are possible). This sealing process is crucial, since it determines bonding strength, tightness, bio-compatibility, uniformity and durability. For thermoplasts several methods exist, including adhesives, thermal bonding and ultrasonic bonding. Adhesives are critical in combination with biomolecules, since remaining free groups can bind DNA or proteins. Thermal and ultrasonic bonding were investigated. Because

of thermal stability and biocompatibility, polycarbonate was chosen as the sealing material. Thin sealing films guarantee low thermal losses, beneficial for PCR. The moulded channels were capped by a polycarbonate film with a thickness of 125 µm. After injection moulding the chip was drilled to access inlet and outlet port via the back side (front side is in contact with heater, see Fig. 3.10). The chip was rinsed with IPA to remove contaminations from production (injection moulding and drilling) and dried at 65 °C overnight to remove moisture. For the sealing process, chip and film were mounted in a planar press between an aluminium plate and a silicone disc for compensation of surface irregularities (Fig. 3.7). Chip, film, aluminium plate and silicone disc have a centre hole for the accurate positioning with a fixed pin, which is screwed into the baseplate of the press. A force of 9 kN was applied to the stack by a spindle. The whole press was transferred into an oven and the chip-film sandwich was bonded for 40 min at 160 °C. Cooling was performed for one hour before the press was unscrewed. Overlapping film was trimmed and Nanoports (N-126, IDEX Health & Science LLC, Oak Harbor, WA, USA) were epoxied over inlet and outlet port, which makes the chip ready for fluidic connection.

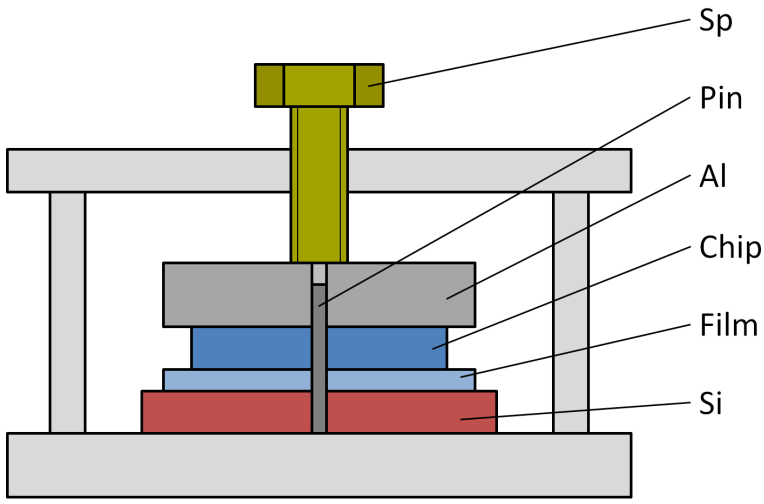

Figure 3.7: Press for thermal bonding (cross-section): A silicone disc (Si) compensates chip irregularities; film and chip are sandwiched between the silicone and an upper aluminium disc; all layers are circular and have a concentric hole and are slipped over the pin mounted in the centre for accurate positioning; pressure is applied by a central spindle (Sp).

As an alternative to thermal bonding, the polycarbonate thin film was bonded by ultrasonic welding. Therefore, channels were sealed locally to test the bonding process. Two different sonotrodes were tested (circular-shaped with 12 mm diameter and ring-shaped with 43 mm diameter and 1 mm ring thickness). Results of the two sonotrodes are discussed in Section 3.5.2. Ultrasonic welding was performed with a Rinco Standard 3000 device (Rinco AG, Romanshorn, Switzerland) in cooperation with Franz Josef Mayer GmbH, Brunn am Gebirge, Austria.

3.3.3 Heater design

For normal operation, the chip is placed on a heating plate with three sections for denaturation, annealing and extension. The side where the channels are sealed with the film is in direct contact with the heater, which minimises the thermal resistance to 125 µm polycarbonate. The heater is driven by Peltier elements, which are run by proportional integral derivative (PID) controllers, sensing the temperature in the middle of each section, as depicted in Fig. 3.8. For homogeneous temperature distribution and high stability, the chip is isolated with 30 mm polystyrene (not shown in Fig. 3.8).

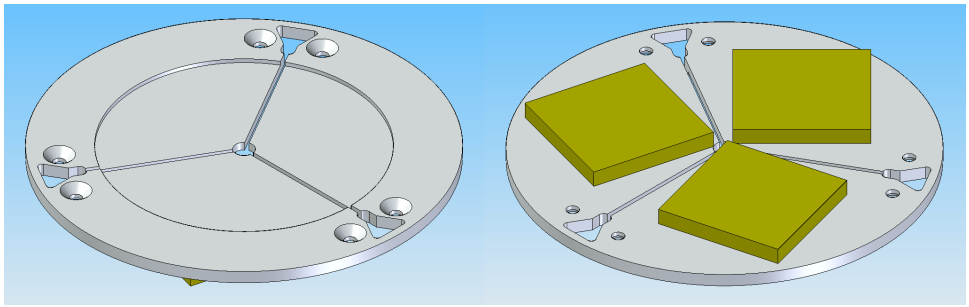

Figure 3.8: Top- and Bottom view of planar heating device: The disc-shaped aluminium plate is divided into three equal sectors by 1 mm slots; These sectors are separately heated by quadratic Peltier elements for denaturation, annealing and extension; The thermo-electric elements are operated by PID controllers.

To assure accurate and homogeneous temperatures, the heater design was benchmarked by thermal simulations. It was assumed, that there is no heat loss to ambient air and that the Peltier elements are perfectly homogeneous and ideally attached to the aluminium heater. The simulation results represent the distribution, which would be possible under ideal conditions.

An alternative design with two heating elements per temperature zone was additionally investigated (Fig. 3.9). The two elements are designed to operate in parallel mode to achieve one homogeneous temperature distribution per sector. Temperature is measured in the middle of each sector for accurate control. The positioning of the Peltier elements on the edges of each heating zone is expected to lead to a more homogeneous temperature distribution, which was assessed by thermal conductivity simulations in COMSOL Multiphysics (COMSOL AB, Stockholm, Sweden). Heat transfer from the Peltier elements to the aluminium heating disc was assessed by finite element method (FEM) solving the heat equation 3.6. Temperature T is related to the heat source Q with density ρ, heat capacity C_P and thermal conductivity k. The temperature distribution of the Peltier elements was assumed to be constant and the attachment to the aluminium lossless. Heat transfer through the $3\,\mathrm{mm}$ thick heating plate was simulated by solving the steady state equation 3.7. The spatial temperature distribution on the surface of the heater T was calculated with the thermal conductivity k and a given thermal flux vector $\mathbf{q}$ originating from the Peltier elements. This temperature simulation was crucial to assess an accurate tempering of the plastic chip.

$$\rho C_p \frac{\partial T}{\partial t} - \nabla \cdot (k \nabla T) = Q \tag{3.6}$$

$$\mathbf{q} = -k \nabla T \tag{3.7}$$

For the reactions, the polycarbonate chip is clamped on the heating device for good thermal contact. The side with the bonded film is in contact with the heater. The thermal resistance between heating plate and fluid stream consists of the $125\,\mu\mathrm{m}$ thin polycarbonate film, which guarantees accurate temperatures in the channels. On the backside of the chip two Nanoports (N-126, IDEX Health & Science LLC, Oak Harbor, WA, USA) were mounted on the inlet and outlet respectively by epoxy adhesive (Fig. 3.10). PTFE tubings are screwed into the Nanoports, to deliver and collect samples.

The temperature distribution of the fabricated heater was experimentally measured by thermography, including heat loss to ambient air and inhomogeneities of Peltier elements and attachment by thermal grease. Because aluminium is reflective in the infrared spectrum, the heater was sprayed with graphite, for visualising the thermal distribution. The measurements were performed with an infrared camera (Silver 450M, FLIR Systems Inc.,

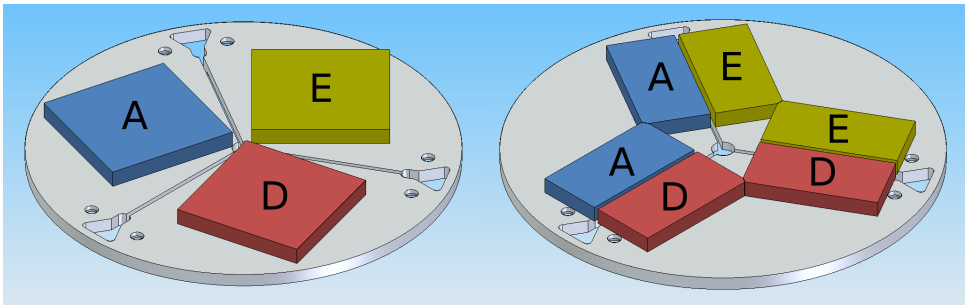

Figure 3.9: Alternative heater design: In contrast to the first design, which utilises one quadratic Peltier element per sector (left), the alternative design uses two rectangular Peltier elements per sector, which are placed on the edges of each heating zone (right); D: Peltier elements used to heat the denaturation zone, A: Peltier elements used to heat the annealing zone; E: Peltier elements used to heat the extension zone.

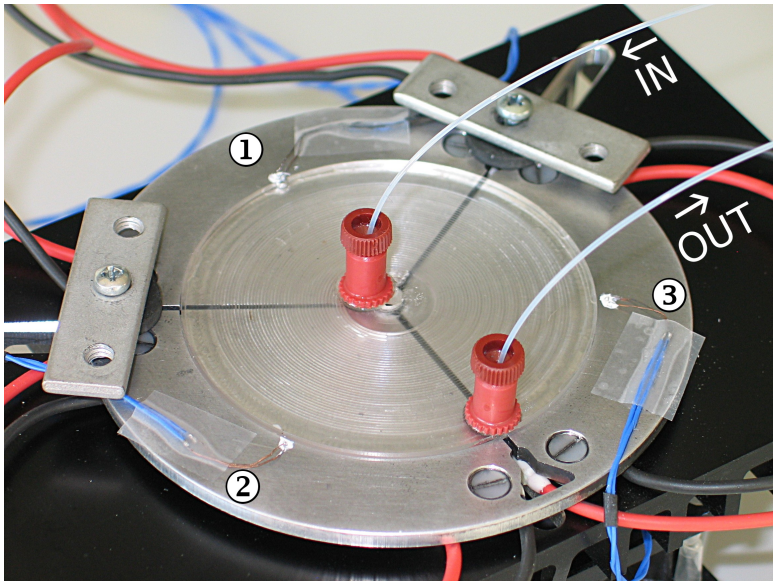

Figure 3.10: Planar heater with chip: The three heating zones are operated by Peltier elements, mounted underneath the aluminium disc for denaturation, annealing and extension; The centre of the plate is lowered by 1 mm to guarantee accurate positioning of the polycarbonate device (compare Fig. 3.8); The three temperature sensors are mounted into the aluminium plate at the outer centre of each sector (1 for denaturation, 2 for annealing and 3 for extension); Inlet (IN) and outlet (OUT) tubing are connected to the chip with Nanoports, which are mounted by epoxy adhesive.

Wilsonville, OR, USA) in cooperation with Profactor GmbH, Vienna, Austria.

3.4 Experimental setup

The fluidic design is based on two syringes for sample aspiration and process operation as presented before [60]. In principle, the sample, including microbial DNA and direct labelling reagents, is driven through the spiral by a low viscous silicon oil. The reaction output is collected manually and further analysed by microarray technology, which is the downstream application. DNA microarrays with 200 individual probes for the genotypic identification of 65 bacterial species were used to benchmark the microfluidic chip. The hybridisation ready mix from the chip and the reference method were both incubated on the microarrays for 1h at $65\,^{\circ}\mathrm{C}$. Afterwards, the slides were washed and spin-dried before they were imaged with a fluorescent scanner. The gained data was further analysed by the image analysis software ImageJ [38] to transform the intensity image into a quantitative line plot. This data was used to compare signals of direct labelling on-chip and the reference method (PCR and primer extension). For statistical classification of bacterial species an R-based software script was used [27].

3.5 Results

3.5.1 Chip quality

Injection moulding of the polycarbonate chip resulted in accurate channel structures and the $290\,\mu\mathrm{m}$ wide channels, inter-spaced with the $150\,\mu\mathrm{m}$ wide rims, could be demoulded without any damage or breaking. The channel quality and the decrease of the channel-depth with increasing angle can be seen in Fig. 3.11. The calculated values for the depth of the channels were confirmed by measurement of cross section images. Overall, the chip fabrication showed high quality and the geometrical design was implemented precisely. After the sealing of the channels by thermal bonding (see Section 3.3.2 for details), the leak-tightness of the whole chip was evaluated by applying a constant flow of transport buffer. No crosstalk between channels could be observed and the film withstood flow velocities of up to $111\,\mathrm{nL\,s^{-1}}$. This flow rate equals the shortest retention time of $15\,\mathrm{s}$ per temperature zone

for the 418 bp target, limited by polymerase activity. Therefore, higher flow rates were not applied. It was shown, that the described method of thermal bonding is suitable to seal microfluidic channels in a polycarbonate substrate. The bonding strength withstands the applied flow rates and is stable at the maximum operating temperature of 95 °C. In addition to the mechanical and thermal properties, it was crucial to utilise a biocompatible polymer. In particular, it has to be inert to nucleic acids, DNA polymerases and fluorescently labelled primers. This inertness could be shown, evidenced by successful synthesis of a hybridisation ready solution. In particular, the impact of a 3.76 m polycarbonate channel, with a total inner surface area of 42.1 cm^2, was shown to have no inhibitory effects on DNA amplification and fluorescence labelling (Surface to volume ratio: 20.2 m^{-1}). These mechanical, thermal and chemical properties qualify the fabricated polymer disc as a suitable reactor for nucleic acid reactions with DNA polymerase and fluorescently conjugated oligonucleotides. This was evidenced by the successful hybridisation mix synthesis as described in Section 3.5.5.

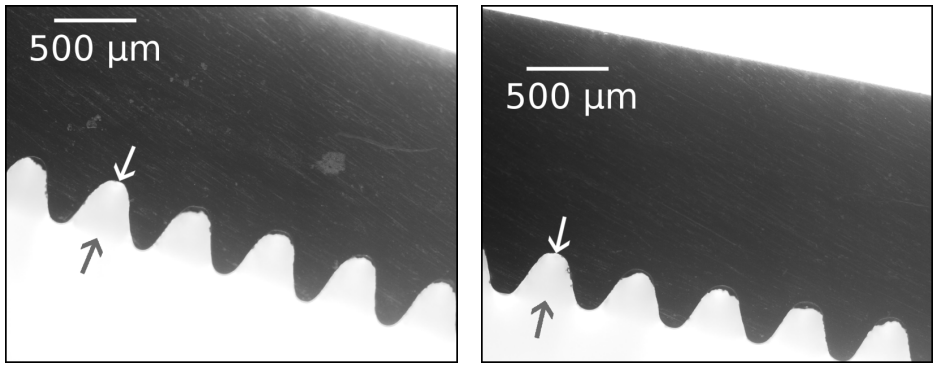

(a) (b)

Figure 3.11: a) cross section of inner channels (turn 10 to 14), calculated channel depth: 355 µm, measured channel depth: 350 µm (arrows); b) cross section of middle channels (turn 17 to 21), calculated channel depth: 281 µm, measured channel depth: 275 µm (arrows).

3.5.2 Ultrasonic bonding

The polycarbonate thin film was alternatively attached to the chip by ultrasonic welding. The sealing of the channels was tested with a circle-shaped

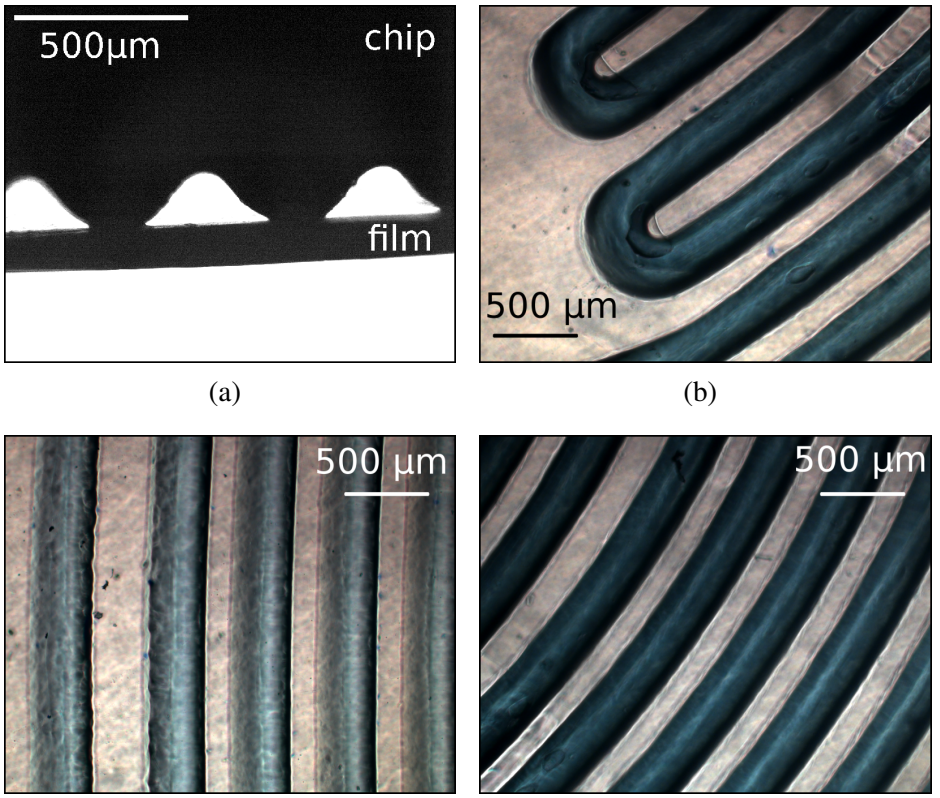

Figure 3.12: Images of thermally bonded chips: a) cross section of sealed channels; b) pre-denaturation meander; c) top view of outer channels; d) top view of inner channels; b-d) channels were filled with an aqueous solution of methylene blue.

sonotrode (D = 12 mm) and a ring-shaped sonotrode (D = 43 mm, ring-width = 1 mm). The bonded areas showed an accurate fusion of film and chip (Fig. 3.13). Although the ultrasonic bonding was successful when tested locally, a chip-wide sealing could not be achieved. When bonding the chip with a large sonotrode, covering the whole chip, only few areas were sealed. Ultrasonic welding requires energy concentrators. Usually they are peak-shaped structures to define the initial point of fusion. Furthermore, welding depth has to be limited by a buffer region. The cross section of the rims is round-shaped and decreases towards the film (Fig. 3.12). However, the geometry was not sufficient for whole-chip welding. More defined energy concentrators in the form of spiky cones on top of the rims, could be one possibility to achieve chip-wide ultrasonic bonding.

3.5.3 Thermal simulations and thermography of heater

For PCR, accurate, homogeneous and stable temperatures are important to achieve high efficiencies and reproducibility. Continuous-flow PCR has the advantage, that temperatures can be kept constant. In contrast to conventional thermocyclers, the heating unit can be designed for steady state, and dynamic temperature alterations occur only during the initial turn-on procedure. Fast heating and cooling rates are therefore not required. Since the channels of the chip are guided through the different temperature zones, the spatial temperature distribution influences the temperature protocol for the samples. Variations in PCR temperatures should not exceed 1 K, to avoid efficiency losses. As shown in Section 3.3.3 the heater has a disc-shaped form for tempering the circular chip. The three temperature zones are heated by quadratic Peltier elements (Fig. 3.8), which transfer heat into the aluminium plate. This heat transfer of the Peltier elements towards the aluminium plate and its resulting temperature distribution on the surface was simulated according to the heat transfer equation for steady state (Equation 3.7), Section 3.3.3).

The simulation results showed homogeneous inner regions, while the outer regions deviate up to 1.5 °C at the interface with the largest temperature difference (95 °C to 55 °C). The smallest deviation of 0.5 K was observed at the region between 72 °C and 55 °C (Fig. 3.14). The thermal distribution was validated by thermography experiments. Because of thermal losses to ambient air, inhomogeneities of the Peltier elements and the lossy attachment by thermal grease, the deviations are larger than in the simulation.

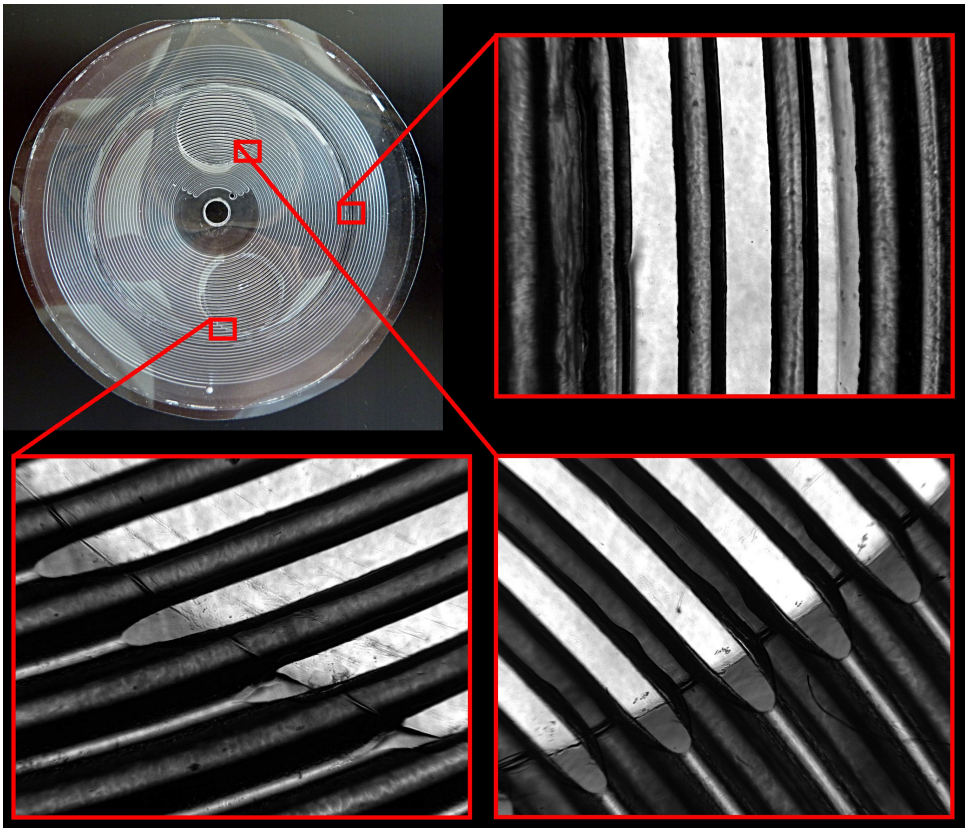

Figure 3.13: Ultrasonic bonding: Two areas were bonded with a circular sonotrode (bottom row) and one area was bonded with a ring-shaped sonotrode (top right); The phase-contrast images show an accurate attachment of the polycarbonate film to the rims of the chip for all test areas.

Deviations up to 3.5 K were observed in the outer regions. Because thermography requires direct access to the surface of interest, this difference was measured at the bare heating plate without chip and any isolation. Punctual measurements of the isolated heater revealed lower deviations in the range of 1.5 K to 2 K at normal operation (chip placed on heater and covered with 30 mm polystyrene). This proves, that convection is a major cause for heat loss and spatial temperature differences. Isolation of the chip and heater is therefore important for temperature homogeneity. The mentioned maximal deviations occur at the boundary and transition regions and are constrained locally (Fig. 3.14). Therefore, their influence on the samples is of limited time.

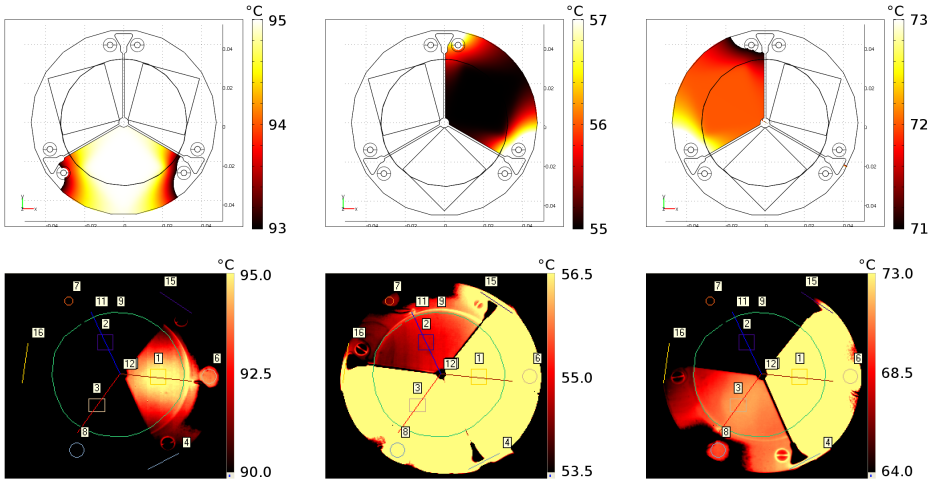

Figure 3.14: Temperature distribution of planar heater: top row: simulation (assumptions: homogeneous Peltier elements with ideal attachment, no losses to ambient air); bottom row: thermography of the heater without polystyrene isolation.

An alternative heater design with two Peltier elements per sector, as depicted in Fig. 3.9, was assessed by thermal simulations. The new design has the potential to improve temperature homogeneity, especially in the boundary regions. The comparison of the simulated temperature distributions of the two designs showed lower temperature deviations for the novel design. In particular, the highest temperature deviations in the outer boundary regions (between 95 °C and 55 °C zone) could be decreased from 1.5 °C to 0.1 °C. Furthermore, the other heating zones show high homogeneity and temperature deviations below 0.1 °C (Fig. 3.15).

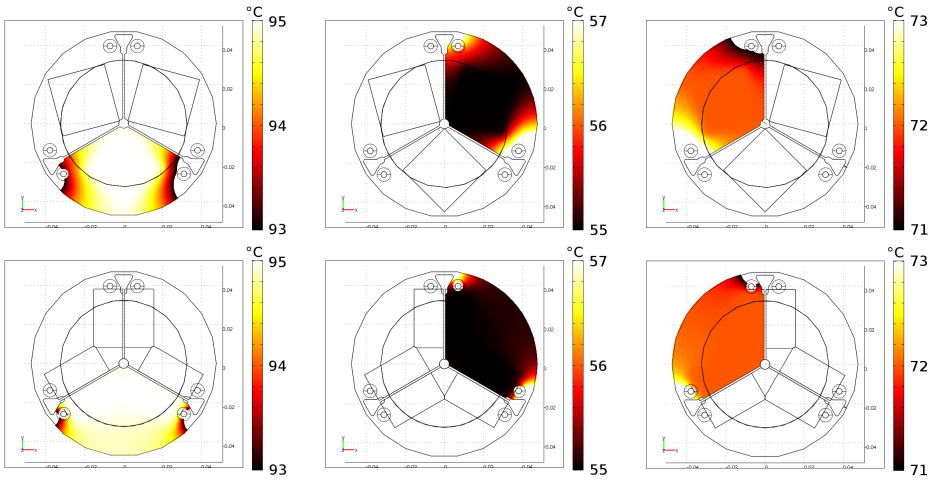

Figure 3.15: Improvements of planar heater: top row: simulation with one quadratic Peltier element (30 mm × 30 mm × 3.9 mm) per heating zone; bottom row: simulation with two rectangular Peltier elements (15 mm × 30 mm × 3.6 mm) per heating zone (assumptions: homogeneous Peltier elements with ideal attachment, no losses to ambient air).

3.5.4 Direct labelling with Cy3-conjugated primers

As described in Section 3.2, primers with attached fluorophores (Cy3) were used for DNA amplification and simultaneous labelling. To assess the efficiency of this approach off-chip, both labelling methods (primer extension and direct labelling) were compared by hybridisation on microarrays. Because the primer extension method incorporates labelled dCTPs into a new DNA strand, overall fluorophore density is approximately one every 30 to 40 nucleotides. This is much higher than the direct labelling approach, where only one fluorophore is attached to one target DNA strand. According to this lower number of fluorophores incorporated per DNA strand, a signal decrease of 15- to 30-fold is expected, when using Cy3-conjugated primers (see Section 3.2). When comparing the signals of the off-chip reactions, a decrease of 33% (efc1), 46% (efc2) and 44% (efc3) was observed (Fig. 3.16). The expected decrease of 15- to 30-fold, which would equal a decrease of 93-96%, could not be measured. The observed decline in signal intensity is therefore not proportional to the reduction of fluorophores.

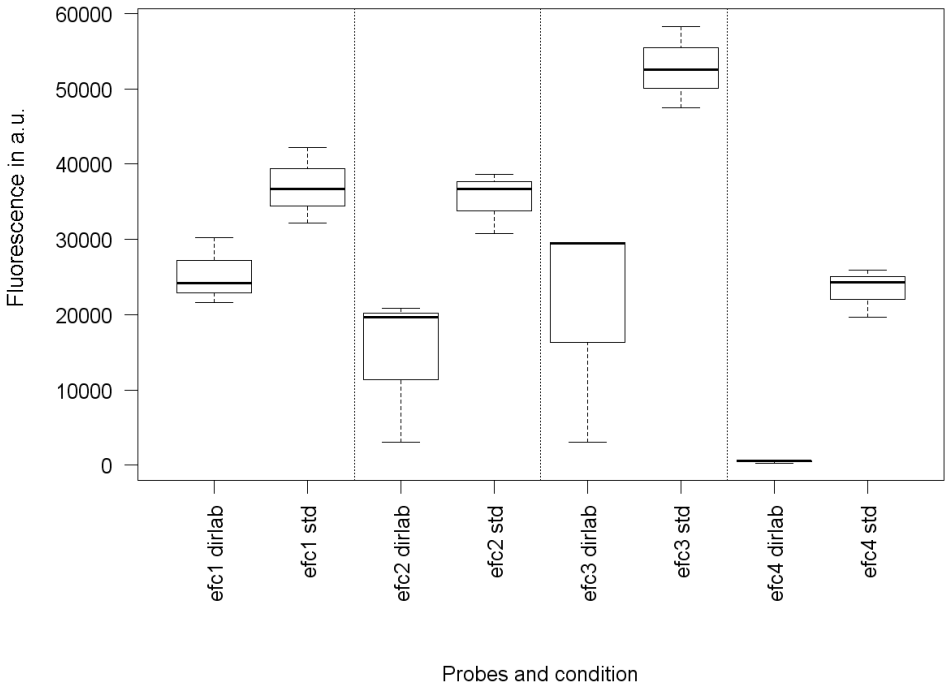

Figure 3.16: Direct labelling method in comparison to primer extension (standard method), processed off-chip; array triplicates of fluorescence intensities of direct labelling and standard method are depicted as boxplots; dirlab: direct labelling with fluorescently labelled primers; std: standard method (primer extension); efc1-4: species specific DNA probes on the microarray; Source species of hybridised DNA: *Enterococcus faecalis*.

3.5.5 DNA Microarray performance

The successful operation of the chip reactor was tested by comparing the synthesised fluorescently labelled product with conventional processed samples, where PCR and labelling were performed separately. The reaction output of the chip and the conventional product were both hybridised on DNA microarrays and the signal intensities were compared (see Section 3.4 for details). When observing the scanned microarray images as seen in Fig. 3.17(a), it can be seen qualitatively, that the biologically correct spots (sar1-3) for *S. aureus* are positive, while the negative control is negative. A quantitative analysis of the spot intensities reveals, that the signal of the chip-synthesised product gave lower absolute values, especially for probe sar3. The signal decrease for sar1 is 56%, for sar2 28% and for sar3 76% (Fig. 3.17(b)). Although chip signal intensities were lower, it did not affect the correct classification of the bacterial species.

3.5.6 Sensitivity

Three different species (*S. aureus*, *E. coli* and *P. aeruginosa*) were tested in terms of sensitivity in the lab-on-chip device. The detection limit was tested for the 720 bp target in the device and with the reference method. While *S. aureus* and *E. coli* were measured with 10^3 cells per reaction, *P. aeruginosa* could be detected with 10^2 cells per reaction. In comparison to the reference method, only *S. aureus* showed lower sensitivity in the chip (Table 3.2).

Table 3.2: Sensitivity for different bacterial species in cells per reaction

Species	Chip	Reference method
S. aureus	10^3	10^2
E. coli	10^3	10^3
P. aeruginosa	10^2	10^2

3.5.7 Processing time

Due to the cyclic-flow PCR and the direct labelling chemistry, the overall processing time could be decreased significantly. In particular, the faster transition times between temperature zones and the utilisation of direct fluorophore conjugation decreased processing time. A flow rate of $56\,\mathrm{nL\,s^{-1}}$

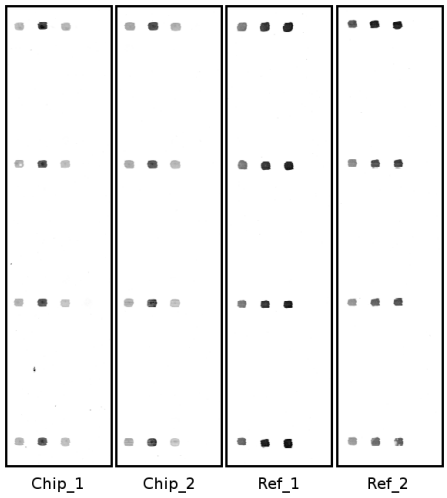

(a)

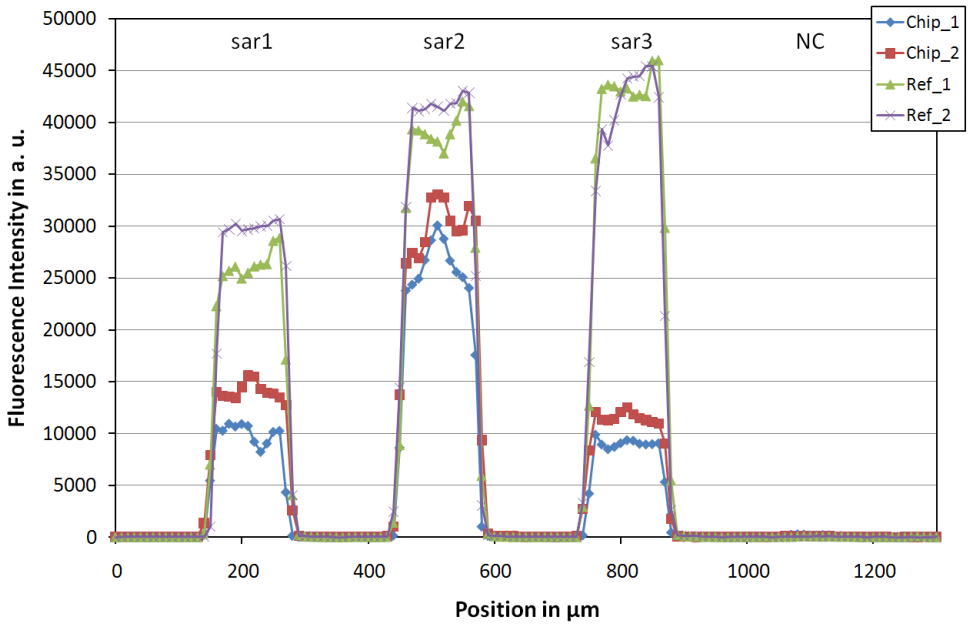

(b)

Figure 3.17: a) Microarray images of the Cy3 channel after scanning and background correction: the four samples have four spot replicates of sar1, sar2, sar3 and negative control; Spot diameter: 120 µm; Target length: 720 bp; 10^5 bacterial cells per reaction; b) signal intensities of biologically relevant probes for *S. aureus* (sar1-3) and the negative control (NC); Although the signal intensities of the chip product are lower in absolute values, the bacterial species could be classified correctly.

was used for the 720 bp target, which resulted in a processing time of 60 min and 30 s per temperature zone. The 418 bp target was processed with a flow rate of 111 nL s^{-1} (15 s per temperature zone), which led to a total reaction time of 30 min. In comparison to the standard protocol, this is a tenfold process acceleration (Table 3.3).

Table 3.3: Processing times for the two different target lengths

Target length	**Flow rate**	**Time per temperature zone**	**Total processing time**
bp	nL s^{-1}	s	min
418	111	15	30
720	56	30	60

3.6 Discussion

As seen in Section 3.5.1, the applied fabrication methods were perfectly suitable to produce a high quality polycarbonate chip for DNA amplification and fluorescence labelling. The combination of two single reactions into one microfluidic reactor represents high system integration in comparison to other publications [33, 61]. In contrast to prototype devices [20, 30], the established fabrication method is capable of large-scale production, which is crucial when used as disposable device. Furthermore, this potential to dispose the chip after the analysis is crucial, when the chip should be used as an in vitro diagnostic test. When synthesising the hybridisation ready mix, a polystyrene isolation block is attached on top of the chip, to reduce temperature losses to ambient air. This increases homogeneity and reduces the deviations seen in the thermography of the outer regions (Fig. 3.14). Because the deviations from the nominal temperature are at the boundary regions, it has not significantly affected the efficiency of the enzymatic reaction. An alternative design, as presented in Fig. 3.9, showed optimised temperature homogeneity in simulations (Fig. 3.15). This may enhance PCR efficiency and therefore microarray signal output. The thermal stability of the fabricated polycarbonate chip is suitable for reactions around 100 °C, where other polymers show already deformation effects (compare Section 3.6.1). This temperature is quite common for DNA denaturation, enzyme inhibition or cell lysis, which represent further applications. In addition to the thermal

properties, polycarbonate is transparent, which makes it suitable for optical readout, such as fluorescence measurements. Because of the planar fabrication technique, further up- and downstream methods can be integrated in an advanced design, such as DNA isolation or hybridisation on chip.

Primer extension was used as the reference method for labelling, which results in a target, conjugated with a fluorophore every 30 to 40 nucleotides. In comparison to the direct labelling method (Cy3-conjugated primers), the standard method has therefore 15- to 30-fold more fluorophores per DNA strand (see Section 3.2), which is equivalent to a decrease of 93% to 96%. As shown in Section 3.5.4 the signal decrease in an off-chip reaction was 33% to 46% (Fig. 3.16). This effect was also observed on-chip with signal reduction ranging from 28% to 76% (Fig. 3.17). Both results (off- and on-chip) are not proportional to the reduction of fluorophores. The distance of the fluorophores in the primer extension method (reference) is approximately 10 nm (30 nucleotides equal 10 nm), which is in the range of the Förster radius of fluorophores (typically 1 nm to 10 nm). Self-quenching of the dyes in the DNA strand, synthesised by the primer extension method, is therefore possible, which would explain the unproportional decrease. The direct labelling method misses the linear extension of the PCR product, which is done by a polymerase with relatively high error rate (Vent (exo-), New England Biolabs, Ipswich, MA, USA). These errors in the standard method can lead to an increased cross reaction on the microarray. In contrast, the direct labelling method is more specific due to less DNA amplification and a lower error rate, which results in less cross reactions on the microarray. The signals for the efc4 probe (Fig. 3.16) differ for the standard method (positive signal) and for the direct labelling approach (negative signal). Unspecific binding might be a reason for the positive efc4, while the more specific direct labelling reaction would result in no signal.

As discussed before, the signal decrease with the direct labelling method lies in the range between 28% to 76%, when tested with the microfluidic chip (Fig. 3.17) and 33% to 46%, when assessed off-chip (Fig. 3.16). Testing on a coarser scale (10^1 to 10^5 cells per reaction) revealed no significant difference in sensitivity between chip and reference. Only *S. aureus* was identified with a detection limit one order of magnitude higher (Table 3.2). Variations in DNA isolation might be a reason for this higher detection limit. Although there was a difference for *S. aureus*, the highest sensitivity (100 cells per reaction) qualifies the system for clinical applications. In addition, the analysis process was significantly accelerated by tenfold and

the extra labelling reaction (Fig. 3.1) was no longer required, which reduced hands-on time. Integration into a disposable microfluidic polycarbonate chip brought miniaturisation and continuous-flow processing. The presented device is therefore a rapid, more automated and compact alternative to standard mircroarray analysis.

3.6.1 Alternative chip materials

As an alternative to polycarbonate, further chip materials were tested with the injection molding process. In addition to plastics, ceramics and metals were assessed with the established method. While plastics are ready for operation directly after moulding, ceramics and metals have to be additionally sintered. For those two materials the chip was produced by powder injection molding to fabricate the green body. This green part is then sintered to its final material composition with a two stage temperature protocol. During this thermal treatment, the part densifies, which results in a shrinkage. This reduction in size can be specified by the shrinkage factor (SF = length of sintered part / length of green part). One additional plastic, polymethyl methacrylate (PMMA), was tested for chip fabrication. It is cheaper than polycarbonate and easier to process. However, for the presented application it was not suitable, due to its low thermal stability ($\mathrm{T_s}$ = 100 °C, Table 3.1). PMMA devices showed deformation of the film and channels, when operated at the heating plate. Like polycarbonate, PMMA does not shrink after molding (SF = 1). In contrast, the further assessed metal and ceramic materials do show a shrinkage up to 24% after sintering. The only metal which was tested was copper (SF = 0.83). Due to its high thermal conductivity of $400\,\mathrm{W\,m^{-1}\,K^{-1}}$), establishing well defined temperature regions requires high thermal fluxes and therefore high power. In addition, all thermal junctions have to be highly thermal conducting, to transport the increased heat flux. More generally, a copper chip would act like a heat sink, blurring temperature steps between the different heating zones. Aluminium oxide (Al_2O_3, SF = 0.85) has a thermal conductivity of $26\,\mathrm{W\,m^{-1}\,K^{-1}}$, which is lower than copper. However it is still higher than those of polymers, which lie in the range of $0.2\,\mathrm{W\,m^{-1}\,K^{-1}}$. This makes it still unsuitable for confined temperatures in the different sectors, without increasing thermal flux significantly. Zinc oxide (ZnO) is expensive and the shrinkage factor was quite high (SF = 0.76), which resulted in smaller channel structures. In conclusion, plastics showed several advantages in comparison to ceramics

or metals. The sealing process by thermal- or ultrasonic bonding is facile and they show good biocompatibility (Fig. 3.5). Furthermore, plastics are cheap and not fragile. Although the alternative materials were not suitable for the presented application, they were all successfully fabricated by injection molding and powder injection molding respectively.

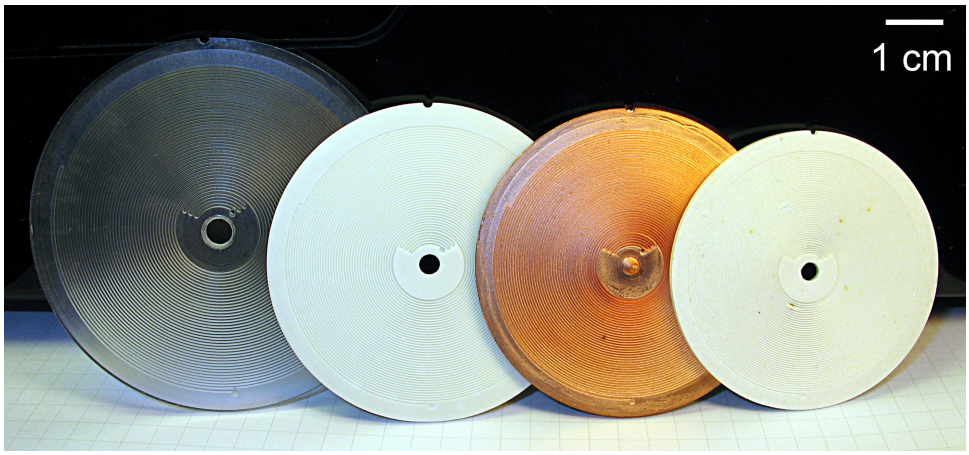

Figure 3.18: Alternative chip materials: PMMA (1), Al_2O_3 (SF = 0.85), Cu (SF = 0.83), ZnO (SF = 0.76); From left to right; SF: shrinkage factor after sintering.

3.7 Conclusion

The presented chip is suitable for the synthesis of a hybridisation ready mix out of bacterial DNA. The fabrication method showed high quality and thermal stability of the chips, required for the reaction. Besides the integration of DNA amplification and fluorophore conjugation into one device, the cyclic flow setting further accelerated the process. Overall a tenfold speed-up was possible and DNA targets of up to 720 bp could be processed. Microarray benchmarking revealed accurate species identification and detection limits down to DNA amounts equivalent to 100 cells per reaction. These specifications enable an accelerated genotyping of pathogens, which has the potential for early and targeted therapeutic intervention. In a further consequence, this increases the probability of patient convalescence and reduces antibiotic resistances.

Chapter 4

Continuous-flow DNA sensor for high-throughput detection of PCR products

Chapter 2 and 3 described continuous flow PCR systems for rapid and high throughput analysis of DNA. Those two systems were evaluated with gel electrophoresis and microarray assays respectively. Electrophoretic separation and measurement of DNA is already performed in microdevices, like the Agilent 2100 Bioanalyzer (Agilent Technologies Inc., Santa Clara, CA, USA) or the Shimadzu MCE-202 MultiNA (Shimadzu Corp., Kyoto, Japan). Those systems are suitable for DNA detection, but their operational principle is batch processing. This means they lack the capability to be integrated into continuous flow process chains, which is also the case for microarrays. One possibility for a flow through DNA sensor is the continuous measurement of the DNA-sensitive fluorescent dye SYBR Green. Such a device is presented in this chapter. Parts of this work have been published in:

J. R. Peham, M. J. Vellekoop, C. Noehammer, H. Wiesinger-Mayr, "PCR Product Detector with LED-Photodiode Fluorescence Sensing in a Nanoliter Flow-Cell for the High-Throughput Detection of Double-Stranded DNA", *Procedia Engineering*, Eurosensors XXV Conference, Athens (accepted for publication), 2011.

4.1 Integrated sensing of PCR products

Polymerase chain reaction is a highly sensitive method, however rapidness (processing time below 1 hour) and high sample throughputs are only achieved with miniaturised and automated PCR systems. Chamber based microdevices [62–64] are difficult to integrate into total analysis systems, since the interfaces between different chamber-based modules (e.g. DNA-extraction, PCR or microarrays) are often not compatible. Continuous flow PCR systems have the great opportunity to be suitable for direct connection to up- and downstream flow-through modules. In addition, continuous flow operation in PCR achieves rapidness, high sample throughput and high sensitivity [55, 60, 65]. However, those systems still rely on DNA detection by gel electrophoresis, which is labour intensive, or require large and costly laser induced fluorescence (LIF) detectors, which have high power consumption (disadvantageous for mobile devices) [29, 66, 67]. Further drawbacks of lasers are limited lifetime and narrow excitation bands, which prevents the simultaneous excitation of multiple fluorophores for multiplexing analysis. In some systems the laser as excitation source is already substituted by light emitting diodes (LED) and LED-arrays, while detection is still performed by photomultiplier tubes (PMT) [68]. A complete shift to LEDs for fluorescence excitation and photodiodes (PD) for sensing emission further reduces costs and increases integration, which has recently been presented [69, 70]. While these articles describe LED-PD systems for sensing uric acid and glucose respectively, our approach provides DNA detection by LED-PD fluorescence sensing. In comparison to [30], we provide a continuous flow sensor without any lenses. High sample throughputs and high sensitivities were achieved with a cost-effective and facile design. The presented system in this chapter is direct applicable to continuous flow PCR systems as presented in Chapter 2 and 3.

4.2 Methods

4.2.1 Measurement Principle

The central part of the PCR product detection system is the heated flow cell, where DNA samples are pumped through for fluorescent measurement. Inlet and outlet tubing as well as optical fibres are screwed into the measurement cell to realise a fully contained continuous flow DNA sensor. Samples, interspaced by silicone oil (Dow Corning Inc., Midland, MI, USA), are pumped through the flow cell by a syringe pump (Cetoni GmbH, Korbußen, Germany), which is controlled by manufacturers' software. The fluorescence signal itself is generated by the fluorophore SYBR Green (Invitrogen, Carlsbad, CA, USA), which is sensitive for double stranded DNA (dsDNA). Excitation is performed with a LED with 480 nm peak wavelength and 4500 mCd maximum brightness (PUR-LED GmbH & Co. KG, Selzen, Germany). The emission is recorded with a standard positive intrinsic negative (PIN) photodiode (Osram AG, München, Germany, $0.62\,\mathrm{A\,W^{-1}}$ spectral sensitivity at 850 nm). The two optical signals are coupled into the flow cell by polymer fibres (Edmund Optics Inc., Barrington, NJ, USA). After high-gain amplification the response of the photodiode is recorded by a data acquisition card (USB-6009, National Instruments Corp., Austin, TX, USA). For melting primer dimers, the cell is additionally heated by a Peltier element regulated by a proportional integral derivative (PID) controller (see Section 4.2.2 for details).

4.2.2 Heated flow cell

The sensing chamber for the DNA samples consists of a 5-port manifold out of black polyether ether ketone (PEEK) with 1 mm through-holes. The inner channels of the manifold are arranged like a perpendicular cross (4 ports), where the fifth channel is perpendicular to all other channels. This gives an optical accessible inner volume of 524 nL. In the horizontal ports, the fluidic inlet and outlet-tubing are screwed in, while the 1 mm optical polymer fibres are attached in the lower vertical port and the centre port respectively to achieve an angle of $90°$ between excitation and emission. The emission port is optically shielded, to avoid noise from ambient light and the upper vertical port is closed with a polytetrafluoroethylene (PTFE) plug. When a sample sequence is pumped through the cell, light is directly coupled into the aqueous DNA sample plugs. The excited fluorophore SYBR Green,

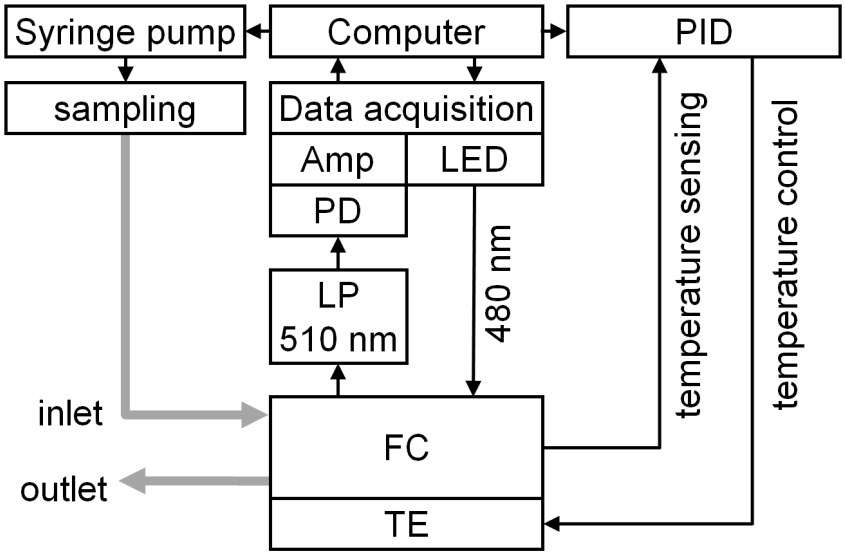

Figure 4.1: Block diagram of PCR product detector: Amp: High-gain amplifier, PD: photodiode, LP: long pass, FC: flow cell, TE: thermoelectric heater, PID: proportional integral derivative controller.

which is dsDNA-sensitive, emits in the range of $520\,\mathrm{nm}$. This emitted light is sensed via a second fibre and the photodiode continuously (Fig. 4.2). The manifold and all nuts, plugs and ferrules are from IDEX Health & Science LLC, Oak Harbor, WA, USA.

While most DNA-sensing microsystems are limited to purified DNA or fractionated DNA fragments by capillary electrophoresis [71], our system is able to measure PCR products. They include primer dimers, which can lead to a fluorescence signal even in the negative control without any PCR product. This primer dimer noise can reach high intensities, which prevents sensitive measurements. To be able to measure unpurified PCR products with sufficient sensitivity, our flow cell is heated by a Peltier element (Tecoolers, Utrecht, The Netherlands) to $60\,^{\circ}\mathrm{C}$. At this temperature small DNA fragments, like primer dimers, are melted into single strands, which avoids SYBR Green intercalation and therefore suppresses a fluorescence signal. Longer fragments, like PCR products, remain in double stranded conformation, allowing SYBR Green to intercalate and emit a fluorescent signal when excited. The Peltier element is attached to the bottom of the manifold by thermal grease and controlled by a proportional integral derivative (PID) controller (TC M PCB, Electron Dynamics Ltd., Southampton, Uni-

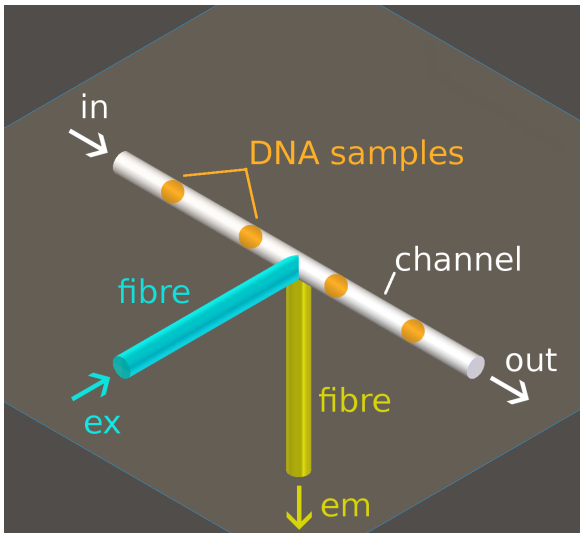

(a) Measurement principle

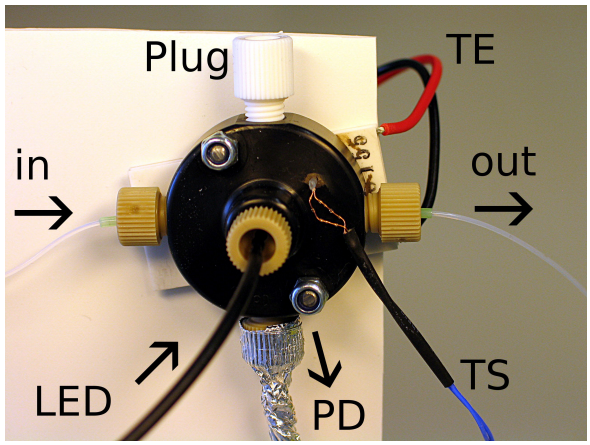

(b) Assembly of flow cell

Figure 4.2: a) Measurement principle: The inner cross-sectional cell volume of 524 nL is excited (ex) by a 480 nm LED through a polymer fibre and the fluorescence emission (em) is measured 90° to excitation by a PIN-photodiode after filtering excitation light (510 nm long pass); b) Assembly of flow cell: the 5-port manifold is heated with a thermoelectric heater (TE); inlet tubing (in), outlet tubing (out) and optical fibres from LED and photodiode (PD) are screwed into the ports; the temperature sensor (TS) is mounted into the bulk of the manifold.

ted Kingdom). The thermal sensor (B57540, EPCOS AG, München, Germany) is mounted into the bulk material of the flow cell at the depth of the through-channel to guarantee accurate temperature control.

4.2.3 Data acquisition

The illuminated dsDNA samples, including SYBR Green, emit in the range of $520\,\mathrm{nm}$. This optical signal is captured by a standard PIN photodiode after filtering ($510\,\mathrm{nm}$ long pass), which generates a proportional electric current. A high gain operational amplifier with low noise transforms the photocurrent to an output voltage between $0\,\mathrm{V}$ and $10\,\mathrm{V}$. This voltage is recorded continuously by a data acquisition card. Because of the high gain, the circuit is shielded, to limit noise from ambient electromagnetic fields. The measured signal represents the fluorescence of the liquid inside the flow cell and a sample sequence of different DNA concentrations results in several peaks of different voltages.

4.2.4 Fluidic sampling

Fluidic control is performed with a syringe pump operated by software. All DNA samples and PCR products were aspirated with a needle into a loading column interspaced with a low-viscous silicone oil as presented before [60]. Because smallest air bubbles cause light scattering in the flow cell and therefore a signal, they have to be avoided. This was realised by a pumping step before each aspiration of a sample plug or oil plug respectively. With this pump step a small drop is pumped out of the injection needle. When this drop is visible, the needle is inserted into the next liquid (sample or silicone oil) to assure direct contact between oil and aqueous sample. The following aspiration step will aspirate the liquid into the tubing without any air bubbles in between sample and silicone oil (Fig. 4.3). From the loading column the samples are pumped through the flow cell for measurement with flow rates of $200\,\mathrm{nL\,s^{-1}}$ and $400\,\mathrm{nL\,s^{-1}}$. These sampling and flow conditions equal a flow-through PCR system, like presented before [60]. Therefore, the sensing system is directly compatible for downstream connection after continuous-flow PCR devices.

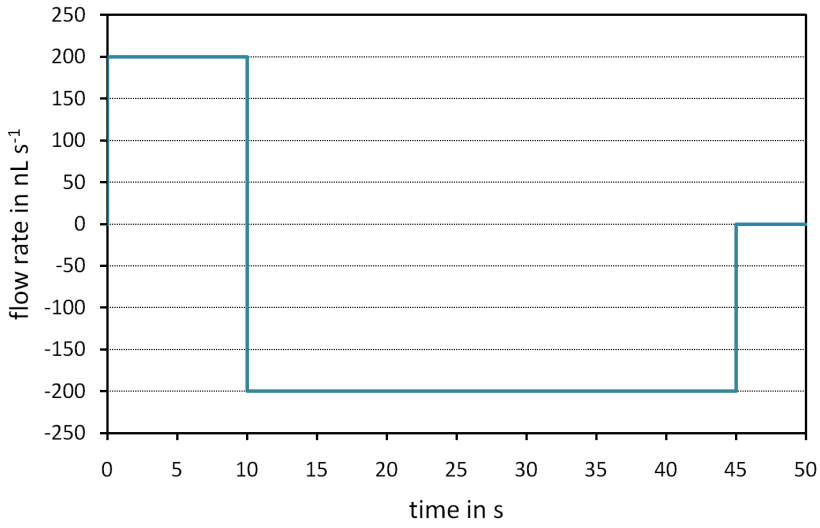

Figure 4.3: Aspiration flow profile: Preceding pumping (0 to 10 s) avoids air bubbles between samples and transport buffer when aspirating (10 to 45 s).

4.2.5 DNA samples and reference measurements

DNA samples were used as PCR products, containing target DNA, primers, polymerases, dNTPs, and PCR buffer. They were derived from *Escherichia coli* and *Acinetobacter baumanii* with a target length of 720 bp. The initial DNA template concentrations are specified in cell equivalents, ranging from 10^1 cells per reaction to 10^4 cells per reaction. This dilution series was used to determine the sensitivity, measured in bacterial cells per reaction. Cell concentrations were determined photometrically and adjusted using the McFarland standard No. 5 as reference. This adjustment of bacterial cell concentration makes the results of different bacterial strains comparable. PCR was performed in a conventional thermocycler (VWR Duo-Cycler, VWR International LLC, Radnor, PA, USA) with the Mastermix 16S Basic (Molzym GmbH & Co. KG, Bremen, Germany) using primers and conditions as presented before [60]. All template DNA was isolated thermally (95 °C, 15 min) from bacterial culture. (See [60] for details).

PCR products contain dNTPs, primers and polymerases. Those biomolecules prevent an accurate calibration (260 nm:280 nm ratio) of the samples to a specific DNA amount in ng µl^{-1}. Therefore, purified DNA samples were tested in addition to the PCR products. With these samples the sensitivity of the device in ng µl^{-1} could be determined. The purified

DNA samples were obtained from PCR products by solid phase extraction using the MSB Spin PCRapace kit (Stratec Molecular GmbH, Berlin, Germany). The source species of the purified samples was *Pseudomonas aeruginosa* with an amplicon length of 1347 bp. After purification, the DNA concentration was obtained photometrically by the 260:280 ratio measured by the Epoch spectrophotometer (BioTek Instruments Inc., Winooski, VT, USA). A 10-fold dilution series in ultrapure water from $0.01\,\mathrm{ng\,\mu L^{-1}}$ to $100\,\mathrm{ng\,\mu L^{-1}}$ was used for sensitivity measurements. The fluorescence dye SYBR Green was added in a 1x concentration following the manufacturers' instructions.

Fluorescence measurements were validated by endpoint detection with a real-time PCR system (LightCycler 480, Roche Applied Science, Basel, Switzerland). Sensitivity measurements of PCR products were validated with a micro capillary electrophoresis system (MCE-202 MultiNA, Shimadzu Corp., Kyoto, Japan).

4.3 Results and Discussion

4.3.1 Signal intensity and sample throughput

The acquired signal with the flow-through detector was compared to a commercial real-time PCR device for validation. Purified DNA samples with concentrations between $10\,\mathrm{ng\,\mu L^{-1}}$ and $100\,\mathrm{ng\,\mu L^{-1}}$ were measured in both systems. A clear discrimination of the negative control, which consists of ultrapure water and 1x SYBR Green, and DNA samples was observed. In both systems, the signal showed a saturation effect from $10\,\mathrm{ng\,\mu L^{-1}}$ onwards. Higher concentrations did not show higher signals, rather a slight decrease was detected. This could result from fluorophore saturation or self-quenching effects [72, 73] because of high concentrations. Although a decrease was observed, the signals from the flow cell showed high correlation with the commercial real-time system, which validates the flow-through detector for DNA measurements (Fig. 4.4).

In addition to the validation of the signal intensity, the throughput of the continuous flow device was tested. With a sample volume of $3\,\mu\mathrm{L}$ a maximum flow rate of $400\,\mathrm{nL\,s^{-1}}$ was possible (Fig. 4.4). This equals a throughput of 240 samples per hour. The signal of higher flow rates could not be resolved due to a slow amplifier response. A discrimination between the different samples was not possible. Faster amplifiers would enable higher flow

rates and therefore an increased sample throughput. The highest possible flow rate (240 samples per hour) of the device is sufficient for continuous flow PCR systems (80 to 200 samples per hour, [60]).

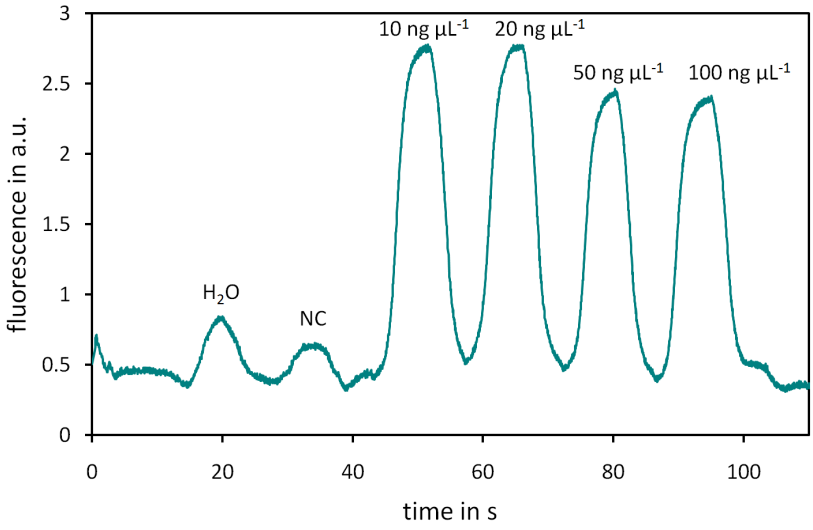

(a) Flow cell detector

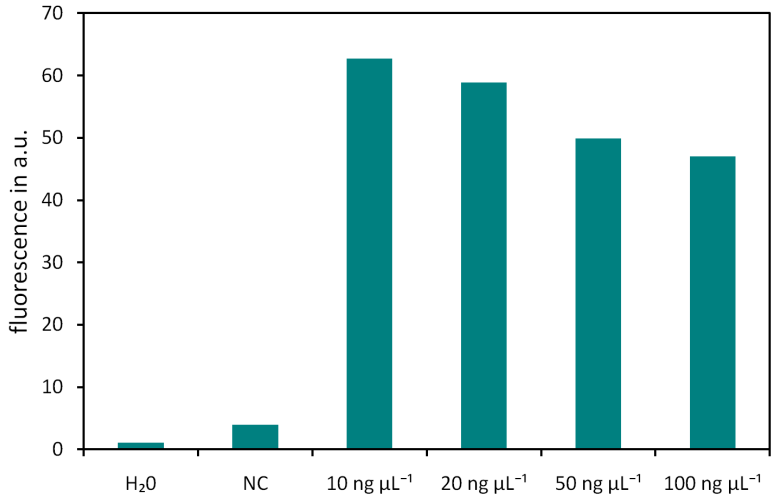

(b) Real-time PCR device

Figure 4.4: Validation of signal intensity: a) Flow cell measurement; b) Measurement with real-time PCR device (Light Cycler 480); flow rate: $400\,\mathrm{nL\,s^{-1}}$; sample volume: 3 µL; throughput: 240 samples per hour; NC: negative control: 1x SYBR Green in ultrapure water, a.u.: arbitrary units.

4.3.2 Sensitivity with purified DNA

Purified dsDNA samples were further diluted ($0.01\,\mathrm{ng\,\mu L^{-1}}$ - $100\,\mathrm{ng\,\mu L^{-1}}$) to test the sensitivity of the system. DNA concentrations of $0.01\,\mathrm{ng\,\mu L^{-1}}$ and $0.1\,\mathrm{ng\,\mu L^{-1}}$ showed the same signal intensity as the negative control. From $1\,\mathrm{ng\,\mu L^{-1}}$ onwards the signals could be clearly discriminated from the negative control (Fig. 4.5). Therefore, the lowest detectable amount of the dilution series was $1\,\mathrm{ng\,\mu L^{-1}}$ for purified DNA samples. Theoretically, a PCR with 40 cycles and an efficiency of 80% can produce $1\,\mathrm{ng\,\mu L^{-1}}$ out of one single $100\,\mathrm{bp}$ copy initial DNA. This means, when the detector is combined with a preceeding continuous-flow PCR, single molecules can be detected.

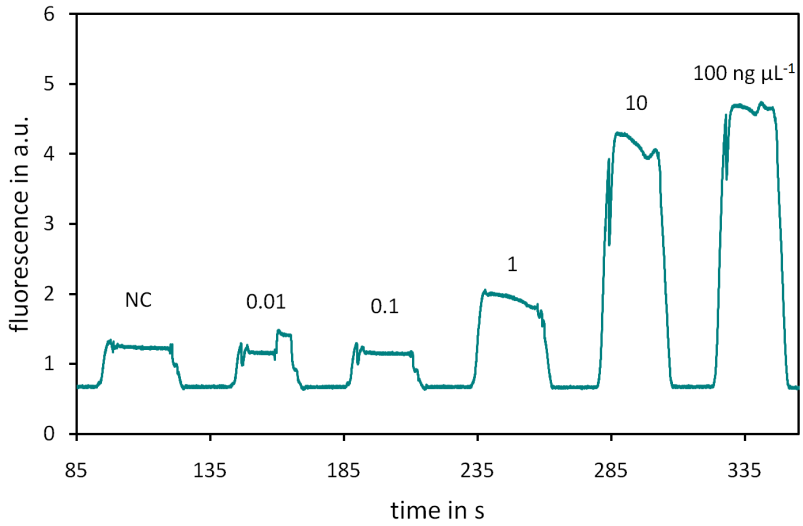

Figure 4.5: Sensitivity with purified DNA samples: five different concentrations and one negative control were measured in a consecutive sample sequence; the lowest concentration still detectable was $1\,\mathrm{ng\,\mu L^{-1}}$; flow rate: $200\,\mathrm{nL\,s^{-1}}$; sample volume: $5\,\mu\mathrm{L}$; throughput: 72 samples per hour; NC: negative control: 1x SYBR Green in ultrapure water; a.u.: arbitrary units.

4.3.3 Sensitivity of PCR products

While purified dsDNA samples could be detected at high sensitivity (Section 4.3.2), the measurements of PCR products showed high background

noise when measured at ambient temperature. This noise prevented a sensitive measurement and a discrimination between negative control (cycled PCR mastermix without target DNA) and low concentrations of DNA (Fig. 4.6). The mentioned effect of air bubbles (Section 4.2.4) can be seen in Fig. 4.6(a). Although it was interrupting an oil plug, it did not influence the sample sequence nor the signal of the different plugs. With the optimised aspiration procedure (Fig. 4.3) air bubbles could be reduced significantly. When observing the electropherogram of the negative control it can be seen, that primer dimers lead to a signal at around 50 bp when fluorescently measured (Fig. 4.6(b) and Fig. 4.8(b)). This signal represents the background noise observed in the flow-through sensor. A detailed measurement of the different components of a PCR mastermix confirmed, that the signal originates from the primers. Comparing PCR mastermix, PCR mastermix including primers and PCR mastermix including primers and polymerase showed a clear signal increase when primers are added (Fig. 4.7). Intercalating fluorophores like SYBR Green attach to this primer agglomeration and generate a fluorescence signal. Even before cycling, which means that the primer dimers were not exponentially amplified, a signal was observed (Fig. 4.7).

Fluorescence signals from primer dimers can be avoided by using alternative reporter molecules like TaqMan probes or molecular beacons. A more cost-effective approach is to measure the PCR product when the primers are dissociated. This can be achieved by heating the entire flow cell with a Peltier element. At $60\,^{\circ}\mathrm{C}$ all primer dimers are melted, which hinders SYBR Green to intercalate. Therefore, primers no longer contribute to the fluorescence signal. All PCR reagents (mastermix, mastermix + primers, mastermix + primers + polymerase) led to a low signal in the range of the negative control (Fig. 4.7(b)). The MM+P+T sample in Fig. 4.7(b) showed two peaks, which means it was interspaced by a small oil droplet. The signal intensities were not influenced by this effect and the samples could be clearly discriminated. One reason for this fractionation might be inhomogeneous flow paths through valves and connectors. In comparison to the measurement at $25\,^{\circ}\mathrm{C}$ (Fig. 4.7), the signals of the primer containing samples were low. Therefore, the overall background signal of PCR products is reduced as well. A sensitive measurement of PCR products is now possible.

With this primer melting function, PCR products could be measured without oversaturation due to primer dimers. The observed fluorescence signal revealed a clear discrimination between negative control and samples.

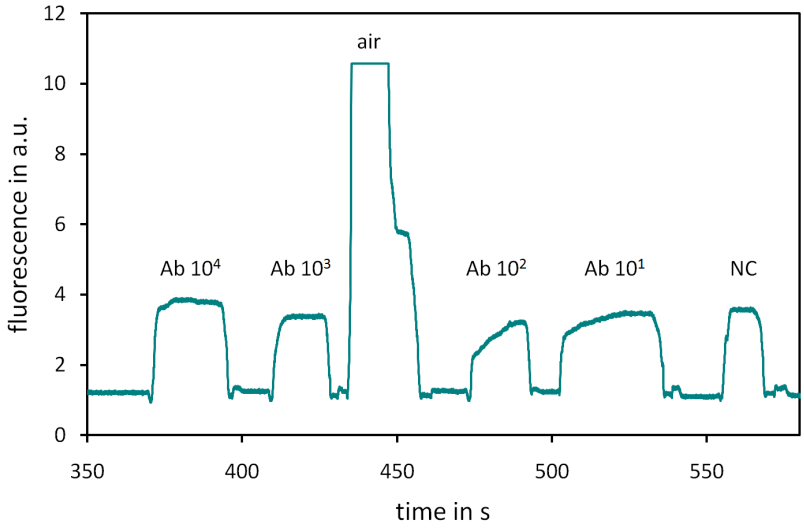

(a) Signal of flow cell at 25 °C

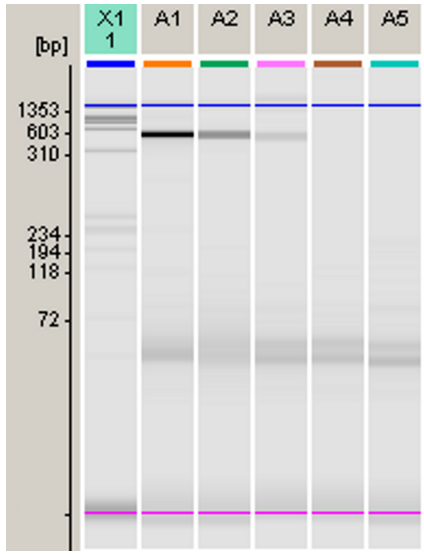

(b) Reference measurement

Figure 4.6: a) Measurement of PCR products in flow cell at 25 °C; PCR products are amplified from bacterial DNA from *Acinetobacter baumanii* (Ab) in different concentrations (cells per reaction); NC: negative control (cycled PCR mastermix without target DNA); flow rate: 200 nL s^{-1}; sample volume: 5 µL; throughput: 72 samples per hour; a.u.: arbitrary units; b) reference measurement from capillary electrophoresis system at 25 °C; primer dimers can be seen at approximately 50 bp; X1: Ladder; A1: 10^4 cells/rxn; A2: 10^3 cells/rxn; A3: 10^2 cells/rxn; A4: 10^1 cells/rxn; A5: negative control.

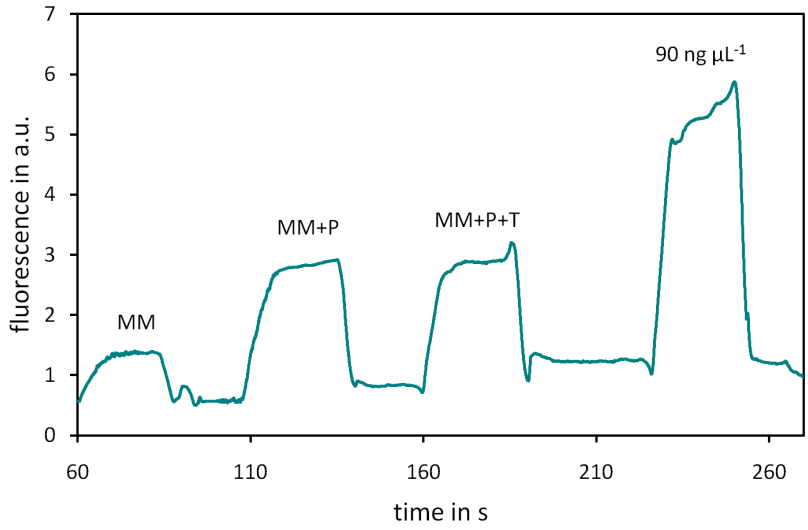

(a) PCR reagents at 25 °C

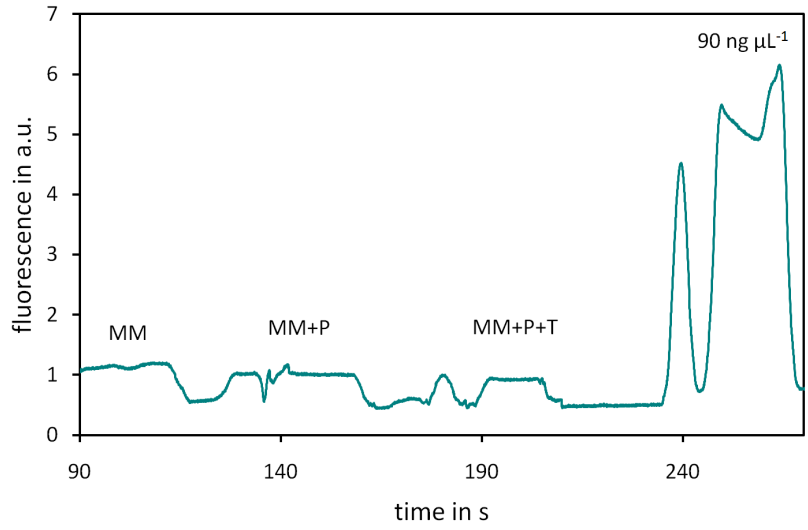

(b) PCR reagents at 60 °C

Figure 4.7: Signal of PCR reagents at different temperatures: a) 25 °C, the primers led to a signal (MM+P, MM+P+T) which is approximately 50% of the signal obtained by high concentrations of DNA (90 ng µL^{-1}); b) 60 °C, the primers no longer contribute to a high signal, while the intensity of the positive control (90 ng µL^{-1}) remains unchanged; double peaks in the signal represent interspacing by small oil droplets, which did not influence signal intensities or sample discrimination; flow rate: 200 nL s^{-1}; sample volume: 5 µL; throughput: 72 samples per hour; MM: mastermix (negative control); P: primers; T: Taq polymerase; a.u.: arbitrary units.

For reference measurements a capillary electrophoresis (CE) system was used. The CE device has no heating function, which means that primer dimers are still visible (Fig. 4.8(b)). With the presented flow-through device DNA concentrations down to 10^1 cells per reaction before PCR were still detectable. When comparing the sensitivity to a capillary electrophoresis system it can be seen, that it is two orders of magnitude higher than the reference measurement (Fig. 4.8). In contrast to UV DNA measurements (sensitive to dNTPs and primers), our system can therefore be applied to PCR products directly.

4.3.4 Future advances and system integration

It has been shown, that the presented device is suitable for PCR product detection with sensitivities down to $1\,\mathrm{ng\,\mu L^{-1}}$. A further increase in sensitivity could open alternative applications such as quality measurements of DNA extracts of clinical samples or DNA detection without PCR. One possibility to increase sensitivity is to switch to photodiodes out of amorphous silicon, which will bring enhancement up to 10-fold [74]. Even further enhancement is achieved with avalanche photodiodes (APD), which are able to detect single photons [75, 76]. While APDs bring high sensitivity, they are still expensive and require high voltages for operation and cooling to reduce the dark current.

The capability of sensing DNA samples in a continuous flow setting at high throughput and sensitivity, qualifies the detector for the facile combination with up- and downstream flow-through applications. Especially the downstream integration after continuous flow PCR systems, as presented before [60], is of major interest. It will lead to a self-contained system for detecting minute amounts of DNA by PCR and endpoint fluorescence sensing. The additional integration of microfluidic DNA extraction methods [77–79] on the upstream of continuous flow PCR is a further step towards a micro total analysis system for the sensitive detection of DNA out of unprocessed samples (e.g. blood, food or water). Applications could range from rapid clinical diagnostics like sepsis or tumour assays, food pathogen assays, biowarfare detection systems, forensics to environmental screening tests.

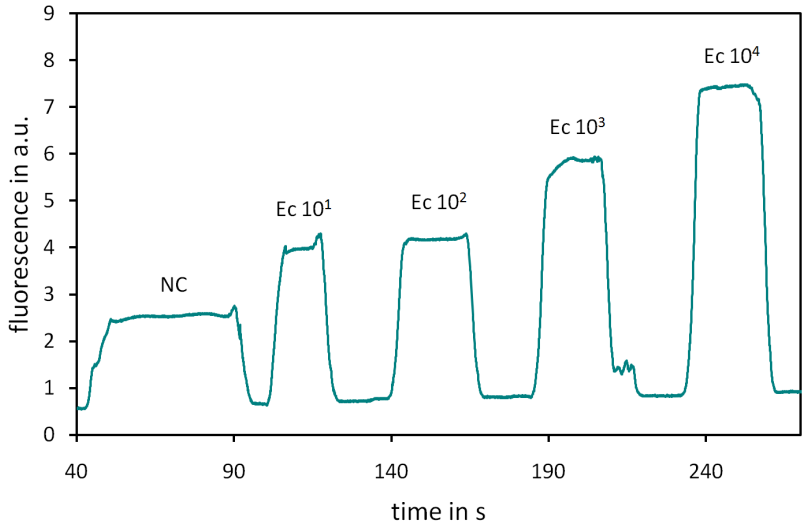

(a) Signal of flow cell at 60 °C

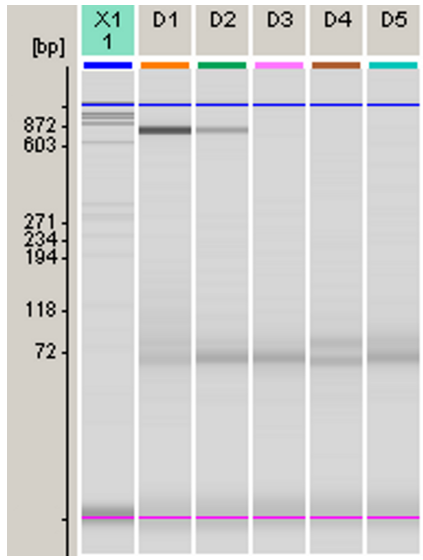

(b) Reference measurement

Figure 4.8: a) measurement of PCR products in flow cell at 60 °C; PCR products are amplified from bacterial DNA from *Escherichia coli* (Ec) in different concentrations (cells per reaction); NC: negative control (cycled PCR mastermix without target DNA); flow rate: 200 nL s^{-1}; sample volume: 5 µL; throughput: 72 samples per hour; a.u.: arbitrary units; b) reference measurement from capillary electrophoresis system at 25 °C; primer dimers can be seen at approximately 72 bp; X1: Ladder; D1: 10^4 cells/rxn; D2: 10^3 cells/rxn; D3: 10^2 cells/rxn; D4: 10^1 cells/rxn; D5: negative control.

4.4 Conclusion

The presented DNA sensor is capable of measuring dsDNA in continuous flow operation. In particular, it was designed for measuring unpurified PCR products including primers and polymerases. Primer dimer signals were suppressed by heating the flow cell to $60\,^{\circ}\mathrm{C}$. This approach enabled high sensitivities when detecting PCR products. Initial microbial DNA amounts before PCR of 10 cell equivalents per reaction were still detectable. Purified DNA samples could be detected down to $1\,\mathrm{ng}\,\mu\mathrm{l}^{-1}$. High sample throughputs of up to 240 samples per hour were achieved. The compact lens-free design with a cost-effective LED-photodiode approach is an attractive alternative to laser-induced-fluorescence systems. The fluidic sampling and the flow conditions equal flow-through PCR systems, which qualifies the detector for direct downstream connection after continuous flow PCR devices. Applications such as portable systems, low priced lab equipment, high-throughput screening or point of care diagnostic devices are possible with the shown performances.

Chapter 5
Enhanced fluorescence

Chapter 3 describes a microfluidic chip for DNA microarray preprocessing to accelerate and automate the analysis workflow. Beside process speed up, sensitivity is another important parameter, when using molecular methods for diagnostic applications. This chapter describes a facile method for the enhancement of fluorescent signals for solid phase based biomolecule detection by employing planar thin metal or metal oxide films. The demonstrated approach was tested with DNA microarrays, where it could be easily integrated into the fabrication process. The achieved signal amplification is interesting for diagnostic applications, since it boosts sensitivity by almost one order of magnitude.

5.1 Introduction

DNA microarray technology is a powerful analytical method for massively parallel sequence testing. Up to several million probe oligonucleotides are currently available on a single assay [80]. These parallel DNA testing methods enable whole genome coverage. Applications include gene expression profiling, single nucleotide polymorphism (SNP) screening or chromatin immunoprecipitation (ChIP) on chip. Beside their utilisation in basic genomic research, they can also be used for diagnostic purposes like cancer assays, pathogen identification [81] and antibiotic resistance testing. In particular, those diagnostic tests can benefit from sensitivity enhancements in several ways. First, the limit of detection can be reduced and therefore diseases with low analyte concentrations get in reach of microarray detectability. Secondly, sensitivity enhancement has the potential to make prior amplification steps (by polymerase chain reaction (PCR)) unnecessary and therefore reduce analysis complexity and processing time. This further enables a one-step assay, applicable for point of care (POC) testing. Finally, cost-effective and miniaturised readout equipment could be used instead of

bulky lasers, optics and photomultiplier tubes. This would make point of care and handheld devices [82] feasible, opening new fields of application for solid phase DNA assays.

In principle, sensitivity is dependent on scanning performance (laser intensity, photomultiplier tube sensitivity and optics), fluorophore performance (quantum yield and photobleaching), binding chemistry (dendrimers, 3D structures and linker density), the geometrical properties of the solid support (surface to volume ratio and nanostructures) and the optical properties of the slides (reflectivity, interference and surface enhanced fluorescence [83]). Several nanostructures have been reported to enhance fluorescence emission, including gold nanoparticles [84], dye doped silica nanoparticles [85], quartz nanopillars [86] and ZnO nanorods [87, 88]. However, nanostructures have several disadvantages in comparison to planar films when applied to microarrays. They are often not stable for contact spotting and reduce reflectivity due to their diffuse optical properties. Therefore, planar thin films were chosen. They have been previously reported to enhance signals in the range of 10-20 fold [89].

The focus of this chapter is to fabricate metal (Au and Ta) and metal oxide (ZnO and TiO_2) thin film coatings for fluorescent signal enhancement. In contrast to multilayer systems, like Bragg mirrors [90], the presented approach employs maximal two enhancement layers and one linker layer for biomolecule attachment. This brings a reduction of fabrication steps and therefore a faster and more cost-effective production.

5.2 Methods

5.2.1 Design of coatings

Fluorescence signal enhancement can be realised in different ways, including the increase of binding site density (e.g. by dendrimers or 3D structures), reflective thin films and nanostructures for enhanced localised field strength [83, 89]. Thin films have the advantage of low complexity and facile integration into the microarray fabrication process. Furthermore, they do not decrease wettability and are stable for contact-spotting. The signal enhancing structure, presented in this chapter, consists of a metal or metal oxide layer, deposited on a bare glass slide. An additional epoxy film serves for covalent attachment of the DNA probes. Excitation (E_{ex}) and emission (E_{em}) light components are reflected at every boundary, which contributes

to an overall field enhancement ($E_{em}{}^{*}$ in Fig. 5.1).

5.2.2 Thin film fabrication

Planar thin films can be fabricated with several methods, including chemical vapour deposition (CVD), physical vapour deposition (PVD), dip coating, spray coating and spin coating. CVD and PVD methods have in common, that the coating material is vaporised in a vacuum chamber and precipitated on the target substrate. CVD include chemical reactions on the target surface, while the vaporised material does not change on the surface in PVD methods. PVD techniques, like sputtering, are common for metal films and more cost-effective than CVD. Therefore, sputtering was used for metal coatings. Thin film fabrication by dip coating starts with the immersion of the target substrate in a solution containing the thin film material. The coating compound can be dissolved in its final form (e.g. ZnO for ZnO films) or as a precursor (e.g. $ZnCl_2$ for ZnO films). After immersion, the substrate is withdrawn from the solution at a certain speed and the solvent is vaporised. The coated substrate is thermally treated for the final thin film. Spin coating is performed with the application of the coating solution onto the centre of the substrate and subsequent spinning. Centrifugal forces cause homogeneous films over the entire substrate. Post spinning treatments include vaporisation of solvent and thermal treatment, similar to dip coating. The presented metal films were deposited by sputtering and the metal oxide films were fabricated by sputtering, dip- and spin coating.

All presented coatings were deposited on bare glass slides (Paul Marienfeld GmbH, Lauda-Königshofen, Germany) after cleaning with isopropyl alcohol. The metal films (Au and Ta) and one part of the zinc oxide films (ZnO266, ZnO133 and ZnO67) were deposited by magnetron sputtering (direct current mode) with an Univex 450 C (Oerlikon Leybold Vacuum GmbH, Cologne, Germany). The other zinc oxide films and titanium dioxide coatings were fabricated by dip- and spin-coating with three different protocols per oxide (ZnO_P1, ZnO_P2, ZnO_P3, TiO2_P1, TiO2_P2 and TiO2_P3 in Table 5.1). The first zinc oxide film (ZnO_P1) was synthesised by dip-coating in a ZnO-epoxy mixture with $85.7\,\mathrm{mm\,min^{-1}}$ dipping velocity and a holding time of $60\,\mathrm{s}$. ZnO_P2 was fabricated by dip-coating in a zinc chloride solution (1M $ZnCl_2$ in isopropyl alcohol + 0.05% acetylacetone) with $85.7\,\mathrm{mm\,min^{-1}}$ dipping velocity and a holding time of $60\,\mathrm{s}$. ZnO_P3 was synthesised like ZnO_P2, but with two identical layers.

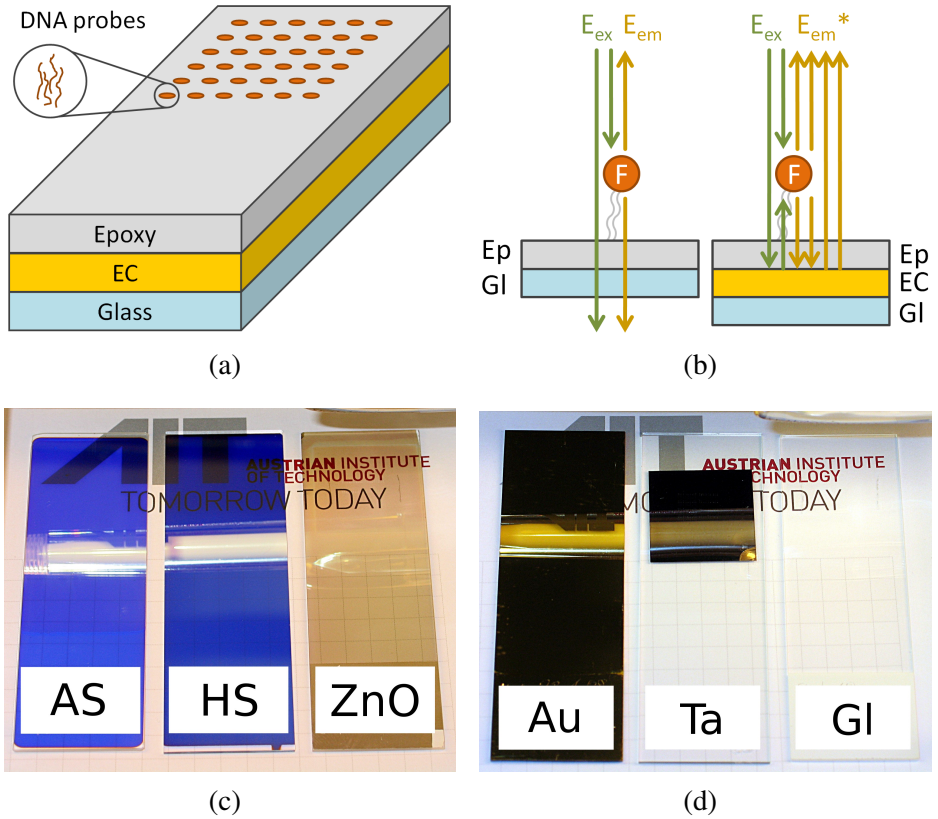

Figure 5.1: Metal and metal oxide coatings: a) Film composition: all enhancement coatings (EC) are deposited on bare glass slides and covered with an epoxy film for DNA attachment; b) Fluorescence enhancement: glass slides lose a part of the fluorescence signal through transmission (left), enhancement coatings result in reflection and interference, which contribute to an enhanced signal E^*_{em} (simplified illustration); c) Comparison of metal oxide slides: Amplislides (AS) and HiSens slides (HS) show low transmission and high reflectivity, while zinc oxide slides (ZnO) show high transmission and low reflectivity; d) Comparison of metal slides: gold slides (Au) and tantalum slides (Ta) show no transmission and high reflectivity, while glass slides (Gl) show high transmission and very low reflectivity; Tantalum films were sputtered on small glass coverslips (22 mm × 22 mm × 0.16 mm), which were glued to standard slides (76 mm × 26 mm × 1 mm); transmission can be seen by the readability of the writing on the underlying paper; reflectivity can be seen by the mirror image of a white pen; EC: enhancement coating; Ep: epoxy layer for DNA attachment; Gl: glass slide; E_{ex}: electrical field strength of excitation; E_{em}: electrical field strength of emission; F: fluorophore.

Table 5.1: Thin film compositions: all samples are additionally coated with a 30 nm epoxy film

Name	Film 1	Film 2	Fabrication
Amplislide	SiO_2	TiO_2	n.a.[a]
HiSens	n.a.[a]	n.a.[a]	n.a.[a]
Au133	5 nm Ta	133 nm Au	sputtering
Au64	5 nm Ta	64 nm Au	sputtering
Ta266	266 nm Ta		sputtering
Ta133	133 nm Ta		sputtering
Ta67	67 nm Ta		sputtering
ZnO266	266 nm ZnO		sputtering[c]
ZnO133	133 nm ZnO		sputtering[c]
ZnO67	67 nm ZnO		sputtering[c]
ZnO_P1	ZnO		HT[b]-ZnO precursor, dip-coated
ZnO_P2	ZnO		$ZnCl_2$ precursor, dip-coated
ZnO_P3	ZnO	ZnO	$ZnCl_2$ precursor, dip-coated
TiO2_P1	TiO_2		$TiCl_4$ precursor, dip-coated
TiO2_P2	TiO_2		$TiCl_4$ precursor, dip-coated
TiO2_P3	TiO_2		$TiCl_4$ precursor, spin-coated

[a] not available (commercial product)
[b] hydrothermally synthesised
[c] unspecific enhancement

The first titanium dioxide film (TiO2_P1) was fabricated by dip-coating ($85.7\,\mathrm{mm\,min^{-1}}$ dipping velocity, $20\,\mathrm{s}$ holding time) in a $TiCl_4$ solution inclusive polyethyleneglycol [91] and a thermal treatment of $500\,°\mathrm{C}$ for 4 hours. TiO2_P2 was synthesised like TiO2_P1, but with a different thermal treatment of $150\,°\mathrm{C}$ for 20 hours. The third titanium dioxide film (TiO2_P3) was fabricated as TiO2_P1, but by spin-coating ($2\,\mathrm{mL}$, $2000\,\mathrm{min^{-1}}$, $40\,\mathrm{s}$) and thermal treatment of $500\,°\mathrm{C}$ for 4 hours.

5.2.3 Dielectric mirrors

The fabricated slides were compared to two different dielectric mirror slides. Amplislides (Genewave, Paris, France) consist of a four period SiO_2/TiO_2 stack with a Bragg wavelength of $612\,\mathrm{nm}$. With this design fluorescent enhancement of up to 15-fold was reported [90]. The second dielectric mirrors were Nexterion HiSens slides (Schott AG, Mainz, Germany), which claim enhancements of up to 12.6 times. Material composition of HiSens slides are not available, but visual appearance is very similar to Amplislides (Fig. 5.1(c)). Also the layer design is not available, but a spectral reflectivity measurement suggests more layers than Amplislides (Fig. 5.6).

5.2.4 Microarray fabrication

Microarray analysis is a powerful analytical method, because of its parallel testing capabilities. Millions of biomolecules can be assessed in a single sample by visualising hybridisation and binding events on a solid support. Fabrication technology determine capture molecule density and therefore total number of sensing probes, microarray sensitivity and costs. Most popular solid support material are microscope glass slides (see Section 5.2.2), which are modified with different linker chemistries (e.g. epoxy or aldehyde) for biomolecule attachment. Alternatively silicon is used for more integrated devices and label-free detection methods [92]. Glass is cost-effective for standard microarray applications and therefore used for the presented method. Attachment of DNA onto the surface can be done in two ways: photolithographic in-situ synthesis of oligonucleotides or spotting of microdroplets. Mask-based and micromirror systems [93, 94] are used in photolithographic methods to selectively activate or deactivate the attachment of the next base. Oligonucleotides are therefore build up from the surface base by base. This method is time consuming and complex,

which makes it feasible for large-scale production only. Research microarrays are still fabricated by contact or non-contact spotters, which transfer microdroplets of oligonucleotide solution to the surface of the slides. The presented slides in this chapter were fabricated by contact-printing, where pins dip into a solution of probe DNA and transfer it to the slide surface. Typical spot volumes lie in the range of $0.5\,\mathrm{nL}$ to $2\,\mathrm{nL}$. After spotting the slides are blocked to avoid unspecific binding, which finalises microarray fabrication (Fig. 5.2).

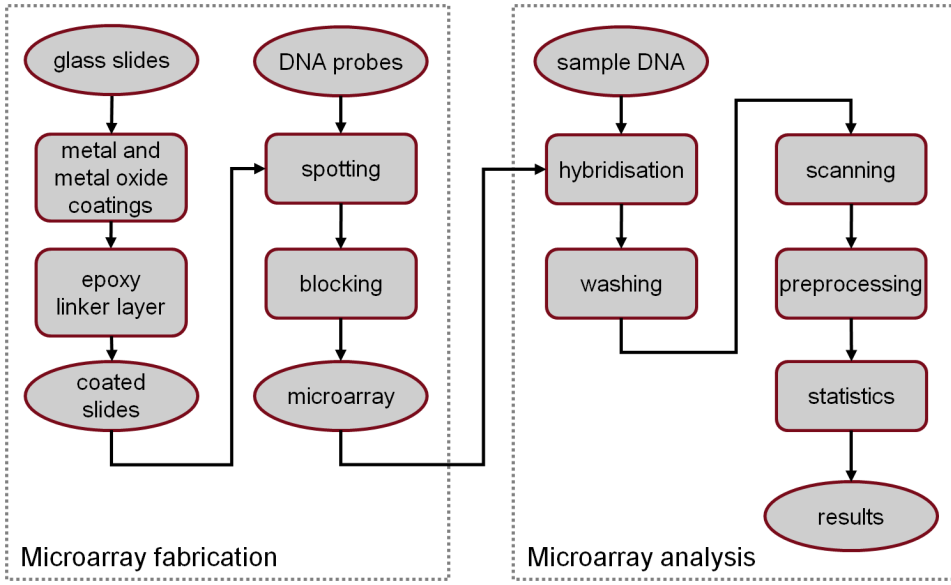

Figure 5.2: Microarray fabrication and analysis: Glass slides are coated with metal and metal oxide thin films by sputtering or dip-coating, including a functional linker layer for DNA attachment; DNA probes are spotted onto the linker layer and subsequently blocked, which leads to the final microarray; Blocking is important to avoid unspecific binding; Analysis is performed by applying labelled sample DNA onto the microarray surface; Hybridisation events are measured by fluorescent scanning and statistical analysis; Depending on the type of microarray, results can represent gene expression, pathogen species (Chapter 3) or SNPs.

Coupling of biomolecules to surfaces can be realised with linker layers including epoxy, aldehyde or amine chemistries. The presented method of microarray fabrication is applicable to glass, metal and metal oxide surfaces and uses an epoxy layer, applicable for DNA and protein capture molecules. All fabricated thin films and commercial products (Table 5.1) were covered

with an epoxy coating to provide functional linker groups for biomolecule attachment (Fig. 5.3). Epoxy thickness $(30(7)\,\mathrm{nm})$ was determined by profilometer measurements. One part of the film was removed by reactive ion etching (RIE) using a shadow mask. Because gold has an etch-rate several magnitudes lower than epoxy, it was possible to remove the epoxy film, without etching into the underlying gold layer.

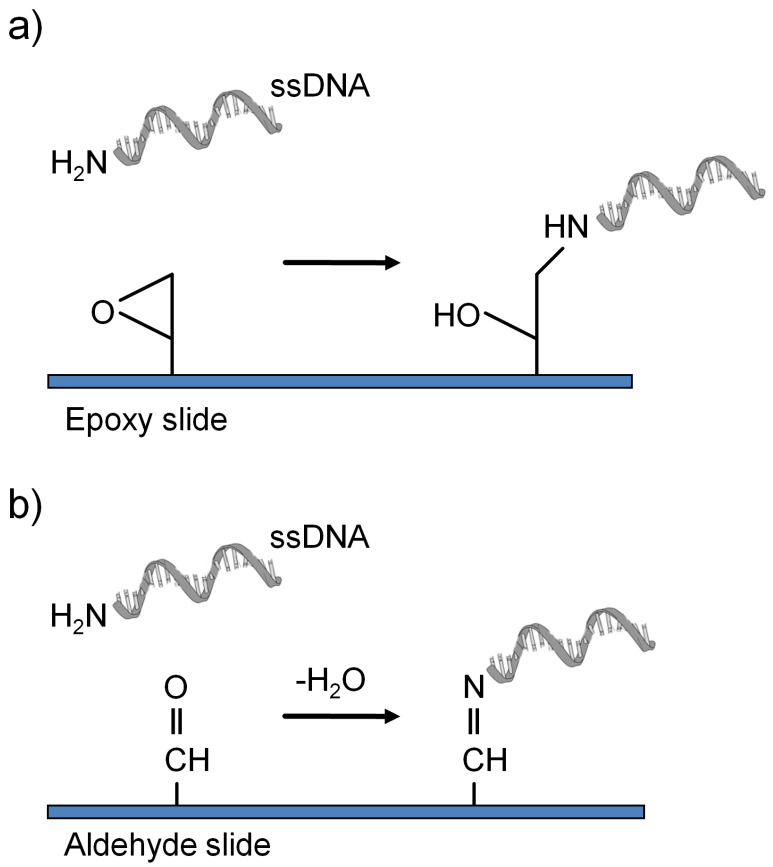

Figure 5.3: Linker systems: a) Epoxy coatings: amino-modified oligonucleotides (ssDNA) are covalently attached by ring opening of the epoxy structure; b) Aldehyde coatings: amino-modified oligonucleotides (ssDNA) are covalently immobilised by Schiff-base formation by dehydration.

To provide a final DNA assay, the fabricated slides (enhancement- and linker layer) were functionalised. This was performed by spotting oligonucleotide probes onto the epoxy surface by a microarray contact spotter (OmniGrid 100, former Genemachines, now Digilab Inc., Holliston, MA,

Table 5.2: Spotting buffers

Name	Composition
B1	0.2 M Na_2HPO_4 + 0.2 M $NaH_2PO_4 \cdot H_2O$, pH 8 + 0.02 % sodium dodecyl sulfate (SDS)
B2	6 M betaine + 3× saline sodium citrate (SSC)
B3	0.2 M $MgCl_2$ + 0.02 % SDS
B4	CaCl, pH 8 + 0.02 % SDS
B5	TE buffer (10 mM Tris, 1 mM EDTA, pH 8)
B6	2× phosphate buffered saline (PBS) + 0.02 % SDS
B7	100 % dimethyl sulfoxide (DMSO)

USA). Four different ssDNA probes (*Escherichia coli* (eco2), *Staphylococcus aureus* (sar2), *Pseudomonas aeruginosa* (psa5) and *Enterococcus faecium* (efa42)) were used for species identification. Two control spots were used for validation of PCR and hybridisation. PCR control was realised by spotting the complementary sequence of the forward primer. PCR products of any microbial DNA can be detected with this probe. Hybridisation was assessed with the BSrev probe (`TTA AAA CGA CGG CCA GTG AGC`). It detects the complementary sequence, which was added to every reaction before hybridisation. Therefore, a validation of the hybridisation event without PCR products is possible (compare Section 5.2.5). In addition, two different linker systems were assessed. Amino-(NH) and thiol-modified (SH) oligonucleotides (5'-modification) were compared. Each probe was spotted four times to account for variation due to spatial- and spotting effects. All slides were tested in triplicates. To optimise signal intensities in association with probe immobilisation, seven different spotting buffers were compared (B1-B7, Table 5.2). Before each experiment the microarrays were blocked in 3 M urea + 0.1 % SDS for 30 min to passivate active epoxy groups. After blocking, the microarray slides were ready for sample measurements (compare Fig. 5.2).

5.2.5 Preprocessing and microarray experiments

Bacterial strains were cultured and DNA isolated by thermal lysis as presented before [60]. Bacterial genomic DNA was amplified by PCR, targeting the 16S rRNA gene. Two universal primers (FW45: `GCY TAA YAC ATG CAA GTC GAR CG`, RV764: `TGT TTG CTC CCC AYG CTT T`) target

conserved regions, which allows species-independent amplification of bacterial DNA. PCR was performed with initial pre-denaturation (5 min, 95 °C), 40 cycles of denaturation (1 min, 95 °C), annealing (1 min, 55 °C) and extension (1 min, 72 °C) and a final extension step (10 min, 72 °C). Primers were ordered from Microsynth AG (Balgach, Switzerland) and the Mastermix 16S Basic (Molzym GmbH, Bremen, Germany) was used for PCR.

After amplification, a labelled product was synthesised with fluorescently conjugated nucleotides. This was performed by primer extension (linear PCR) with forward primers and ATTO532-labelled dCTPs (ATTO-TEC GmbH, Siegen, Germany). Fluorescently labelled forward strands were synthesised with initial pre-denaturation (3 min, 95 °C), 25 cycles of denaturation (20 s, 95 °C), annealing (20 s, 55 °C) and extension (20 s, 72 °C) and a final extension step (3 min, 72 °C). Vent (exo-) polymerase from New England Biolabs (Ipswich, MA, USA) was used due to its lack of proofreading exonuclease activity. This enabled the incorporation of ATTO532-conjugated dCTPs (compare Chapter 3, Fig. 3.2).

The labelled product was mixed with hybridisation buffer (ExpressHyb, Clontech Laboratories Inc., Mountain View, CA, USA) at a ratio of 1:1 and the hybridisation control BSrev (ATTO620 (ATTO-TEC GmbH, Siegen, Germany) conjugated oligonucleotide) was added with a final concentration of 166 nM (compare Section 5.2.4). The hybridisation mix was applied onto the microarrays and capped by a cover slip. The slides were incubated in a humid chamber at 65 °C for 45 min. After hybridisation the arrays were washed in Wash1 (2x SSC, 0.1% SDS) for 5 min, Wash2 (0.2x SSC) for 2 min and Wash3 (0.1x SSC) for 1 min and subsequently dryed by centrifugation (172 g, 2 min).

5.2.6 Scanning and data analysis

Processed slides were scanned at 532 nm (for dye ATTO532) and 635 nm (for dye ATTO620) with a Genepix 4000A microarray scanner (Former Axon Instruments, now Molecular Devices, LLC, Sunnyvale, CA, USA) at a resolution of 10 µm. Images were analysed by Genepix software, which transformed spot intensities into numerical values. Spots were detected and the background signal was subtracted from the spot intensity. Signal increase of different coatings was assessed with the enhancement factor (EF), which is defined as ratio between intensity of enhanced slides and intensity of glass slides (Fig. 5.1 and Equation 5.1). Enhancements are given when

EF is greater than one. Glass slides have per definition an enhancement factor of 1.0.

$$EF = \frac{|{E_{em}}^*|^2}{|E_{em}|^2} \tag{5.1}$$

5.3 Results and discussion

5.3.1 Integration of thin films into microarray fabrication

Conventional microarrays are based on glass slides. Therefore, most linker systems for oligonucleotide immobilisation are based on glass surfaces like silane-based chemistries [95]. These coatings require hydroxyl groups, which are present on glass and metal oxide surfaces. In contrast, the used epoxy approach is applicable to metal surfaces as well. This was important for the comparability between the different metal and metal oxide thin films. The fabricated enhancement coatings consist of up to two layers, excluding the additional epoxy linker. This is a straightforward design in comparison to the commercial dielectric mirrors. They require multiple double layers for their wavelength-dependant enhancement, which makes them more complex.

Alternative metal coatings (Ag, Al and Pd) were fabricated by sputtering, but they were not stable during hybridisation, which makes them unsuitable for DNA microarray applications. The hybridisation mix (see Section 5.2.5) corroded the metal films and delaminated them from the glass substrate, even with the covering epoxy film. One reason could be small pin holes in the epoxy layer, giving access to the underlying metal films. Although this permeability was destructive for unstable metals (Ag, Al and Pd), it was not affecting DNA attachment or hybridisation adversely on other coatings. Metal films (Au and Ta) showed high stability and biocompatibility with DNA probes and samples. The metal oxide films (ZnO and TiO_2) showed high stabilities and no delamination as well.

5.3.2 Surface topology

As discussed in Section 5.1, surface structures in the nanometre range can contribute to signal enhancement. Several nanostructures were reported to enhance fluorescence including pillars and rods [86–88]. However, those

nanopatterns have reduced wettability, making spotting more difficult. Furthermore, when those structures are in the micrometre range, the surface shows diffuse optical properties (compare Section 5.3.6). This reduces reflectivity, which further decreases signal strength. Therefore, surface roughness was assessed by atomic force microscopy (AFM) and root mean squared roughness R_{RMS} was calculated from the measured topology.

Bare glass slides show a low roughness of 3.1 nm, which does not lead to diffuse optical properties. The topology shows several peaks with maximal heights of 22 nm, which are distributed randomly (Fig. 5.4(a)). Additional epoxy coating results in higher roughness of 7.7 nm, still not contributing to diffuse optical properties. Peaks are higher with a maximal length of 61 nm and their density is lower compared to bare glass (Fig. 5.4(b)). The epoxy film covered the glass surface and showed peaks with increased height, which may result from impurities during the coating process. Increased surface area, in comparison to atomic flatness, may further enhance capture probe density and therefore signal strength. However, this effect remains to be investigated. Roughness and peak heights are low and therefore do not reduce reflectivity or adversely affect the optical properties of the slides. Sputtered gold thin films show a lower roughness of 2.5 nm compared to glass and epoxy coatings. Clusters have a maximal height of 29 nm and are randomly distributed (Fig. 5.5). These variations in structure do not decrease reflectivity of the gold coatings.

5.3.3 Reflectivity

Reflection of excitation and emission intensity can significantly increase fluorescence signal (Fig. 5.1). Therefore, the spectral reflectivity was measured for the different enhancement coatings. Dielectric mirror slides (Amplislide and HiSens) show increased reflectance in the range between 500 nm and 700 nm. Gold slides have increased reflectance from 500 nm onwards and tantalum slides have medium reflectance in the range of 50 % (Fig. 5.6). Although there is a reflection of tantalum slides, fluorescence enhancement could not be measured (Fig. 5.8), which could be caused by destructive interferences. Metal oxide coatings show low reflectivity in the range between 5 % and 20 %, which is comparable with bare glass slides (Fig. 5.7). High reflectance of dielectric mirrors and gold slides correlates with increased fluorescence depicted in Fig. 5.8.

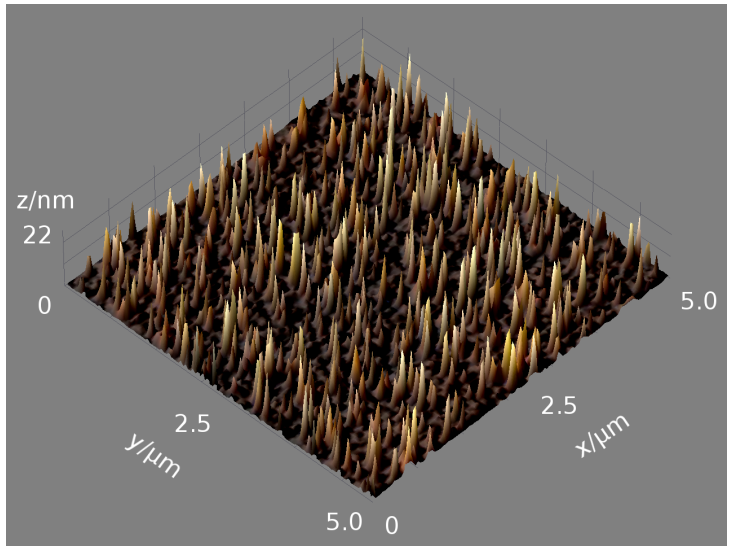

(a)

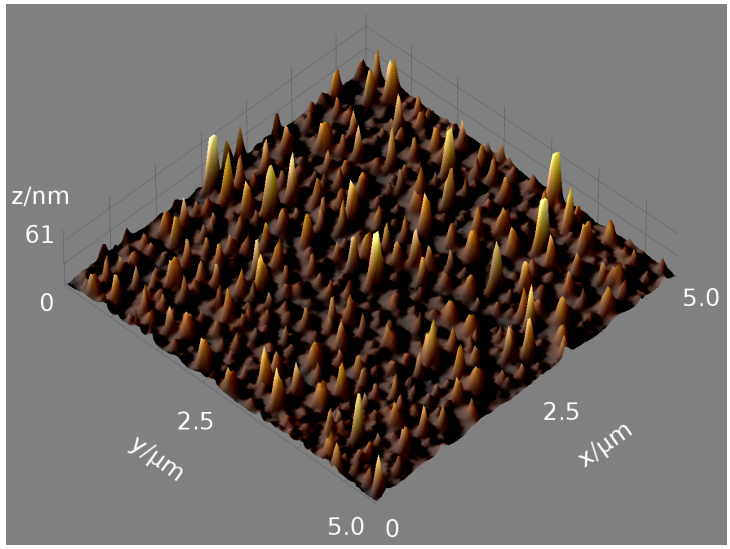

(b)

Figure 5.4: Surface topology: a) Bare glass slides ($R_{RMS} = 3.1\,\text{nm}$); b) Epoxy coating ($R_{RMS} = 7.7\,\text{nm}$); R_{RMS}: surface roughness, root mean squared, measured along the diagonal (top corner to bottom corner).

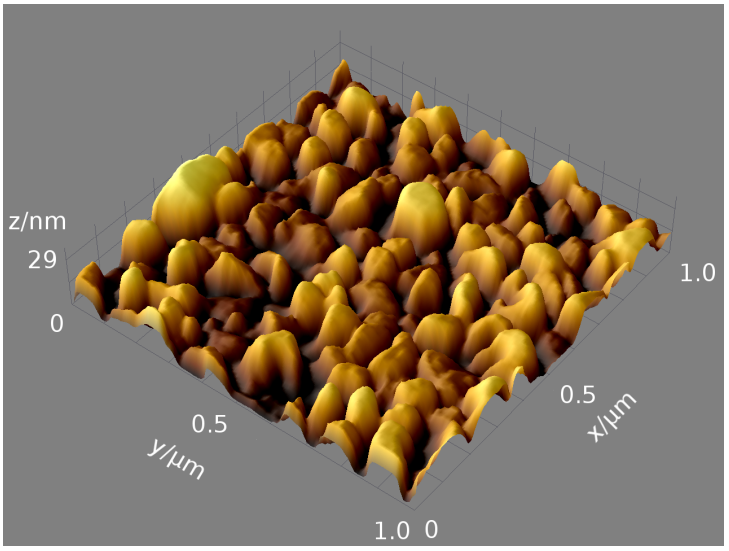

Figure 5.5: Surface topology of gold coating with a layer composition of glass, 5 nm Ta, 133 nm Au ($R_{RMS} = 2.5$ nm); R_{RMS}: surface roughness, root mean squared, measured along the diagonal (top corner to bottom corner).

5.3.4 Spotting buffers

The comparison of the different spotting buffers revealed, that buffer B1 showed the highest signals and best reproducibilities on all slides (defined as 100% on Au133 coating). Buffer B6 resulted in lower signals (53% (NH) and 95% (SH) of B1) and reproducibility was low. The chlorine-containing buffers B3 and B4 (see Section 5.2.4) led to high signals on the ZnO surfaces, but positive negative controls were observed (see Section 5.3.5 and Fig. 5.9). On the other coatings their performance was lower than B1 (B3: 6% (NH) and 95% (SH) of B1, B4: 59% (NH) and 78% (SH) of B1). Buffers B2, B5 and B7 did not perform well on the established epoxy surface (B2: 13% (NH) and 38% (SH) of B1, B5: 12% (NH) and 11% (SH) of B1, B7: 17% (NH) and 23% (SH) of B1). Because B1 resulted in the highest signals, all presented enhancement factors were obtained with this spotting buffer.

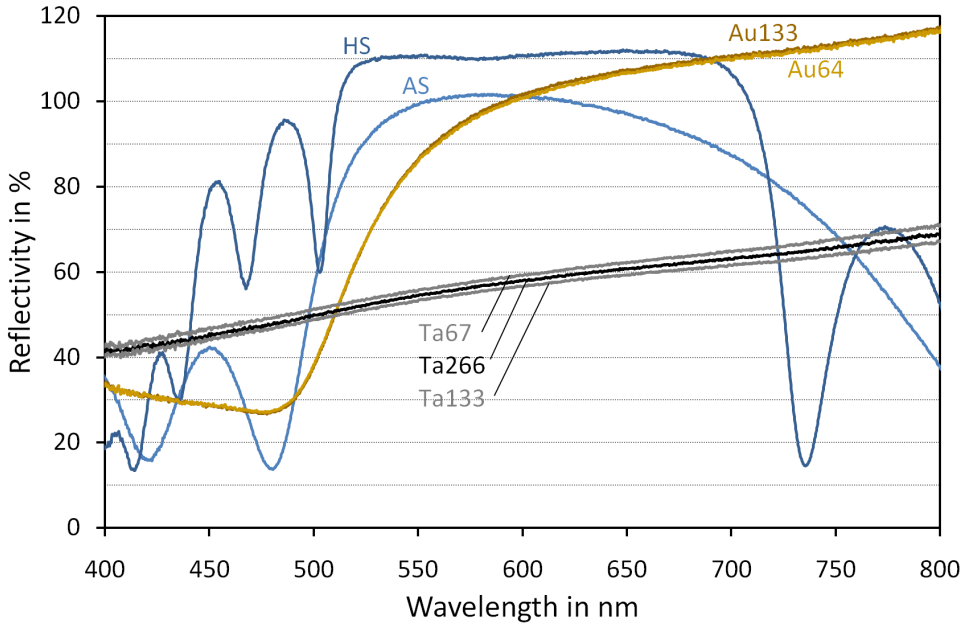

Figure 5.6: Reflectivity of metal coatings: Amplislide (AS) and HiSens slides (HS) show increased reflectance between 500 nm and 700 nm; Their multiple minima and maxima result from their multi-layer design representing interference patterns; Gold films with 64 nm (Au64) and 133 nm (Au133) have low reflectance in the UV-range with an increase at 500 nm; Tantalum slides with film thicknesses between 67 nm and 266 nm (Ta67, Ta133 and Ta266) show medium reflectance between 40 % and 60 %; Reflectivity in % is referenced to a standard mirror (STAN-SSH, Ocean Optics Inc., Dunedin, FL, USA), which is defined as 100 %.

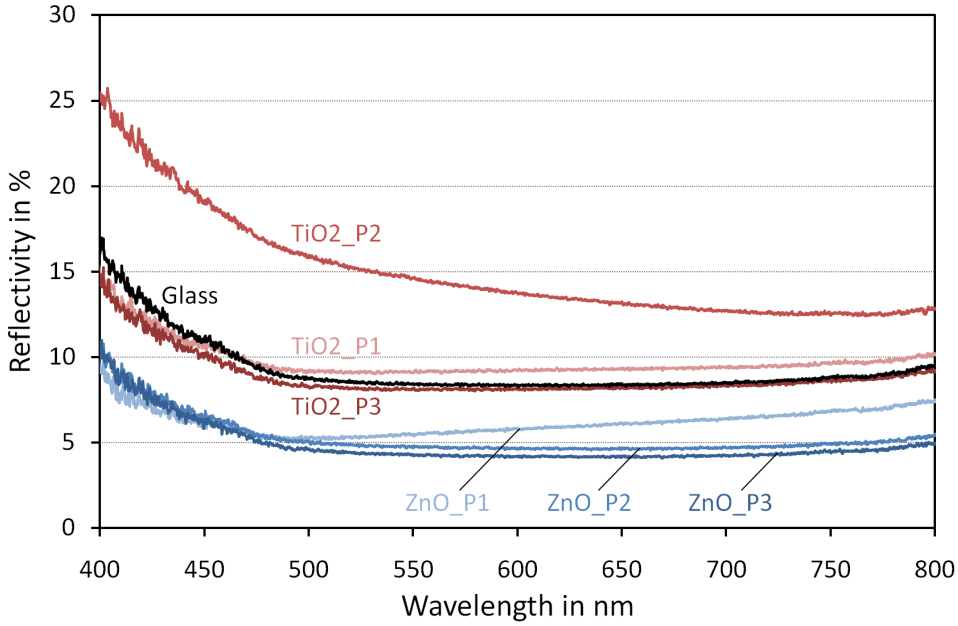

Figure 5.7: Reflectivity of metal oxide coatings: Dip-coated titanium dioxide films (TiO2_P1 and TiO2_P3) show reflectivities in the range of bare glass slides (Glass); Titanium dioxide films with reduced thermal treatment (compare Section 5.2.2) show higher reflectivities in the range of 13 % to 25 %; Dip-coated zinc oxide coatings (ZnO_P1 and ZnO_P3) led to the lowest reflectivities in the range of 5 % to 10 %; Synthesis by dipping in a ZnO-epoxy mixture (compare Section 5.2.2) resulted in slightly higher reflectivity between and 500.800 nm (ZnO_P1); Reflectivity in % is referenced to a standard mirror (STAN-SSH, Ocean Optics Inc., Dunedin, FL, USA), which is defined as 100 %.

5.3.5 Enhancement of different surfaces and probe modifications

Different metal and metal oxide surfaces were compared in aspect of fluorescent signal enhancement of ATTO532 (Cy3 derivate). Commercial dielectric mirror slides (Amplislide and HiSens, see Section 5.2.3 for details) showed the highest enhancements. Amplislides resulted in enhancements of 13-fold (SH) and 10-fold (NH) respectively. HiSens slides led to signal increases of 10-fold (NH). This high enhancements result from multiple constructive interference at multiple double layers and the optimisation to the fluorophore wavelength [90]. Although dielectric mirror slides showed higher enhancements, the presented fabrication procedure can compete due to its low complexity. The best metal slides were gold thin films with 133 nm, which achieved signal enhancements of 8.9-fold (SH) and 5.6-fold (NH) respectively. Thinner gold films with 64 nm showed lower enhancement factors of 7.4 (SH) and 4.2 (NH) respectively. Tantalum slides resulted in no enhancement, but reduction of signal intensities with factors ranging from 0.6 (266 nm, NH) to 1.0 (133 nm, NH). This proves, that the enhancement effect is highly material dependent. Generally, gold layers showed high enhancements, while tantalum layers led to signal decrease. This is consistent with reports of high enhancement by gold and silver thin films, while signal increase by aluminium thin films was low [96]. Sol-gel ZnO films led to signal decrease with factors ranging from 0.8 (ZnO_P2, NH) to low enhancement of 1.2 (ZnO_P1, SH). TiO_2 films showed signal amplification of up to 1.7-fold (TiO2_P3, SH). Thiol-modified oligonucleotide probes (SH) outperformed amino-modified probes (NH) in terms of signal intensity at all different coatings, except TiO2_P1. Signal increase due to thiol-modified probes ranges from 10% for low enhancing surfaces (TiO2_P2) to 75% for high enhancing surfaces (Au64). All enhancement factors are summarised in Fig. 5.8.

While dip-coated ZnO films (ZnO_P1-3) showed signal decreases, sputtered ZnO films showed signal increases of up to 10-fold for 266 nm film thickness. This increase was only observed with the chlorine-containing spotting buffers B3 and B4. Although there was signal enhancement, it was unspecific and could not be linked to the DNA hybridisation event. This was evidenced by positive negative controls (Fig. 5.9(a)). Furthermore, the background signal of these slides was high. One reason could be the formation of zinc chloride between surface atoms and spotting buffer. Zinc

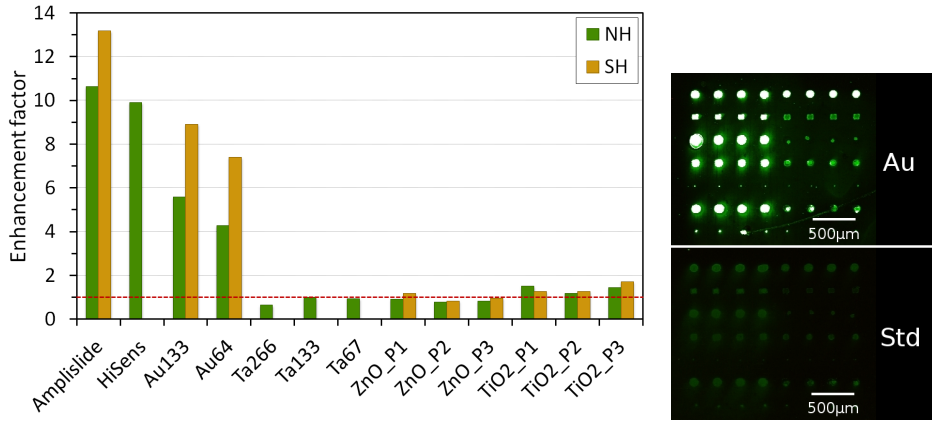

(a) (b)

Figure 5.8: a) Enhancement factors of different film materials: Dielectric mirrors (Amplislide, HiSens) resulted in the highest increases; Strongest enhancement of metal coatings were achieved with 133 nm gold films (Au133); TiO_2 sol-gel slides (TiO2_P3) led to the highest gain in the metal oxide category; Enhancement factors are referenced to epoxy-coated glass slides; The values represent the median of slide triplicates; spot replicates were averaged; NH: amino-modified probes; SH: thiol-modified probes; b) Microarray image of hybridised slides: The signal enhancement of a gold slide (Au) in comparison to a standard glass slide (Std) can be seen by brighter DNA spots.

chloride was reported as fluorescent agent [97], which would explain the unspecific signals. Intrinsic fluorescence was also obtained with alternative ZnO dip-coating protocols (ZnO_P1 without stearic acid). However, there it was not linked to a specific spotting buffer, but fluorescent islands were observed all over the slide (Fig. 5.9(c)). In contrast to the sputtered films, this effect does not correlate with chlorine-containing spotting buffers. Photoluminescence of zinc oxide [98, 99] could be a reason for the signals. Like with the sputtered ZnO films, this intrinsic fluorescence of the films was only observed in the green channel ($\lambda_{ex} = 532\,\text{nm}, \lambda_{em} = 553\,\text{nm}$). Specific fluorescence enhancement due to ZnO [88, 100, 101] could not be confirmed with the presented design. Neither sputtered ZnO thin films, nor dip-coated ZnO films showed signal enhancements for the DNA binding event of microarray assays.

Beside DNA sensing, the presented enhancement films can be applied for protein and peptide biochips [102]. Especially the epoxy linker is suitable for the direct application to protein microarrays. Another field, where the signal enhancement could be used, are chemiluminescence reactions, like for enzyme linked immunosorbent assays. Dendrimers and 3D structures are another possibility to enhance signal intensities, due to increased binding site density [103]. A combination of this technology with the presented enhancements has the potential for a further increase of fluorescence signal.

5.3.6 Structured surfaces

Planar thin films led to enhancements of up to 8-fold in comparison to bare glass slides. As discussed in Section 5.1, ZnO nanorods have the potential for fluorescent signal enhancement [87, 88]. Drawbacks of structured surfaces are their low wettability, which adversely affects spot conformity. Furthermore, contact spotting with pins can destroy nanopatterns, which has to be considered when applied to microarrays. Electrochemically synthesised ZnO nanowires were assessed for their signal enhancement capability and their stability in microarray fabrication. The wires were grown on a gold film and are between $1.8\,\mu\text{m}$ and $2.7\,\mu\text{m}$ long and have a thickness of $150\,\text{nm}$ to $520\,\text{nm}$ (Fig. 5.10). Nanowires were coated with epoxy and ATTO532-labelled DNA probes were spotted onto the surface. Signal intensities of fluorescent probe oligonucleotides were compared to standard glass slides and gold thin films without hybridisation to sample DNA. Spot

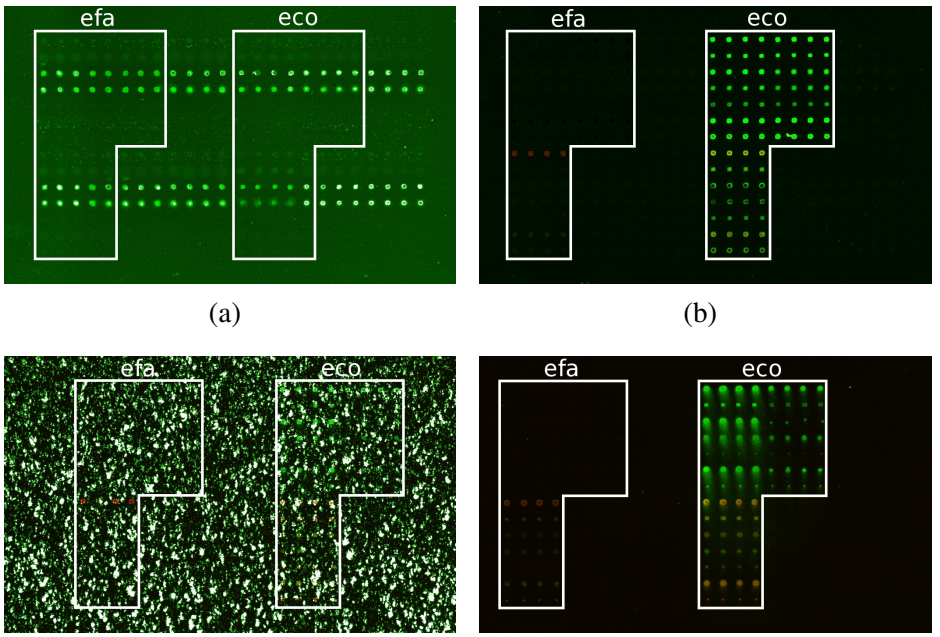

Figure 5.9: Unspecific signals of ZnO coating: a) Sputtered ZnO film with 266 nm thickness; chlorine-containing buffers (B3 and B4) led to high unspecific signals, where pure spotting buffer without DNA probes led to signals (positive negative controls) and the background signal was high; b) Reference glass slide hybridised with the same sample DNA as in a) led to specific signals (eco); c) Dip-coated ZnO slides (ZnO_P1 without stearic acid); ZnO clusters showed high intrinsic fluorescence leading to high background signals; d) Reference glass slide hybridised with the same sample DNA as in c) led to specific signals (eco); All images are a composition of 532 nm channel (green) and 635 nm channel (red); Specific DNA probes are framed: efa for *Enterococcus faecium*, eco for *Escherichia coli*; Spot rows represent different spotting buffers (two times B1-B7); Spots outside the frames are negative controls (spotting buffer without DNA probes).

morphology on the ZnO nanowire surface reveals increased spot diameters and diffuse spot borders for buffers B1 and B6 in Fig. 5.11(b). This led to low probe densities and therefore to decreased signal strength. Buffers B3 and B4 led to the highest signals on ZnO nanowires. As discussed in Section 5.3.5, these signals can result from intrinsic fluorescence, due to ZnCl formation (shown in Fig. 5.9(a)). While the nanowires led to enhancements, compared to glass slides, they showed lower enhancement factors than gold thin films (Fig. 5.11). This effect can result from their diffuse appearance caused by their structure in the micrometre range. It is also possible, that the underlying gold film is responsible for the measured enhancement. Further measurements of hybridised microarrays are necessary to assess specific nanowire effects on fluorescence signal enhancement for DNA binding events.

5.4 Conclusion

We have shown a facile method of integrating sputtered, dip- and spin-coated thin films into microarray fabrication. A maximum of two enhancement layers and one biomolecule linker layer were used, reducing fabrication steps and therefore costs. Gold, tantalum, zinc oxide and titanium dioxide films were stable at hybridisation conditions and did not adversely affect DNA probes and samples. The used epoxy linker system was suitable for oligonucleotide immobilisation and applicable to all surfaces, which was important for comparability. Furthermore, it can be directly applied to protein microarrays. Gold coatings with 133 nm film thickness showed the highest enhancement of up to 8-fold for ATTO532 fluorophores. Dip-coated titanium dioxide films led to enhancements of 1.7-fold. The presented thin films have the power of enhancing microarray sensitivity by almost one order of magnitude. This is of great interest for diagnostic applications like cancer assays or pathogen detection.

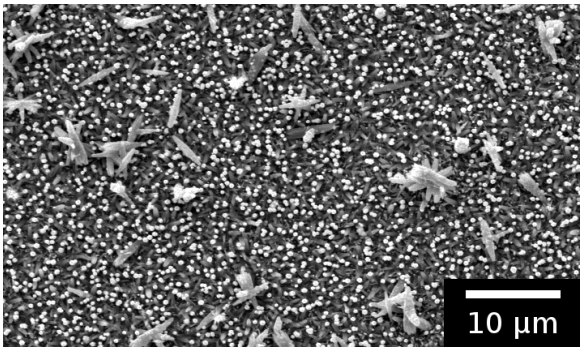

(a)

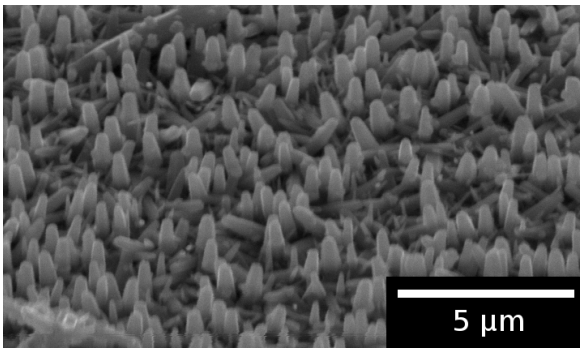

(b)

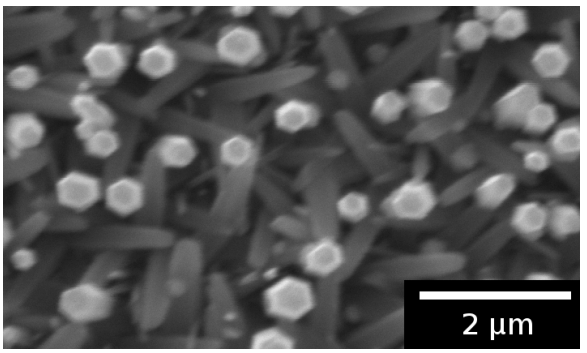

(c)

Figure 5.10: ZnO nanowires: electrochemically synthesised nanowires grown on a gold substrate; Nanowire length: 1.8 µm to 2.7 µm; Nanowire thickness: 150 nm to 520 nm.

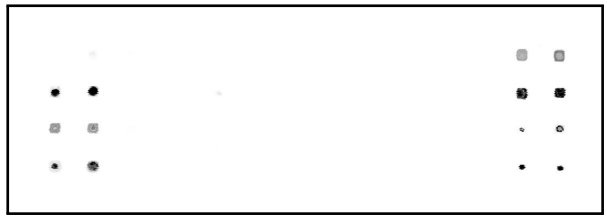

(a)

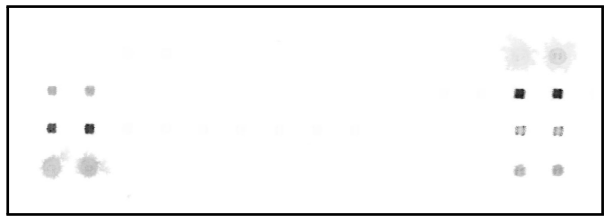

(b)

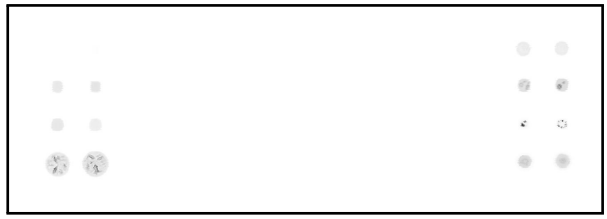

(c)

			B1 NH (*)	B1 SH (*)
B2 NH (*)	B2 SH (*)		B3 NH (*)	B3 SH (*)
B4 NH (*)	B4 SH (*)		B5 NH (*)	B5 SH (*)
B6 NH (*)	B6 SH (*)		B7 NH (*)	B7 SH (*)

(d)

Figure 5.11: Signal enhancement of ZnO nanowires: a) Gold slides with 158 nm thickness; b) ZnO nanowires; c) Aldehyde reference slide; d) spotting pattern with different buffers (B1-B7, Table 5.2) and modifications (NH: amino-modified, SH: thiol-modified); (*): ATTO532-conjugated; Signal represents the intensity of ATTO532-labelled probe oligonucleotides directly after spotting without hybridisation; Intensity is depicted as grey-scale image, where white equals 0% and black 100%.

Chapter 6
Conclusions and Outlook

6.1 Conclusions

Molecular methods have several potentials in medical diagnostics. In comparison to classical methods like cultivation, medical imaging or invasive approaches such as colonoscopy, they have multiple advantages. They are sensitive, rapid, capable for high-throughput analysis and have low invasiveness with the analysis of sputum, urine or blood. Especially high-throughput approaches enable not only patient testing itself, but the discovery of biomarkers on a large scale. This is important to find specific and sensitive biomolecule panels, which correlate with disease status and have a reliable diagnostic value. Therefore, molecular methods can be used for the discovery of biomarkers and for medical diagnostics. Beside their benefits, currently they cannot fulfil further improvements like very short analysis times in the range of minutes, their integration into miniaturised and mobile devices, increased sensitivity, cost-effective high-throughput systems or their automation with reduced hands-on time (sample-in result-out devices).

Microdevices have the potential to achieve these improved performance requirements with the application of novel processing or sensing concepts. In addition, optimised fabrication methods have the capability for cost-effective disposable devices, which is important for single-use diagnostic approaches. Chapter 2 covers rapidness and high-throughput with a cost-effective tubing-based continuous-flow PCR device. In comparison to other publications, this concept is capable of amplifying long targets at high-throughput. It can be used for the discovery of nucleotide biomarkers on a large scale or for the diagnosis of numerous patient samples. Chapter 3 addresses miniaturisation, process automation and rapidness with a disposable polycarbonate chip for PCR and fluorescent labelling in a single reaction. The microfluidic chip was fabricated by injection moulding and thermal bonding, presenting a method for large-scale production. The device can be applied to microarray analysis for shortening the total analysis time or for

the direct detection of DNA biomarkers or genotyping pathogens. Chapter 4 presents a lens-free fluorescent-based DNA sensor for the high-throughput detection of PCR products in continuous flow. The concept is based on a LED-photodiode approach, which makes the system cost-effective. It is applicable for PCR product sensing after CF-PCR devices, which were presented in Chapter 2 and Chapter 3. Chapter 5 addresses increased diagnostic sensitivity by fluorescence enhancement. Metal and metal oxide coatings are integrated into microarray fabrication for the amplification of fluorescence signal.

Continuous-flow PCR was realised with a tubing-approach presented in Chapter 2. The device consists of three heating plates (denaturation, annealing and extension), arranged in a three-sided prism, which are operated by Peltier elements and PID-controllers. PTFE tubing is coiled around the heater with a total of 40 turns, representing 40 PCR cycles and polystyrene isolation guaranteed homogeneous temperatures. This design represents a robust and cost-effective approach, which can be adapted easily. The thermal and fluidic setup was appropriate for processing PCR samples. In particular, the system was tested with the species specific bacterial DNA region (16S rRNA) in a microfluidic sequential droplet setting. Three different species (*Escherichia coli*, *Staphylococcus aureus* and *Pseudomonas aeruginosa*) were tested in the device. They are under the top five causative pathogens for infectious diseases and are responsible for more than 50% of infections (sepsis, pneumonia and urinary tract infections). High sensitivities down to DNA concentrations equivalent to 1×10^2 cells per reaction were achieved, which is appropriate for clinical applications. DNA was extracted from bacterial cells by thermal lysis without any purification, which proves the robustness of the system. Cross-contaminations could be avoided, which qualifies the system for high-throughput sequential sampling. The 418 bp fragment was proven to be processed in 30 min, resulting in a 3-fold acceleration in comparison to a conventional thermocycler. Most importantly the device has overcome the trade-off between target length and sample throughput with the presented design. In particular, the system is capable to amplify regions with 1.3 kbp in consecutive droplets at a throughput of 26.7 samples per hour (80 samples per hour for 418 bp). This performance is superior to other publications (Chapter 2, Fig. 2.10), which is achieved by very inert PTFE tubing, a BSA-containing mastermix and droplet sampling with silicone oil as transport buffer. The achieved target length and sample rate is appropriate for accurate bacterial genotyping

by DNA microarrays at high-throughput. Genomic screening for biomarker discovery can benefit from the achieved sample throughput, process acceleration and reduction of sample volume. Large sample sets can be processed in less time with less reagents and sample material. In addition to the reduces running costs, the presented continuous-flow system has a cost-effective design, which makes parallelisation of multiple reactors feasible. It is therefore an attractive alternative to plate-based PCR systems. Integration and coupling to other continuous-flow systems is straight forward and can bring additional functionalities, like up-stream DNA extraction or down-stream microarray analysis. Long targets, high sensitivity and rapid processing qualify the device for application in DNA microarray testing. It brings acceleration of the workflow, which enables early diagnostics and species specific antibiotic intervention. In the end, patient convalescence will be improved by such biomedical microdevices.

Direct fluorescence labelling was achieved with a continuous-flow approach in a microfluidic polycarbonate chip presented in Chapter 3. Fluorophore conjugated primers were used in a CF-PCR reaction to synthesise (amplify and label) a hybridisation ready mix out of sample DNA in a one-step reaction. The device consists of a spiral channel in a plastic disc, which varies in depth to achieve a constant volume per turn. The chip was placed on a planar heating device with three temperature zones for denaturation, annealing and extension. The temperature distribution of the heater was simulated by finite element method and validated by thermography. The used design was appropriate for homogeneous temperatures, important for high PCR efficiencies. Samples were processed in consecutive droplets transported by buffer. The channels of the device were fabricated by injection moulding of polycarbonate and sealed by thermal bonding with a polycarbonate film. These techniques are capable for large-scale production, which is crucial for cost-effective disposable devices. The used material and fabrication method showed high quality and thermal stability at the maximal operating temperature of $95\,°C$, which is crucial for successful reactions. Beside the integration of DNA amplification and fluorescent labelling into one device, the cyclic flow setting further accelerated the process. Overall, a tenfold speed-up was possible and DNA targets of up to $720\,bp$ could be processed. Detection limits down to DNA amounts equivalent to 100 cells per reaction were possible. The achieved performance enables accelerated nucleotide fluorescence labelling in a disposable device, which can be used for down-stream DNA hybridisation measurement by fluorescence,

like microarrays or bead-based assays. Microarray benchmarking revealed accurate species identification with the hybridisation mix synthesised in the chip. This qualifies the device for the application of genotyping or gene expression analysis. Especially the rapid identification of pathogens has the potential for early and targeted therapeutic intervention in the case of infectious diseases. In a further consequence, this increases the probability of patient convalescence and reduces antibiotic resistances.

DNA sensing was performed with a flow-through fluorescence detector presented in Chapter 4. SYBR Green was used as dsDNA-sensitive dye, mixed to the aqueous DNA samples. Excitation light originated from a LED and emission was filtered and recorded by a standard photodiode. Excitation and emission light was coupled directly into the flow cell by optical fibres, which makes the system lens-free. With the presented design the DNA sensor is capable of measuring dsDNA in continuous flow operation. In particular, it was designed for measuring unpurified PCR products including primers and polymerases. Primer dimer signals were suppressed by heating the flow cell to $60\,^{\circ}\mathrm{C}$ by a Peltier element. This approach enabled high sensitivities when detecting PCR products. Initial microbial DNA amounts, before PCR, of 10 cell equivalents per reaction were still detectable. Purified DNA samples could be detected down to $1\,\mathrm{ng\,\mu L^{-1}}$ at a throughput of 240 samples per hour. The compact lens-free design with a cost-effective LED-photodiode approach is an attractive alternative to laser-induced-fluorescence systems. The continuous-flow design of the device, makes it direct applicable after CF-PCR systems, as presented in Chapter 2 and 3, for PCR product sensing. This enables a rapid diagnostic device for high-throughput applications with single molecule sensitivity.

Fluorescence enhancement was achieved with metal and metal oxide thin films presented in Chapter 5. The coatings were deposited on glass slides and amplified excitation and emission light of fluorescence sensing. The thin films were applied to DNA microarrays for the enhancement of fluorescence readout of the DNA hybridisation event. A facile method of integrating sputtered, dip- and spin-coated thin films into microarray fabrication was presented. A maximum of three layers, including biomolecule linker, was used, reducing fabrication steps and therefore costs. Gold, tantalum, zinc oxide and titanium dioxide films were stable at hybridisation conditions and did not adversely affect DNA probes and samples. The used epoxy linker system was suitable for oligonucleotide immobilisation and applicable to all surfaces, which was important for comparability. Further-

more, it can be directly applied to protein microarrays. Gold coatings with 133 nm film thickness showed the highest enhancement of up to 8-fold for ATTO532 fluorophores. Dip-coated titanium dioxide films led to enhancements of 1.7-fold. The presented thin films have the power of enhancing microarray sensitivity by almost one order of magnitude. This is of great interest for diagnostic applications like cancer assays or pathogen detection.

All presented devices and approaches were designed to be applicable as advanced methods for molecular diagnostics. In particular, the systems were superior in aspects of costs, process integration, sample throughput, miniaturisation, sensitivity and rapidness. High throughput and reduced reaction volumes achieved with the tubing-based CF-PCR device enables faster and cheaper screening for biomarkers. Furthermore, numerous samples can be processed, which is crucial in large diagnostic laboratories. Rapidness, miniaturisation, higher system integration and the applicability as disposable assay was achieved with the polycarbonate chip for fluorescence labelling. This is important for in vitro diagnostic (IVD) single-use tests, mobile devices and low sample volumes. High throughput, a cost-effective approach and sufficient sensitivity for PCR products were achieved with the DNA sensing flow cell. This is important for the direct combination with CF-PCR systems like the tubing-based system or the spiral polycarbonate chip. Increased sensitivity was achieved by metal and metal oxide thin films, which is crucial for disease detection in an early stage. A summary of the developed devices, their performance, application and outlook is shown in Table 6.1.

6.2 Outlook

Tubing-based CF-PCR was constructed in a cost-effective and facile manner. On the basis of the achieved results, multiple tubings can achieve even higher sample throughputs. Parallelisation of fluidic paths can be realised by placing multiple spirals on the same heater. The results of the DNA sensing flow cell qualifies the system for the direct combination with the continuous-flow PCR systems. Especially the integration of one DNA sensor after each turn, will construct a quantitative PCR device in continuous-flow. In comparison to conventional plate-based qPCR devices, this approach does not require bulky and expensive readout systems. In addition, it is a cost-effective alternative with high-throughput capability.

Polycarbonate chip fabrication was shown to be suitable for biomole-

Table 6.1: Summary

Device	Performance	Diagnostic application	Outlook
CF-PCR	long targets, high-throughput, cost-effective, rapid, CF[a]	Biomarker discovery, laboratory devices for numerous samples	Combination with DNA sensing device for quantitative PCR, parallelisation of multiple devices
Fluorescence labelling chip	disposable, rapid, two reactions in one device, low volumes, CF[a]	DNA microarray preprocessing, mobile and automated devices, single-use IVD[b] tests	Apply fabrication method to more integrated devices
DNA sensing	PCR products measurable, cost-effective, lens-free, CF[a]	Endpoint detection of biomarkers after PCR, DNA quantification	Combination with tubing-based CF-PCR and fluorescence labelling chip for quantitative PCR
Enhanced fluorescence	facile layer design, 8-fold signal increase, biocompatible	Solid phase biomolecule assays like DNA and protein microarrays	Apply to other assays

[a] continuous flow
[b] in vitro diagnostic

cule reactions at temperatures in the range of $100\,°C$. Injection moulding and thermal bonding can therefore be used for more complex and integrated devices. One example would be a sample-in result-out system, integrating DNA extraction, PCR and readout in a single device. Patient samples will be directly applied to the system, where DNA is extracted and transferred to the amplification stage. After PCR the product is measured directly by fluorescence sensing or hybridised to an on-chip microarray. Such an integrated miniaturised and mobile system has the potential for point of care diagnostics, aiming for the application as a handheld testing device for the clinician, a decentralised diagnostic instrument for the general practitioner or a device for patient self-testing.

Acknowledgements

Herbert Wiesinger was my supervisor at AIT and initiated the project for diagnostic microdevices, which made this PhD thesis possible. I want to thank him for his input, constructive criticism and his support of my new ideas. His cooperative and friendly character guaranteed a warm and productive working atmosphere, which was important for the progress of my thesis.

Christa Nöhammer headed the former Molecular Medicine group at AIT. I am very thankful for her support of my project and her valuable comments to my manuscripts, which were important for the final publications. She granted my attendance on national and international conferences, which enabled proceeding papers, talks, contact with other researchers and companies and inspired me with novel concepts.

Michiel Vellekoop was my supervisor at the TU Wien. I owe him my deepest gratitude for his support and diligent review of my work. Numerous critical discussions led to important improvements and revisions of the dissertation and helped me to stay focused.

Zlatko Trajanoski agreed to be my second referee. I want to thank him for carefully reviewing my thesis and for being my co-examiner at the PhD defence.

Walter Grienauer was a colleague at the Powder Injection Moulding group at AIT. He was responsible for the realisation of the injection moulding of the microfluidic chip and helped me with the thermal bonding. I am very thankful for his commitment, openness and active attitude, which led to fruitful discussions and creative new approaches.

Hannes Steiner from the Surface Engineering group at AIT helped me with the dip- and spin-coated thin films and spectroscopic measurements. I owe him my gratitude for his cooperation and short term support, which were important to keep on schedule.

Martin Jenni helped me with the 3D-design of the spiral channel of the direct labelling chip. Thank you very much for your support.

Matthias Wielscher shared the Seibersdorf-office with me. I am very thankful for the initial discussions and coffee breaks, from which a cooperation in the field of data analysis evolved. I want to thank him for offering

me a co-authorship and the resulting teamwork for the final paper. Most importantly I am grateful for the off-work activities, which were important to recover and establish a loyal friendship.

Silvia Schönthaler helped me in the lab and spotted the DNA microarrays. I wish to thank her for the cooperation and helpful attitude. Her friendly character allowed a warm working atmosphere in the Muthgasse-office, which I enjoyed very much.

Lisa Recnik conducted a student project in the field of PCR and microarray analysis of bacterial pathogens, which I was supervising. She performed some of the microarray experiments in Chapter 3, for which I am very thankful.

Naranbold Nyamdavaa worked on a student project for microfluidic DNA extraction under my supervision. I wish to thank him for his cooperation and results, which inspired me for future designs and approaches.

Michaela Nittmann helped me with administrative issues ranging from orders to conference registrations. I want to express my gratitude for her commitment and uncomplicated and friendly attitude. She enabled fast and diligent accomplishment of the tasks, which gave me more time for scientific work.

All members of the Molecular Diagnostics group contributed to a friendly and helpful atmosphere at work. Numerous discussions about bioinformatics, novel lab methods, biomarker screening and tumour assays helped me to maintain an actual broad view of molecular medicine and diagnostic approaches.

Rudolf Heer gave me the opportunity to fabricate sputtered thin films and to characterise them. I want to thank him for his support, creative input and precise reviewing of my work. Debating with him revealed creative ideas and inspired me with novel concepts.

Theodoros Dimopoulos helped me with sputtering metal and metal oxide thin films and performing AFM measurements. I owe him my gratitude for his collaboration and introduction into the sputtering method.

Leire Yarza Irusta provided ZnO nanowire samples for the assessment of fluorescence enhancement. I am thankful for her contribution and her accurate documentation.

This thesis is dedicated to my father **Peter Peham** and grandfather **Karl Schöpf**, who both passed away during my PhD years. They were both medical doctors, inspiring my interdisciplinary career in the fields of engineering and medicine. My father always encouraged me during my studies and PhD

work and supported my stays in England and The Netherlands. I am very thankful for his guidance as a father and the numerous happy and enjoyable hours I had with him. My grandfather inspired me with his impetus and assertiveness, which helped me to accomplish difficult tasks. I want to thank him for his encouragement and the pleasant and valuable time with him during our holidays.

I want to thank my mother **Erdmuth Peham** for her assistance and advice. She always supported my career and was there for me.

My friends helped me to recover after busy working-days. Thank you for the time together and the recreational activities.

Most importantly I want to thank my beloved partner **Birgit** for her love, encouragement and for keeping me grounded. Especially during the busy final phase she gave me motivation and drive for finishing the thesis. Thank you for being with me.

List of Publications

Journal Papers

J. R. Peham, W. Grienauer, H. Steiner, R. Heer, M. J. Vellekoop, C. Noehammer, and H. Wiesinger-Mayr, "Long target droplet polymerase chain reaction with a microfluidic device for high-throughput detection of pathogenic bacteria at clinical sensitivity," *Biomedical Microdevices*, vol. 13, no. 3, pp. 463–473, 2011. doi:10.1007/s10544-011-9514-x

J. R. Peham, L.-M. Recnik, W. Grienauer, M. J. Vellekoop, C. Nöhammer, and H. Wiesinger-Mayr, "Disposable microfluidic chip for rapid pathogen identification with DNA microarrays," *Microsystem Technologies [Online First]*, pp. 1–8. doi:10.1007/s00542-011-1401-0

In submission:

J. R. Peham, M. J. Vellekoop, C. Nöhammer, and H. Wiesinger-Mayr, "High-throughput DNA sensor for continuous flow detection of PCR products," *Submitted to Sensors and Actuators B: Chemical*, 2011.

Proceedings International Conferences

J. R. Peham, L.-M. Recnik, W. Grienauer, M. J. Vellekoop, C. Noehammer, and H. Wiesinger-Mayr, "Hybridisation mix synthesis in a spiral lab-on-chip device for fast-track microarray genotyping of human pathogens," in *Proceedings of SPIE*, vol. 8068, 2011, Conference on Bioelectronics, Biomedical, and Bioinspired Systems V/Nanotechnology V, Prague, Czech Republic, Apr 18-20, 2011. doi:10.1117/12.886620

J. R. Peham, M. J. Vellekoop, C. Nöhammer, and H. Wiesinger-Mayr, "PCR Product Detector with LED-Photodiode Fluorescence Sensing in a Nanoliter Flow-Cell for the High-Throughput Detection of Double-Stranded DNA," in *Procedia Engineering (accepted for publication)*, 2011, 25th Eurosensor Conference, Athens, Greece, Sep 04-07, 2011.

Other Publications

J. R. Peham, H. Steiner, W. Grienauer, R. Heer, M. J. Vellekoop, C. Nöhammer, and H. Wiesinger-Mayr, "Microfluidic PCR device for diagnostic pathogen detection," 2009, Lab on Chip European Congress 2009, Stockholm, Sweden, May 19-20, 2009.

J. R. Peham, H. Steiner, W. Grienauer, R. Heer, M. J. Vellekoop, C. Nöhammer, and H. Wiesinger-Mayr, "Bacterial detection with a microfluidic reactor for polymerase chain reaction," in *Clinical Microbiology and Infection*, vol. 16, 2010, p. S511, 20^{th} European Congress of Clinical Microbiology and Infectious Diseases, Vienna, Austria, 10-13 April, 2010.

J. R. Peham, L.-M. Recnik, W. Grienauer, H. Steiner, R. Heer, M. J. Vellekoop, C. Nöhammer, and H. Wiesinger-Mayr, "Direct fluorescent labeling in a microfluidic PCR chip for fast-track DNA microarray analysis for pathogen identification," 2010, p. 86, 2^{nd} OeGMBT Annual Meeting 2010, Vienna, Austria, Sep 27-29, 2010.

J. R. Peham, L.-M. Recnik, W. Grienauer, M. J. Vellekoop, C. Nöhammer, and H. Wiesinger-Mayr, "Diagnostic Polymer Disc for Process Speed-Up in Microarray-based Bacterial Classification," in *GMe Forum 2011 - Proceedings of the Seminar at the Vienna University of Technology*, K. Riedling, Ed. Vienna, Austria: Gesellschaft für Mikro- und Nanoelektronik (GMe), TU Wien, 2011, pp. 109–112.

Journal Papers Related to other Projects

M. Wielscher, W. Pulverer, J. Peham, M. Hofner, C. Rappaport, C. Singer, C. Jungbauer, C. Nohammer, and A. Weinhausel, "Methyl-binding domain protein-based dna isolation from human blood serum combines dna analyses and serum-autoantibody testing," *BMC Clinical Pathology*, vol. 11, no. 1, p. 11, 2011. doi:10.1186/1472-6890-11-11

Supervision of Students

L.-M. Recnik, "Bacterial diagnostics with polymerase chain reaction and microarrays," 2009-2010, Internship conducted at the Austrian Institute of Technology in collaboration with the Vienna University of Technology.

N. Nyamdavaa, “Microfluidic DNA extraction,” 2011-2012, Internship conducted at the Austrian Institute of Technology in collaboration with the Medical University of Vienna.

Bibliography

[1] K. Mullis, F. Faloona, S. Scharf, R. Saiki, G. Horn, and H. Erlich, "Specific enzymatic amplification of DNA in vitro: the polymerase chain reaction," *Cold Spring Harb. Symp. Quant. Biol.*, vol. 51 Pt 1, pp. 263–273, 1986, [PubMed:3472723].

[2] P. SYKES, S. NEOH, M. BRISCO, E. HUGHES, J. CONDON, and A. MORLEY, "QUANTITATION OF TARGETS FOR PCR BY USE OF LIMITING DILUTION," *BIOTECHNIQUES*, vol. 13, no. 3, pp. 444–449, SEP 1992.

[3] B. Vogelstein and K. Kinzler, "Digital PCR," *PROCEEDINGS OF THE NATIONAL ACADEMY OF SCIENCES OF THE UNITED STATES OF AMERICA*, vol. 96, no. 16, pp. 9236–9241, AUG 3 1999. doi:10.1073/pnas.96.16.9236

[4] World Health Organization, *World Health Statistics 2011*. World Health Organization, 2011.

[5] K. Kupferschmidt, "INFECTIOUS DISEASES As E. coli Outbreak Recedes, New Questions Come to the Fore," *SCIENCE*, vol. 333, no. 6038, p. 27, JUL 1 2011.

[6] W. Linde-Zwirble and D. Angus, "Severe sepsis epidemiology: sampling, selection, and society," *CRITICAL CARE*, vol. 8, no. 4, pp. 222–226, AUG 2004. doi:10.1186/cc2917

[7] K. E. Hodgin and M. Moss, "The epidemiology of sepsis," *CURRENT PHARMACEUTICAL DESIGN*, vol. 14, no. 19, pp. 1833–1839, JUL 2008. doi:10.2174/138161208784980590

[8] D. Angus, W. Linde-Zwirble, J. Lidicker, G. Clermont, J. Carcillo, and M. Pinsky, "Epidemiology of severe sepsis in the United States: Analysis of incidence, outcome, and associated costs of care," *CRITICAL CARE MEDICINE*, vol. 29, no. 7, pp. 1303–1310, JUL 2001. doi:10.1097/00003246-200107000-00002

[9] N. Wellinghausen, A.-J. Kochem, C. Disque, H. Muehl, S. Gebert, J. Winter, J. Matten, and S. G. Sakka, "Diagnosis of Bacteremia in Whole-Blood Samples by Use of a Commercial Universal 16S rRNA Gene-Based PCR and Sequence Analysis," *JOURNAL OF CLINICAL MICROBIOLOGY*, vol. 47, no. 9, pp. 2759–2765, SEP 2009. doi:10.1128/JCM.00567-09

[10] N. Wellinghausen, B. Wirths, A. Franz, L. Karolyi, R. Marre, and U. Reischl, "Algorithm for the identification of bacterial pathogens in positive blood cultures by real-time LightCycler polymerase chain reaction (PCR) with sequence-specific probes," *DIAGNOSTIC MICROBIOLOGY AND INFECTIOUS DISEASE*, vol. 48, no. 4, pp. 229–241, APR 2004. doi:10.1016/j.diagmicrobio.2003.11.005

[11] J. Barenfanger, C. Drake, and G. Kacich, "Clinical and financial benefits of rapid bacterial identification and antimicrobial susceptibility testing," *JOURNAL OF CLINICAL MICROBIOLOGY*, vol. 37, no. 5, pp. 1415–1418, MAY 1999.

[12] J. M. Rothberg, W. Hinz, T. M. Rearick, J. Schultz, W. Mileski, M. Davey, J. H. Leamon, K. Johnson, M. J. Milgrew, M. Edwards, J. Hoon, J. F. Simons, D. Marran, J. W. Myers, J. F. Davidson, A. Branting, J. R. Nobile, B. P. Puc, D. Light, T. A. Clark, M. Huber, J. T. Branciforte, I. B. Stoner, S. E. Cawley, M. Lyons, Y. Fu, N. Homer, M. Sedova, X. Miao, B. Reed, J. Sabina, E. Feierstein, M. Schorn, M. Alanjary, E. Dimalanta, D. Dressman, R. Kasinskas, T. Sokolsky, J. A. Fidanza, E. Namsaraev, K. J. McKernan, A. Williams, G. T. Roth, and J. Bustillo, "An integrated semiconductor device enabling non-optical genome sequencing," *NATURE*, vol. 475, no. 7356, pp. 348–352, JUL 21 2011. doi:10.1038/nature10242

[13] N. Pamme, "Continuous flow separations in microfluidic devices," *LAB ON A CHIP*, vol. 7, no. 12, pp. 1644–1659, 2007. doi:10.1039/b712784g

[14] M. Curcio and J. Roeraade, "Continuous segmented-flow polymerase chain reaction for high-throughput miniaturized DNA amplification," *ANALYTICAL CHEMISTRY*, vol. 75, no. 1, pp. 1–7, JAN 1 2003. doi:10.1021/ac0204146

[15] K. Dorfman, M. Chabert, J. Codarbox, G. Rousseau, P. de Cremoux, and J. Viovy, "Contamination free continuous flow microfluidic polymerase chain reaction for quantitative and clinical applications," *ANALYTICAL CHEMISTRY*, vol. 77, no. 11, pp. 3700–3704, JUN 1 2005. doi:10.1021/ac050031i

[16] S. Park, Y. Zhang, S. Lin, T.-H. Wang, and S. Yang, "Advances in microfluidic PCR for point-of-care infectious disease diagnostics," *BIOTECHNOLOGY ADVANCES*, vol. 29, no. 6, pp. 830–839, NOV-DEC 2011. doi:10.1016/j.biotechadv.2011.06.017

[17] Y. Zhang and P. Ozdemir, "Microfluidic DNA amplification-A review," *ANALYTICA CHIMICA ACTA*, vol. 638, no. 2, pp. 115–125, APR 13 2009. doi:10.1016/j.aca.2009.02.038

[18] C. Zhang and D. Xing, "Miniaturized PCR chips for nucleic acid amplification and analysis: latest advances and future trends," *NUCLEIC ACIDS RESEARCH*, vol. 35, no. 13, pp. 4223–4237, 2007. doi:10.1093/nar/gkm389

[19] C. Zhang, J. Xu, W. Ma, and W. Zheng, "PCR microfluidic devices for DNA amplification," *BIOTECHNOLOGY ADVANCES*, vol. 24, no. 3, pp. 243–284, MAY-JUN 2006. doi:10.1016/j.biotechadv.2005.10.002

[20] I. Pjescic, C. Tranter, P. L. Hindmarsh, and N. D. Crews, "Glass-composite prototyping for flow PCR with in situ DNA analysis," *BIOMEDICAL MICRODEVICES*, vol. 12, no. 2, pp. 333–343, APR 2010. doi:10.1007/s10544-009-9389-2

[21] M. Mahalanabis, J. do, H. ALMuayad, J. Y. Zhang, and C. M. Klapperich, "An integrated disposable device for DNA extraction and helicase dependent amplification," *BIOMEDICAL MICRODEVICES*, vol. 12, no. 2, pp. 353–359, APR 2010. doi:10.1007/s10544-009-9391-8

[22] C. Zhang and D. Xing, "Microfluidic gradient PCR (MG-PCR): a new method for microfluidic DNA amplification," *BIOMEDICAL MICRODEVICES*, vol. 12, no. 1, pp. 1–12, FEB 2010. doi:10.1007/s10544-009-9352-2

[23] Y. Li, D. Xing, and C. Zhang, "Rapid detection of genetically modified organisms on a continuous-flow polymerase chain reaction microfluidics," *ANALYTICAL BIOCHEMISTRY*, vol. 385, no. 1, pp. 42–49, FEB 1 2009. doi:10.1016/j.ab.2008.10.028

[24] A. F. Sauer-Budge, P. Mirer, A. Chatterjee, C. M. Klapperich, D. Chargin, and A. Sharon, "Low cost and manufacturable complete microTAS for detecting bacteria," *LAB ON A CHIP*, vol. 9, no. 19, pp. 2803–2810, 2009. doi:10.1039/b904854e

[25] N. Park, S. Kim, and J. Hahn, "Cylindrical compact thermal-cycling device for continuous-flow polymerase chain reaction," *ANALYTICAL CHEMISTRY*, vol. 75, no. 21, pp. 6029–6033, NOV 1 2003. doi:10.1021/ac0346959

[26] P. Obeid, T. Christopoulos, H. Crabtree, and C. Backhouse, "Microfabricated device for DNA and RNA amplification by continuous-flow polymerase chain reaction and reverse transcription-polymerase chain reaction with cycle number selection," *ANALYTICAL CHEMISTRY*, vol. 75, no. 2, pp. 288–295, JAN 15 2003. doi:10.1021/ac0260239

[27] H. Wiesinger-Mayr, K. Vierlinger, R. Pichler, A. Kriegner, A. M. Hirschl, E. Presterl, L. Bodrossy, and C. Noehammer, "Identification of human pathogens isolated from blood using microarray hybridisation and signal pattern recognition," *BMC MICROBIOLOGY*, vol. 7, AUG 14 2007. doi:10.1186/1471-2180-7-78

[28] X. Yu, M. Susa, C. Knabbe, R. Schmid, and T. Bachmann, "Development and validation of a diagnostic DNA microarray to detect quinolone-resistant Escherichia coli among clinical isolates," *JOURNAL OF CLINICAL MICROBIOLOGY*, vol. 42, no. 9, pp. 4083–4091, SEP 2004. doi:10.1128/JCM.42.9.4083-4091.2004

[29] D. P. Manage, Y. C. Morrissey, A. J. Stickel, J. Lauzon, A. Atrazhev, J. P. Acker, and L. M. Pilarski, "On-chip PCR amplification of genomic and viral templates in unprocessed whole blood," *MICROFLUIDICS AND NANOFLUIDICS*, vol. 10, no. 3, pp. 697–702, MAR 2011. doi:10.1007/s10404-010-0702-4

[30] N. Ramalingam, Z. Rui, H.-B. Liu, C.-C. Dai, R. Kaushik, B. Ratnaharika, and H.-Q. Gong, "Real-time PCR-based microfluidic array chip for simultaneous detection of multiple waterborne pathogens," *SENSORS AND ACTUATORS B-CHEMICAL*, vol. 145, no. 1, pp. 543–552, MAR 4 2010. doi:10.1016/j.snb.2009.11.025

[31] G. Hairer, M. Vellekoop, M. Mansfeld, and C. Nohammer, "Biochip for DNA amplification and label-free DNA detection," in *Proceedings of IEEE Sensors 2007 Conference*. Piscataway, NJ, USA: IEEE, Conference Paper, pp. 724–7, IEEE Sensors 2007 Conference, 28-31 Oct. 2007, Atlanta, GA, USA.

[32] Y. Sun, Y. C. Kwok, and N. T. Nguyen, "A circular ferrofluid driven microchip for rapid polymerase chain reaction," *LAB ON A CHIP*, vol. 7, no. 8, pp. 1012–1017, 2007. doi:10.1039/b700575j

[33] R. Hartung, A. Broesing, G. Szczepankiewicz, U. Liebert, N. Haefner, M. Duerst, J. Felbel, D. Lassner, and J. M. Koehler, "Application of an asymmetric helical tube reactor for fast identification of gene transcripts of pathogenic viruses by micro flow-through PCR," *BIOMEDICAL MICRODEVICES*, vol. 11, no. 3, pp. 685–692, JUN 2009. doi:10.1007/s10544-008-9280-6

[34] N. Panaro, X. Lou, P. Fortina, L. Kricka, and P. Wilding, "Surface effects on PCR reactions in multichip microfluidic platforms," *BIOMEDICAL MICRODEVICES*, vol. 6, no. 1, pp. 75–80, MAR 2004.

[35] W. Ludwig, O. Strunk, R. Westram, L. Richter, H. Meier, Yadhukumar, A. Buchner, T. Lai, S. Steppi,

G. Jobb, W. Forster, I. Brettske, S. Gerber, A. Ginhart, O. Gross, S. Grumann, S. Hermann, R. Jost, A. Konig, T. Liss, R. Lussmann, M. May, B. Nonhoff, B. Reichel, R. Strehlow, A. Stamatakis, N. Stuckmann, A. Vilbig, M. Lenke, T. Ludwig, A. Bode, and K. Schleifer, "ARB: a software environment for sequence data," *NUCLEIC ACIDS RESEARCH*, vol. 32, no. 4, pp. 1363–1371, FEB 2004. doi:10.1093/nar/gkh293

[36] W. Dunn, S. Jacobson, L. Waters, N. Kroutchinina, J. Khandurina, R. Foote, M. Justice, L. Stubbs, and J. Ramsey, "PCR amplification and analysis of simple sequence length polymorphisms in mouse DNA using a single microchip device," *ANALYTICAL BIOCHEMISTRY*, vol. 277, no. 1, pp. 157–160, JAN 1 2000.

[37] N. Friedman and D. Meldrum, "Capillary tube resistive thermal cycling," *ANALYTICAL CHEMISTRY*, vol. 70, no. 14, pp. 2997–3002, JUL 15 1998.

[38] W. Rasband, *ImageJ*. U. S. National Institutes of Health, Bethesda, Maryland, USA, 1997-2009, http://rsb.info.nih.gov/ij/.

[39] J. Kim, J. Lee, S. Seong, S. Cha, S. Lee, J. Kim, and T. Park, "Fabrication and characterization of a PDMS-glass hybrid continuous-flow PCR chip," *BIOCHEMICAL ENGINEERING JOURNAL*, vol. 29, no. 1-2, pp. 91–97, APR 1 2006, 10th Symposium of the Young-Asian-Biochemical-Engineers-Community (YABEC), Osaka City, JAPAN, SEP 23-25, 2004. doi:10.1016/j.bej.2005.02.032

[40] J. Chen, M. Wabuyele, H. Chen, D. Patterson, M. Hupert, H. Shadpour, D. Nikitopoulos, and S. Soper, "Electrokinetically synchronized polymerase chain reaction microchip fabricated in polycarbonate," *ANALYTICAL CHEMISTRY*, vol. 77, no. 2, pp. 658–666, JAN 15 2005. doi:10.1021/ac048758e

[41] K. Sun, A. Yamaguchi, Y. Ishida, S. Matsuo, and H. Misawa, "A heater-integrated transparent microchannel chip for continuous-flow PCR," *SENSORS AND ACTUATORS B-CHEMICAL*, vol. 84, no. 2-3, pp. 283–289, MAY 15 2002.

[42] I. Schneegass, R. Brautigam, and J. Kohler, "Miniaturized flow-through PCR with different template types in a silicon chip thermocycler," *LAB ON A CHIP*, vol. 1, no. 1, pp. 42–49, 2001. doi:10.1039/b103846j

[43] E. Lagally, P. Simpson, and R. Mathies, "Monolithic integrated microfluidic DNA amplification and capillary electrophoresis analysis system," *SENSORS AND ACTUATORS B-CHEMICAL*, vol. 63, no. 3, pp. 138–146, MAY 15 2000.

[44] N. Crews, T. Ameel, C. Wittwer, and B. Gale, "Flow-induced thermal effects on spatial DNA melting," *LAB ON A CHIP*, vol. 8, no. 11, pp. 1922–1929, 2008. doi:10.1039/b807034b

[45] M. Hashimoto, P. Chen, M. Mitchell, D. Nikitopoulos, S. Soper, and M. Murphy, "Rapid PCR in a continuous flow device," *LAB ON A CHIP*, vol. 4, no. 6, pp. 638–645, 2004. doi:10.1039/b406860b

[46] Z. Chunsun, X. Jinliang, W. Jianqin, and W. Hanping, "Experimental study of continuous-flow polymerase chain reaction microfluidics based on polytetrafluoroethylene capillary," *CHINESE JOURNAL OF ANALYTICAL CHEMISTRY*, vol. 34, no. 8, pp. 1197–1202, AUG 2006.

[47] A. Fluit, F. Schmitz, J. Verhoef, and E. S. P. Grp, "Frequency of isolation of pathogens from bloodstream, nosocomial pneumonia, skin and soft tissue, and urinary tract infections occurring in European patients," *EUROPEAN JOURNAL OF CLINICAL MICROBIOLOGY & INFECTIOUS DISEASES*, vol. 20, no. 3, pp. 188–191, MAR 2001. doi:10.1007/s10096-001-8078-8

[48] A. Walsh, M. Smith, V. Wuthiekanun, Y. Suputtamongkol, W. Chaowagul, D. Dance, B. Angus, and N. White, "Prognostic significance of quantitative bacteremia in septicemic melioidosis," *CLINICAL INFECTIOUS DISEASES*, vol. 21, no. 6, pp. 1498–1500, DEC 1995.

[49] P. Bowler, B. Duerden, and D. Armstrong, "Wound microbiology and associated approaches to wound management," *CLINICAL MICROBIOLOGY REVIEWS*, vol. 14, no. 2, pp. 244+, APR 2001. doi:10.1128/CMR.14.2.244-269.2001

[50] T. Fukuba, T. Yamamoto, T. Naganuma, and T. Fujii, "Microfabricated flow-through device for DNA amplification - towards in situ gene analysis," *CHEMICAL ENGINEERING JOURNAL*, vol. 101, no. 1-3, pp. 151–156, AUG 1 2004, 7th International Conference on Microreaction Technology (IMRET 7), Lausanne, SWITZERLAND, SEP, 2003. doi:10.1016/j.cej.2003.11.016

[51] D. Chen, M. Mauk, X. Qiu, C. Liu, J. Kim, S. Ramprasad, S. Ongagna, W. R. Abrams, D. Malamud, P. L. A. M. Corstjens, and H. H. Bau, "An integrated, self-contained microfluidic cassette for isolation, amplification, and detection of nucleic acids," *BIOMEDICAL MICRODEVICES*, vol. 12, no. 4, pp. 705–719, AUG 2010. doi:10.1007/s10544-010-9423-4

[52] L.-J. Chien, J.-H. Wang, T.-M. Hsieh, P.-H. Chen, P.-J. Chen, D.-S. Lee, C.-H. Luo, and G.-B. Lee, "A micro circulating PCR chip using a suction-type membrane for fluidic transport," *BIOMEDICAL MICRODEVICES*, vol. 11, no. 2, pp. 359–367, APR 2009. doi:10.1007/s10544-008-9242-z

[53] N. Ramalingam, H.-B. Liu, C.-C. Dai, Y. Jiang, H. Wang, Q. Wang, K. M. Hui, and H.-Q. Gong,

"Real-time PCR array chip with capillary-driven sample loading and reactor sealing for point-of-care applications," *BIOMEDICAL MICRODEVICES*, vol. 11, no. 5, pp. 1007–1020, OCT 2009. doi:10.1007/s10544-009-9318-4

[54] F. Wang and M. A. Burns, "Performance of nanoliter-sized droplet-based microfluidic PCR," *BIOMEDICAL MICRODEVICES*, vol. 11, no. 5, pp. 1071–1080, OCT 2009. doi:10.1007/s10544-009-9324-6

[55] J. R. Peham, L.-M. Recnik, W. Grienauer, M. J. Vellekoop, C. Noehammer, and H. Wiesinger-Mayr, "Hybridisation mix synthesis in a spiral lab-on-chip device for fast-track microarray genotyping of human pathogens," in *Proceedings of SPIE*, vol. 8068, 2011, Conference on Bioelectronics, Biomedical, and Bioinspired Systems V/Nanotechnology V, Prague, Czech Republic, Apr 18-20, 2011. doi:10.1117/12.886620

[56] X. Qiu, D. Chen, C. Liu, M. G. Mauk, T. Kientz, and H. H. Bau, "A portable, integrated analyzer for microfluidic - based molecular analysis," *BIOMEDICAL MICRODEVICES*, vol. 13, no. 5, pp. 809–817, OCT 2011. doi:10.1007/s10544-011-9551-5

[57] N. B. Trung, M. Saito, H. Takabayashi, P. H. Viet, E. Tamiya, and Y. Takamura, "Multi-chamber PCR chip with simple liquid introduction utilizing the gas permeability of polydimethylsiloxane," *SENSORS AND ACTUATORS B-CHEMICAL*, vol. 149, no. 1, pp. 284–290, AUG 6 2010. doi:10.1016/j.snb.2010.06.013

[58] e. a. Charles E. Wilkes, *PVC Handbook*. Hanser Gardner Publications, 2005.

[59] S. Haenle, *Werkstoff-Fhrer Kunststoffe*. Hanser Fachbuchverlag, 2004.

[60] J. R. Peham, W. Grienauer, H. Steiner, R. Heer, M. J. Vellekoop, C. Noehammer, and H. Wiesinger-Mayr, "Long target droplet polymerase chain reaction with a microfluidic device for high-throughput detection of pathogenic bacteria at clinical sensitivity," *Biomedical Microdevices*, vol. 13, no. 3, pp. 463–473, 2011. doi:10.1007/s10544-011-9514-x

[61] Y. Sun, M. V. D. Satyanarayan, N. T. Nguyen, and Y. C. Kwok, "Continuous flow polymerase chain reaction using a hybrid PMMA-PC microchip with improved heat tolerance," *SENSORS AND ACTUATORS B-CHEMICAL*, vol. 130, no. 2, pp. 836–841, MAR 28 2008. doi:10.1016/j.snb.2007.10.058

[62] G. Wu, N. Yang, T. Zhang, Z. Wang, X. Lu, and J. Kang, "Fabrication and application of a new dna biosensor based on on-substrate pcr and electrochemistry," *Sensors and Actuators B: Chemical*, vol. In Press, Accepted Manuscript, pp. –, 2011. doi:DOI: 10.1016/j.snb.2011.08.034. [Online]. Available: http://www.sciencedirect.com/science/article/pii/S092540051100757X

[63] K.-Y. Hwang, S.-Y. Jeong, Y.-R. Kim, K. Namkoong, H.-K. Lim, W.-S. Chung, J.-H. Kim, and N. Huh, "Rapid detection of bacterial cell from whole blood: Integration of dna sample preparation into single micro-pcr chip," *Sensors and Actuators B: Chemical*, vol. 154, no. 1, pp. 46 – 51, 2011, transducers 2009. doi:DOI: 10.1016/j.snb.2009.11.005. [Online]. Available: http://www.sciencedirect.com/science/article/pii/S0925400509008703

[64] P. Bembnowicz, M. Malodobra, W. Kubicki, P. Szczepanska, A. Gorecka-Drzazga, J. Dziuban, A. Jonkisz, A. Karpiewska, T. Dobosz, and L. Golonka, "Preliminary studies on LTCC based PCR microreactor," *SENSORS AND ACTUATORS B-CHEMICAL*, vol. 150, no. 2, pp. 715–721, OCT 28 2010. doi:10.1016/j.snb.2010.08.015

[65] Y. Li, C. Zhang, and D. Xing, "Integrated microfluidic reverse transcription-polymerase chain reaction for rapid detection of food- or waterborne pathogenic rotavirus," *ANALYTICAL BIOCHEMISTRY*, vol. 415, no. 2, pp. 87–96, AUG 15 2011. doi:10.1016/j.ab.2011.04.026

[66] H. J. Kim, H.-S. Moon, B. S. Kwak, and H.-I. Jung, "Microfluidic device to separate micro-beads with various fluorescence intensities," *Sensors and Actuators B: Chemical*, vol. In Press, Corrected Proof, pp. –, 2011. doi:DOI: 10.1016/j.snb.2011.08.013. [Online]. Available: http://www.sciencedirect.com/science/article/pii/S0925400511007362

[67] A. J. Hopwood, C. Hurth, J. Yang, Z. Cai, N. Moran, J. G. Lee-Edghill, A. Nordquist, R. Lenigk, M. D. Estes, J. P. Haley, C. R. McAlister, X. Chen, C. Brooks, S. Smith, K. Elliott, P. Koumi, F. Zenhausern, and G. Tully, "Integrated Microfluidic System for Rapid Forensic DNA Analysis: Sample Collection to DNA Profile," *ANALYTICAL CHEMISTRY*, vol. 82, no. 16, pp. 6991–6999, AUG 15 2010. doi:10.1021/ac101355r

[68] J. E. Dickens, M. S. Vaughn, M. Taylor, and M. Ponstingl, "An led array-based light induced fluorescence sensor for real-time process and field monitoring," *Sensors and Actuators B: Chemical*, vol. 158, no. 1, pp. 35 – 42, 2011. doi:DOI: 10.1016/j.snb.2011.04.077. [Online]. Available: http://www.sciencedirect.com/science/article/pii/S0925400511003741

[69] C.-P. Chang, D. J. Nagel, M. T. Velasquez, and M. E. Zaghloul, "Compact optical microfluidic uric acid analysis system," *BIOSENSORS & BIOELECTRONICS*, vol. 26, no. 10, pp. 4155–4161, JUN 15 2011. doi:10.1016/j.bios.2011.04.013

[70] R. Irawan, Y. H. Cheng, W. M. Ng, M. M. Aung, I. K. Lao, and V. Thaveeprungsriporn, "Polymer waveguide sensor for early diagnostic and wellness monitoring," *BIOSENSORS & BIOELECTRONICS*, vol. 26, no. 8, pp. 3666–3669, APR 15 2011. doi:10.1016/j.bios.2010.10.004

[71] F. Yang, X.-c. Li, W. Zhang, J.-b. Pan, and Z.-g. Chen, "A facile light-emitting-diode induced fluorescence detector coupled to an integrated microfluidic device for microchip electrophoresis," *TALANTA*, vol. 84, no. 4, pp. 1099–1106, MAY 30 2011. doi:10.1016/j.talanta.2011.03.020

[72] J. Wilhelm and A. Pingoud, "Real-time polymerase chain reaction," *CHEMBIOCHEM*, vol. 4, no. 11, pp. 1120–1128, NOV 7 2003. doi:10.1002/cbic.200300662

[73] G. Cosa, K. Focsaneanu, J. McLean, J. McNamee, and J. Scaiano, "Photophysical properties of fluorescent DNA-dyes bound to single- and double-stranded DNA in aqueous buffered solution," *PHOTOCHEMISTRY AND PHOTOBIOLOGY*, vol. 73, no. 6, pp. 585–599, JUN 2001. doi:10.1562/0031-8655(2001)073¡0585:PPOFDD¿2.0.CO;2

[74] T. Kamei, B. Paegel, J. Scherer, A. Skelley, R. Street, and R. Mathies, "Integrated hydrogenated amorphous Si photodiode detector for microfluidic bioanalytical devices," *ANALYTICAL CHEMISTRY*, vol. 75, no. 20, pp. 5300–5305, OCT 15 2003. doi:10.1021/ac0301550

[75] A. Singh, V. Srivastav, and R. Pal, "HgCdTe avalanche photodiodes: A review," *OPTICS AND LASER TECHNOLOGY*, vol. 43, no. 7, pp. 1358–1370, OCT 2011. doi:10.1016/j.optlastec.2011.03.009

[76] S. Marangoni, I. Rech, M. Ghioni, P. Maccagnani, M. Chiari, M. Cretich, F. Damin, G. Di Carlo, and S. Cova, "A 6 x 8 photon-counting array detector system for fast and sensitive analysis of protein microarrays," *SENSORS AND ACTUATORS B-CHEMICAL*, vol. 149, no. 2, pp. 420–426, AUG 19 2010. doi:10.1016/j.snb.2010.05.012

[77] K.-Y. Hwang, J.-H. Kim, K.-Y. Suh, J. S. Ko, and N. Huh, "Low-cost polymer microfluidic device for on-chip extraction of bacterial DNA," *SENSORS AND ACTUATORS B-CHEMICAL*, vol. 155, no. 1, pp. 422–429, JUL 5 2011. doi:10.1016/j.snb.2010.12.026

[78] G. R. M. Duarte, C. W. Price, B. H. Augustine, E. Carrilho, and J. P. Landers, "Dynamic Solid Phase DNA Extraction and PCR Amplification in Polyester-Toner Based Microchip," *ANALYTICAL CHEMISTRY*, vol. 83, no. 13, pp. 5182–5189, JUL 1 2011. doi:10.1021/ac200292m

[79] S. M. Azimi, G. Nixon, J. Ahern, and W. Balachandran, "A magnetic bead-based DNA extraction and purification microfluidic device," *MICROFLUIDICS AND NANOFLUIDICS*, vol. 11, no. 2, pp. 157–165, AUG 2011. doi:10.1007/s10404-011-0782-9

[80] T. Mockler and J. Ecker, "Applications of DNA tiling arrays for whole-genome analysis," *GENOMICS*, vol. 85, no. 1, pp. 1–15, JAN 2005. doi:10.1016/j.ygeno.2004.10.005

[81] P. Arora, A. Sindhu, N. Dilbaghi, and A. Chaudhury, "Biosensors as innovative tools for the detection of food borne pathogens," *Biosensors and Bioelectronics*, vol. 28, no. 1, pp. 1 – 12, 2011. doi:10.1016/j.bios.2011.06.002. [Online]. Available: http://www.sciencedirect.com/science/article/pii/S0956566311003502

[82] G. Zhang, C. Li, Y. Lu, H. Hu, G. Xiang, Z. Liang, P. Liao, P. Dai, W. Xing, and J. Cheng, "Validation of a mobile phone-assisted microarray decoding platform for signal-enhanced mutation detection," *BIOSENSORS & BIOELECTRONICS*, vol. 26, no. 12, pp. 4708–4714, AUG 15 2011. doi:10.1016/j.bios.2011.05.031

[83] J. R. Lakowicz, K. Ray, M. Chowdhury, H. Szmacinski, Y. Fu, J. Zhang, and K. Nowaczyk, "Plasmon-controlled fluorescence: a new paradigm in fluorescence spectroscopy," *ANALYST*, vol. 133, no. 10, pp. 1308–1346, 2008. doi:10.1039/b802918k

[84] J. H. Kim, S. H. Han, and B. H. Chung, "Improving Pb(2+) detection using DNAzyme-based fluorescence sensors by pairing fluorescence donors with gold nanoparticles," *BIOSENSORS & BIOELECTRONICS*, vol. 26, no. 5, pp. 2125–2129, JAN 15 2011. doi:10.1016/j.bios.2010.09.018

[85] R. Ricco, A. Meneghello, and F. Enrichi, "Signal enhancement in DNA microarray using dye doped silica nanoparticles: Application to Human Papilloma Virus (HPV) detection," *BIOSENSORS & BIOELECTRONICS*, vol. 26, no. 5, pp. 2761–2765, JAN 15 2011. doi:10.1016/j.bios.2010.10.024

[86] J. S. Kim, J. B. Cho, B. G. Park, W. Lee, K. B. Lee, and M.-K. Oh, "Size-controllable quartz nanostructure for signal enhancement of DNA chip," *BIOSENSORS & BIOELECTRONICS*, vol. 26, no. 5, pp. 2085–2089, JAN 15 2011. doi:10.1016/j.bios.2010.09.010

[87] K.-Y. Ahn, K. Kwon, J. Huh, G. T. Kim, E. B. Lee, D. Park, and J. Lee, "A sensitive diagnostic assay of rheumatoid arthritis using three-dimensional zno nanorod structure," *Biosensors and Bioelectronics*, vol. 28, no. 1, pp. 378 – 385, 2011. doi:10.1016/j.bios.2011.07.052. [Online]. Available: http://www.sciencedirect.com/science/article/pii/S0956566311004994

[88] W. Hu, Y. Liu, H. Yang, X. Zhou, and C. M. Li, "ZnO nanorods-enhanced fluorescence for sensitive microarray detection of cancers in serum without additional reporter-amplification," *BIOSENSORS &*

BIOELECTRONICS, vol. 26, no. 8, pp. 3683–3687, APR 15 2011. doi:10.1016/j.bios.2011.01.045

[89] E. Fort and S. Gresillon, "Surface enhanced fluorescence," *JOURNAL OF PHYSICS D-APPLIED PHYSICS*, vol. 41, no. 1, JAN 7 2008. doi:10.1088/0022-3727/41/1/013001

[90] H. Choumane, N. Ha, C. Nelep, A. Chardon, G. Reymond, C. Goutel, G. Cerovic, F. Vallet, C. Weisbuch, and H. Benisty, "Double interference fluorescence enhancement from reflective slides: Application to bicolor microarrays," *APPLIED PHYSICS LETTERS*, vol. 87, no. 3, JUL 18 2005. doi:10.1063/1.1999018

[91] M. Addamo, V. Augugliaro, A. Di Paola, E. Garcia-Lopez, V. Loddo, G. Marci, and L. Palmisano, "Preparation and photoactivity of nanostructured TiO(2) particles obtained by hydrolysis of TiCl(4)," *COLLOIDS AND SURFACES A-PHYSICOCHEMICAL AND ENGINEERING ASPECTS*, vol. 265, no. 1-3, pp. 23–31, SEP 1 2005, 3rd International Conference on Interfaces Against Pollutions, Julich, GERMANY, MAY 24-27, 2004. doi:10.1016/j.colsurfa.2004.11.048

[92] A. J. Qavi, T. M. Mysz, and R. C. Bailey, "Isothermal Discrimination of Single-Nucleotide Polymorphisms via Real-Time Kinetic Desorption and Label-Free Detection of DNA Using Silicon Photonic Microring Resonator Arrays," *ANALYTICAL CHEMISTRY*, vol. 83, no. 17, pp. 6827–6833, SEP 1 2011. doi:10.1021/ac201659p

[93] E. Nuwaysir, W. Huang, T. Albert, J. Singh, K. Nuwaysir, A. Pitas, T. Richmond, T. Gorski, J. Berg, J. Ballin, M. McCormick, J. Norton, T. Pollock, T. Sumwalt, L. Butcher, D. Porter, M. Molla, C. Hall, F. Blattner, M. Sussman, R. Wallace, F. Cerrina, and R. Green, "Gene expression analysis using oligonucleotide arrays produced by maskless photolithography," *GENOME RESEARCH*, vol. 12, no. 11, pp. 1749–1755, NOV 2002. doi:10.1101/gr362402

[94] D.-S. Shin, K.-N. Lee, B.-W. Yoo, J. Kim, M. Kim, Y.-K. Kim, and Y.-S. Lee, "Automated Maskless Photolithography System for Peptide Microarray Synthesis on a Chip," *JOURNAL OF COMBINATORIAL CHEMISTRY*, vol. 12, no. 4, pp. 463–471, JUL-AUG 2010. doi:10.1021/cc100009g

[95] S. L. Seurynck-Servoss, A. M. White, C. L. Baird, K. D. Rodland, and R. C. Zangar, "Evaluation of surface chemistries for antibody microarrays," *ANALYTICAL BIOCHEMISTRY*, vol. 371, no. 1, pp. 105–115, DEC 1 2007. doi:10.1016/j.ab.2007.07.010

[96] E. G. Matveeva, I. Gryczynski, A. Barnett, Z. Leonenko, J. R. Lakowicz, and Z. Gryczynski, "Metal particle-enhanced fluorescent immunoassays on metal mirrors," *ANALYTICAL BIOCHEMISTRY*, vol. 363, no. 2, pp. 239–245, APR 15 2007. doi:10.1016/j.ab.2007.01.030

[97] M. J. Choi, K. E. McBean, P. H. R. Ng, A. M. McDonagh, P. J. Maynard, C. Lennard, and C. Roux, "An evaluation of nanostructured zinc oxide as a fluorescent powder for fingerprint detection," *JOURNAL OF MATERIALS SCIENCE*, vol. 43, no. 2, pp. 732–737, JAN 2008, 5th Meeting of the Brazilian-Society-for-Materials-Research, Florianopolis, BRAZIL, OCT 08-12, 2006. doi:10.1007/s10853-007-2178-5

[98] S. Aksoy, Y. Caglar, S. Ilican, and M. Caglar, "Sol-gel derived zinc oxide films: Effect of deposition parameters on structure, microstructure and photoluminescence properties," *SUPERLATTICES AND MICROSTRUCTURES*, vol. 50, no. 5, pp. 470–479, NOV 2011. doi:10.1016/j.spmi.2011.08.008

[99] N. L. Tarwal, P. R. Jadhav, S. A. Vanalakar, S. S. Kalagi, R. C. Pawar, J. S. Shaikh, S. S. Mali, D. S. Dalavi, P. S. Shinde, and P. S. Patil, "Photoluminescence of zinc oxide nanopowder synthesized by a combustion method," *POWDER TECHNOLOGY*, vol. 208, no. 1, pp. 185–188, MAR 10 2011. doi:10.1016/j.powtec.2010.12.017

[100] L. Armelao, M. Pascolini, E. Biasiolo, E. Tondello, G. Bottaro, M. D. Carbonare, A. D'Arrigo, and A. Leon, "Innovative metal oxide-based substrates for DNA microarrays," *INORGANICA CHIMICA ACTA*, vol. 361, no. 12-13, pp. 3603–3608, SEP 1 2008. doi:10.1016/j.ica.2008.03.121

[101] N. Kumar, A. Dorfman, and J.-i. Hahm, "Ultrasensitive DNA sequence detection using nanoscale ZnO sensor arrays," *NANOTECHNOLOGY*, vol. 17, no. 12, pp. 2875–2881, JUN 28 2006. doi:10.1088/0957-4484/17/12/009

[102] V. Adalsteinsson, O. Parajuli, S. Kepics, A. Gupta, W. B. Reeves, and J.-i. Hahm, "Ultrasensitive detection of cytokines enabled by nanoscale ZnO arrays," *ANALYTICAL CHEMISTRY*, vol. 80, no. 17, pp. 6594–6601, SEP 1 2008. doi:10.1021/ac800747q

[103] R. Benters, C. Niemeyer, D. Drutschmann, D. Blohm, and D. Wohrle, "DNA microarrays with PAMAM dendritic linker systems," *NUCLEIC ACIDS RESEARCH*, vol. 30, no. 2, JAN 15 2002. doi:10.1093/nar/30.2.e10

About the Author

Johannes R. Peham was born in Grieskirchen, Austria in 1980. In 1999 he graduated with distincion from the Federal Secondary College of Electrical Engineering (Höhere Technische Bundeslehranstalt HTL für Elektrotechnik), Wels, Austria. He received the M.Sc. degree in molecular medicine from the Cranfield University, United Kingdom in 2007. His master thesis was conducted at the VU University Medical Center, Amsterdam, The Netherlands in the field of bioinformatics for cancer diagnostics. At the Graz University of Technology, Austria he graduated with distinction in electrical engineering with the Dipl. Ing. (M.Sc.) degree and received the award for the best master thesis in 2008. Between 2008 and 2011 he worked at the Austrian Institute of Technology, Vienna as a PhD candidate on microdevices for molecular diagnostics in collaboration with the Institute of Sensor and Actuator Systems, Vienna University of Technology. He authored journal and proceeding papers, gave talks and poster presentations on international conferences and supervised project students. Research interests are microfluidic PCR, DNA sensors, miniaturised DNA extraction systems, automated microarrays and diagnostic microdevices.